Acta Universitatis Szegediensis

Acta Biologica Szegediensis

Volume 48, Number 1-4, 2004

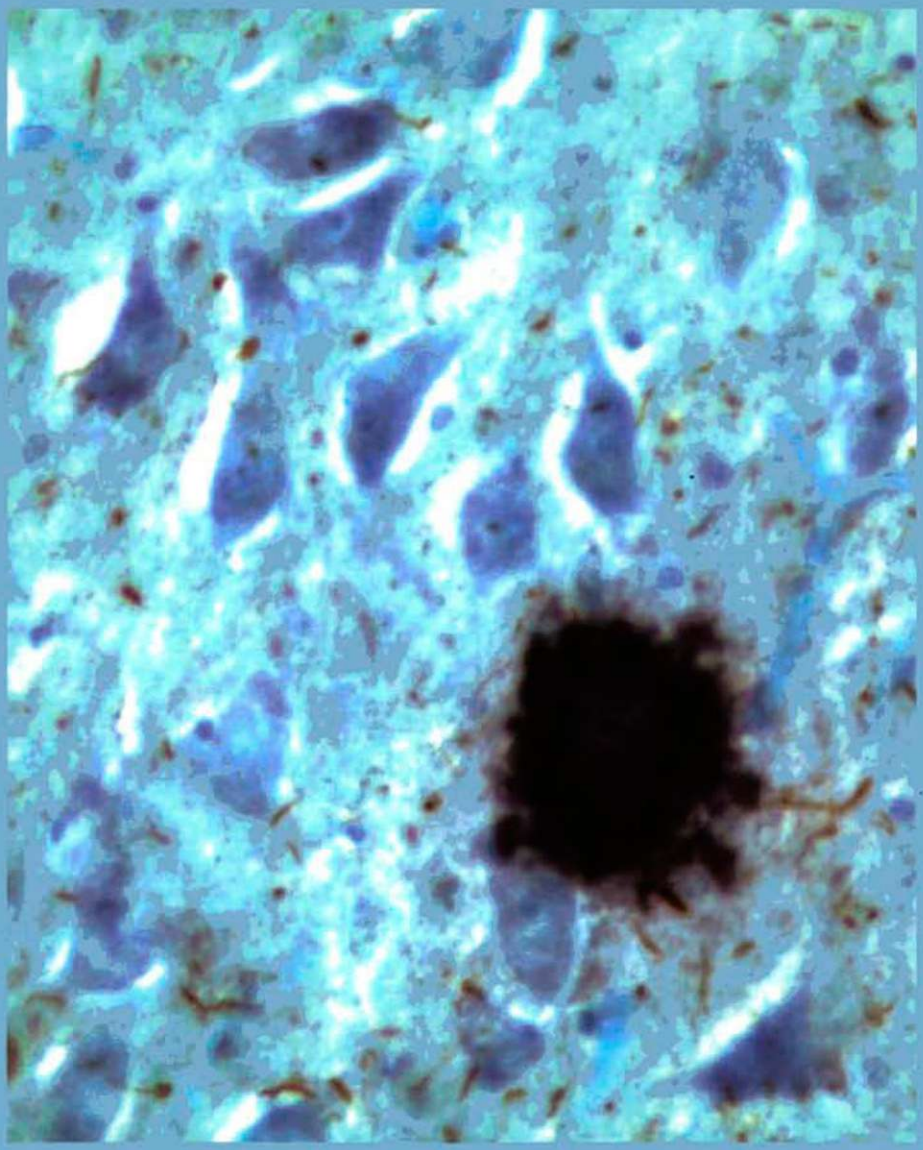

University of Szeged, Szeged, Hungary

Acta Biologica Szegediensis

Acta Biologica Szegediensis (ISSN 1588-385X print form; ISSN 1588-4082 online form), a member of the Acta Universitatis Szegediensis family of scientific journals (ISSN 0563-0592), is published yearly by the University of Szeged. Acta Biologica Szegediensis covers the growth areas of modern biology and publishes original research articles and reviews, involving, but not restricted to, the fields of anatomy, embryology and histology, anthropology, biochemistry, biophysics, biotechnology, botany and plant physiology, all areas of clinical sciences, conservation biology, ecology, genetics, microbiology, molecular biology, neurosciences, paleontology, pharmacology, physiology and pathophysiology, and zoology. Occasionally, Acta Biologica Szegediensis will publish symposium materials. Acta Biologica Szegediensis particularly encourages young investigators and clinicians to submit novel results of interest.

Submission of manuscripts

Manuscripts should be prepared in accordance with the Instructions to Authors published in each issue, also available at http://www.sci.u-szeged.hu/ABS, and submitted to:

Károly Gulya
Acta Biologica Szegediensis, Editorial Office
Department of Zoology and Cell Biology
University of Szeged
2 Egyetem u., POB 659, H-6722 Szeged, Hungary
Phone: 36 (62) 544-048, fax: 36 (62) 544-049
E-mail: gulyak@bio.u-szeged.hu

Correspondence relating to the status of the manuscripts, proofs, publication, reprints and advertising should be sent to:

Lidia Bakota
Acta Biologica Szegediensis, Editorial Office
Department of Zoology and Cell Biology
University of Szeged
2 Egyetem u., POB 659, H-6722 Szeged, Hungary
Phone: 36 (62) 544-125, fax: 36 (62) 544-049
E-mail: bakotal@bio.u-szeged.hu

Subscriptions

Acta Biologica Szegediensis is published yearly in four issues per volume. All subscriptions relate to the calendar year and must be pre-paid. The annual subscription rate is currently 50 USD and includes air mail delivery and handling.

Acta Biologica Szegediensis is indexed in BIOSIS Database, EMBASE, Excerpta Medica, Elsevier BIOBASE (Current Awareness in Biological Sciences) and Zoological Record.

The Table of Contents for the current issue and those for previous issues can be found at http://www.sci.u-szeged.hu/ABS.

ACTA BIOLOGICA SZEGEDIENSIS

VOLUME 48(1-4), 2004

Table of Contents

Articles

Dissertation Summaries

On the cover: Immunohistochemical localization of Aβ in hippocampal area CA1 (Kasa et. al).

Volume 48(1-4):1-6, 2004
Acta Biologica Szegediensis
http://www.sci.u-szeged.hu/ABS

ARTICLE

Presynaptic axonal amyloid-β induces caspase-3 activation and neurodegeneration in the postsynaptic neuron

Peter Kasa[1]*, Henrietta Papp[1], Zsuzsanna Beke[1], David Vadasz[1], Janos Zombori[2]

[1]Alzheimer's Disease Research Centre, Department of Psychiatry, and University of Szeged, Szeged, Hungary, and [2]Department of Pathology, Elisabeth Hospital, Hodmezovasarhely, Hungary

ABSTRACT It is assumed that the amyloid-beta peptide (Aβ) contributes to the neurodegeneration in Alzheimer's disease (AD). Activation of an apoptotic pathway may play a key role in this process. The apoptotic signal may be driven by caspases. The presynaptic Aβ protein may be an activator of caspase-3 and could initiate a series of cascade events, which results in neurofibrillary degeneration in a postsynaptic cell. We report here that the axonic Aβ in the AD brain may be associated with caspase-3 activation. Our data suggest that caspase-3 in fact has a significant role in the widespread neuronal cell death that occurs in AD brain. A subset of pyramidal cells in hippocampus area CA1 demonstrated widespread accumulation of tau-protein. Individual postsynaptic neurons contained intracellular activated caspase-3 and were co-localized with neurofibrillary tangles. The results presented here support the suggestion that caspase-3 activation may lead to the neuronal cell death associated with AD. However, we are aware that, besides Aβ, other factors too may initiate a series of events which lead to the development of neurofibrillary tangles in the postsynaptic neurons.
Acta Biol Szeged 48(1-4):1-6 (2004)

KEY WORDS

Alzheimer's disease
amyloid-beta
apoptosis
caspase-3
neurofibrillary tangle

In Alzheimer's disease (AD), the most common type of dementia in advanced age, the loss of cortical and hippocampal neurons and synapses, is accompanied by the extracellular deposition of amyloid-beta peptide (Aβ) in senile plaques (SPs; Braak and Braak 1991). Paired helical filaments containing hyperphosphorylated tau-protein forms the neurofibrillary tangles (NFTs). The mechanism by which neurodegeneration occurs in AD is not yet understood (Bossy-Wetzel et al. 2004). Some investigators speculate that much of the cell loss may be due to apoptosis, a highly regulated form of programmed cell death (Cotman 1998). The caspases are therefore critical effectors of neuronal apoptosis and may be inappropriately activated in AD (Cowan et al. 2001; Cribbs et al. 2004; Johnson 1994). In particular, the analysis of caspase-3-deficient mice has revealed a decrease in apoptosis in the developing brain, suggesting that caspase-3 is necessary for the apoptosis of developing neurons. In AD brains, the protein level of caspase-3 is also increased (Rohm et al. 2001).

Some reports have indicated that Aβ (Estus et al. 1997) induces morphological and biochemical changes, with characteristic apoptosis of the neurons. Aβ deposits have also been shown to be associated with both the presence of dystrophic neurites and the neuronal loss found in severely affected brain regions in AD (Selkoe 2002).

These observations prompted us to investigate the possible involvement of caspase-3 in Aβ-induced apoptosis in autopsied human brain hippocampal samples. To study the relationship between presynaptic Aβ deposition and the activation of caspase-3 in the postsynaptic neuron, we investigated the structural relationships of these proteins in autopsied human brain hippocampal samples.

Accepted Oct 21, 2004
*Corresponding author. E-mail: kp@comser.szote.u-szeged.hu

Materials and Methods

The primary antibodies used in this study were rabbit anti-Aβ1-42 affinity-purified polyclonal antibody from Chemicon International Inc. (Temecula, CA, USA), caspase-3 active form (biotin-conjugated, polyclonal rabbit from BD Biosciences Pharmingen, San Diego, CA, USA) and monoclonal anti-τ(tau) antibody produced in mouse (Sigma-Aldrich, St. Louis, MO, USA). Normal goat serum, normal sheep serum and 3,3'-diaminobenzidine tetrahydrochloride (DAB) were from Sigma-Aldrich (St. Louis, MO, USA). Biotin-SP-AffiniPure-sheep anti-mouse IgG (H+L), peroxidase-streptavidin from Jackson (West Grove, PA, USA). Histoclear II and Histomount were from National Diagnostics (Atlanta, GA, USA). All chemicals used were of the highest grade available, from various suppliers.

Immunohistochemistry

Autopsied brain tissues from the hippocampus of 5 neuropathologically confirmed AD cases and 6 non-demented cases displaying no evidence of NFTs were studied. The age

at death was not significantly different for the AD (mean, 69 ± 7.2 years) and the controls (mean, 64 ± 6.8). The autopsied brain tissues used in this study were provided by the Department of Pathology, Elisabeth Hospital, Hodmezovasarhely, Hungary.

Coronal sections 30-μm in thickness were cut with a freezing microtome. Sections were soaked for 20 min in 3% H_2O_2, washed in phosphate-buffered saline (PBS; pH 7.4), treated with 0.1 M PBS containing 2.5% Triton X-100 for 20 min and then incubated with the normal blocking serum for 60 min. The sections were thereafter incubated with the primary antibody at 4°C overnight. The dilutions of the individual antibodies were as follows: Aβ: 1:2000, activated caspase-3: 1:800 and tau: 1:2000. After three 10-min washes in PBS, the brain slices were incubated with the secondary antibody. When single staining was applied for demonstration of the localization either of Aβ or of activated caspase-3, the peroxidase complex was visualized by incubating the sections with 0.05 M Tris-HCl (pH 7.5) containing 0.05% DAB, 0.1% $NiCl_2$ and 0.005% H_2O_2, resulting in a bluish-black colour. When double-stained sections were prepared (stained either for Aβ and tau or for activated caspase-3 and tau), the samples were developed first in DAB dissolved in 0.05 M Tris-HCl buffer. This staining resulted in a brownish colour. Thereafter, the sections were treated for 30 min with 0.6% H_2O_2 to eliminate the possibility persistent activity of the marker enzyme. After the staining for the second antibody, the peroxidase complex was visualized by incubating the sections in a DAB-$NiCl_2$ mixture. In these double-stained sections, a brownish colour could be detected in some cell bodies, intermingled with a bluish-black colour (Kasa et al. 2001). Controls were performed to rule out non-specific immunostaining by eliminating the primary or secondary antibody. The sections were next mounted, air-dried, dehydrated in an ethyl alcohol series, cleared in Histoclear, and finally coverslipped using Histomount. Photos were taken under normal light field microscopy conditions (Nikon Microphot-FXA microscope).

Results

To investigate the morphological localization of Aβ in hippocampus area CA1, an affinity-purified polyclonal antibody was used. The immunoreactivity was revealed not only in the SPs (Fig. 1A), but also in the axon varicosities (at the synaptic sites; Fig. 1B) and within the neuronal cell body (Fig. 1C). Some of the stained axon varicosities could be localized near the perikaryon and attached to the primary dendrite of a pyramidal cell (Fig. 1D).

When the samples were double-stained for Aβ and for tau, much to our surprise, a number of Aβ-stained axon varicosities were revealed on the surface of the tau-immunopositive neurons (Figs. 2A, B). It was interesting that the axon varicosities were not uniformly distributed over the dendrite, but were rather located consecutively, separated by distance of a few microns.

In the control hippocampal samples, very few activated-caspase-3-positive pyramidal cells were detected (Fig. 2C). Similarly, in the area dentate, stained neurons were rarely seen. The most interesting observation concerned the appearance of the staining. It appeared intermittently rather than evenly in the dendrites. In a Braak and Braak stage II AD sample, some tau were immunopositive for activated caspase-3 (Fig. 2E), while many more NFT-positive cells stained for caspase-3 (Fig. 2F) in a severe AD case (Braak and Braak stages V and VI).

To examine a possible relationship between caspase-3 activation and tau-positive neurons, double-labelling experiments were undertaken, using the caspase-3 active form and monoclonal anti-tau antibody as markers for NFT formation. As shown in Fig. 3A, only a subset of neurons was caspase-3-positive, and the number of cells was even lower for which tau could be clearly be seen in the same neuron. The co-localization of caspase-3 and tau was evident within individual neurons (Figs. 3A, B). Figure 3B illustrates a high-magnification image of typical caspase-3 and tau staining in the pyramidal neuron in hippocampus area CA1. Interestingly, the appearance of neurons labelled with caspase-3 was similar to that of those with tau. Other stained samples provided further evidence that not all caspase-3-positive neurons contain tau pathology (Figs. 3C, D). Taken together, these results suggest that caspase-3 activation may occur in only a subset of the tau-bearing neurons. This suggestion is supported in Figs. 3E, F, where many more labelled neurons are present than in Fig. 3D.

Discussion

In this report, we have demonstrated that Aβ is not only present in the SPs and neuronal perikarya, but may also be localized in the axons (Chen et al. 2004). There is experimental evidence suggests that Aβ accumulation in the cells may precede tau formation in the AD brain, and can potentiate the development of NFTs in transgenic mice. Furthermore, Aβ-induced neurodegeneration requires tau expression and the intracellular assembly of pathological tau filaments (Rissman et al. 2004). The appearance of intracellular Aβ is also observed in Down syndrome patients with AD, indicating that intraneuronal Aβ may be a common feature of AD subtypes.

The activation of caspase-3 (Stadelmann et al. 1999; Su et al. 2001) in the postsynaptic dendrite by presynaptic Aβ again precedes the appearance of tau positivity in the pyramidal cells of hippocampus area CA1 in human brain samples. By using antibodies specific for the active form of caspase-3, tau and Aβ, we could underline such a sequence of events. It is suggested that the various caspases (among them caspase-3) are activated only during apoptosis (Rohn et al. 2001; Sal-

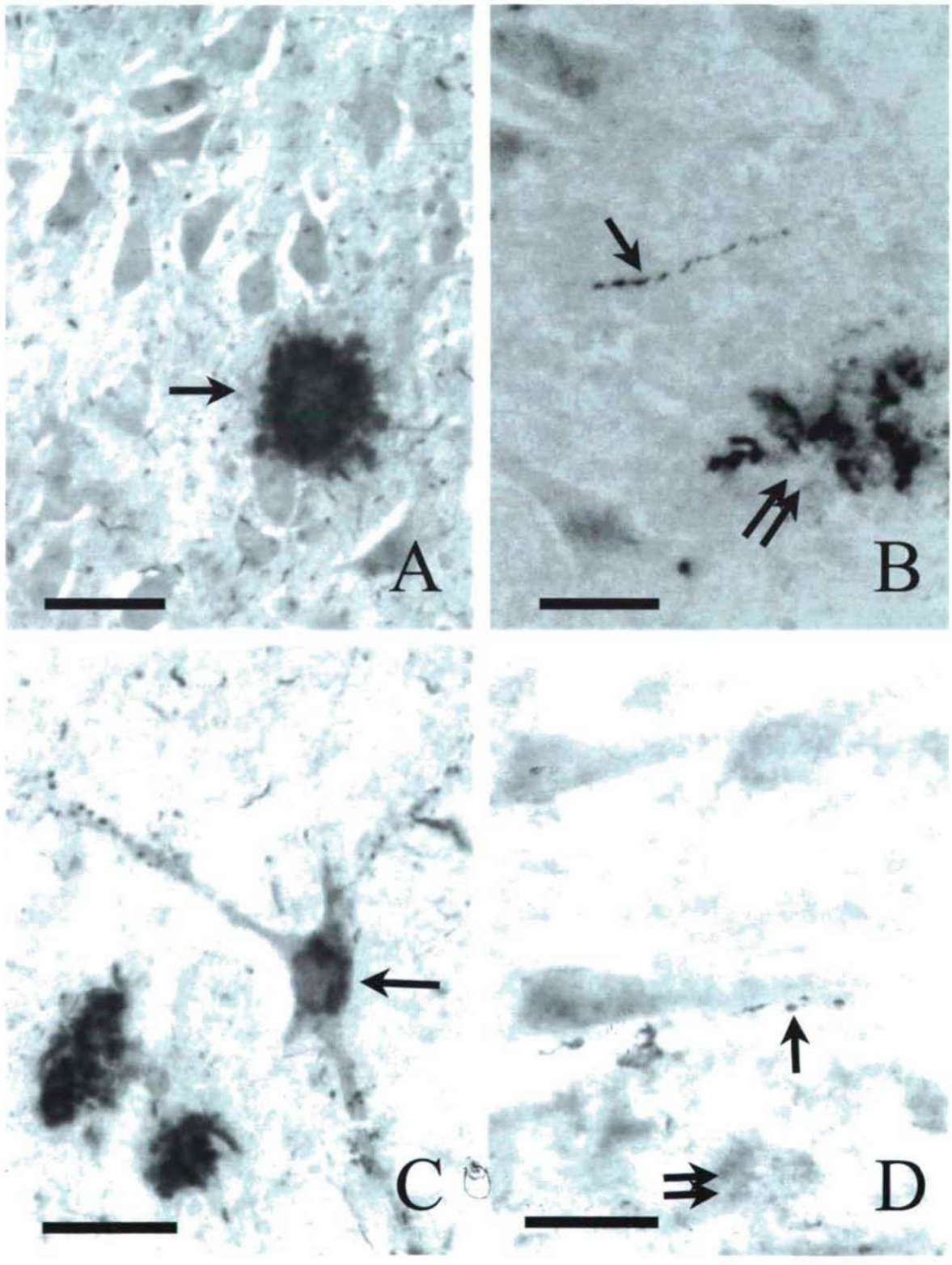

Figure 1. Immunohistochemical localization of Aβ in hippocampal area CA1. Specific Aβ staining appears in the SPs (A, arrow), in the axon varicosities (B, arrow) and in the SPs (B, double arrows). In C, specific Aβ immunoreactivity is present in the perikarya of a neuron (arrow). Some other neurons are covered with Aβ-positive axon varicosities (arrow), while diffuse staining (double-arrow) is to be seen among the neuropil. Scale bar: 50 μm

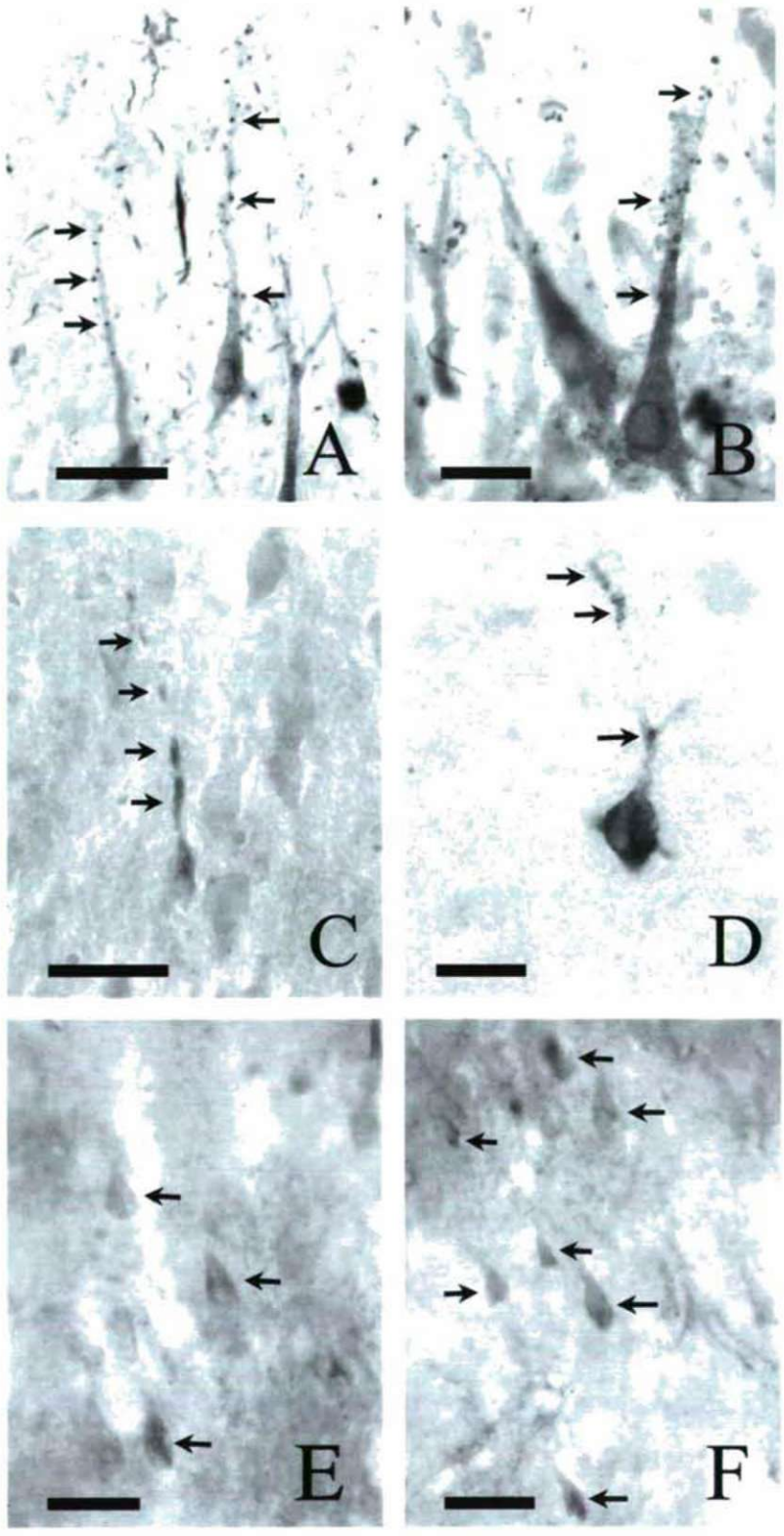

Figure 2. Double-labelling immunohistochemical analysis for Aβ and tau. In A and B, the brownish staining within the neurons indicates the presence of tau, while the black dots (A and B, arrows) on the surface of the pyramidal cells illustrate the Aβ-positive axon varicosities. Figure 2C,D reveal the activated caspase-3 in the dendrites and the cell body in a control sample. The staining pattern appears intermittently in the dendrites (arrows). In contrast, in Braak and Braak stages II (E, arrows) and VI (F, arrows), the caspase-3 appears in the cell bodies. Scale bar = 50 μm

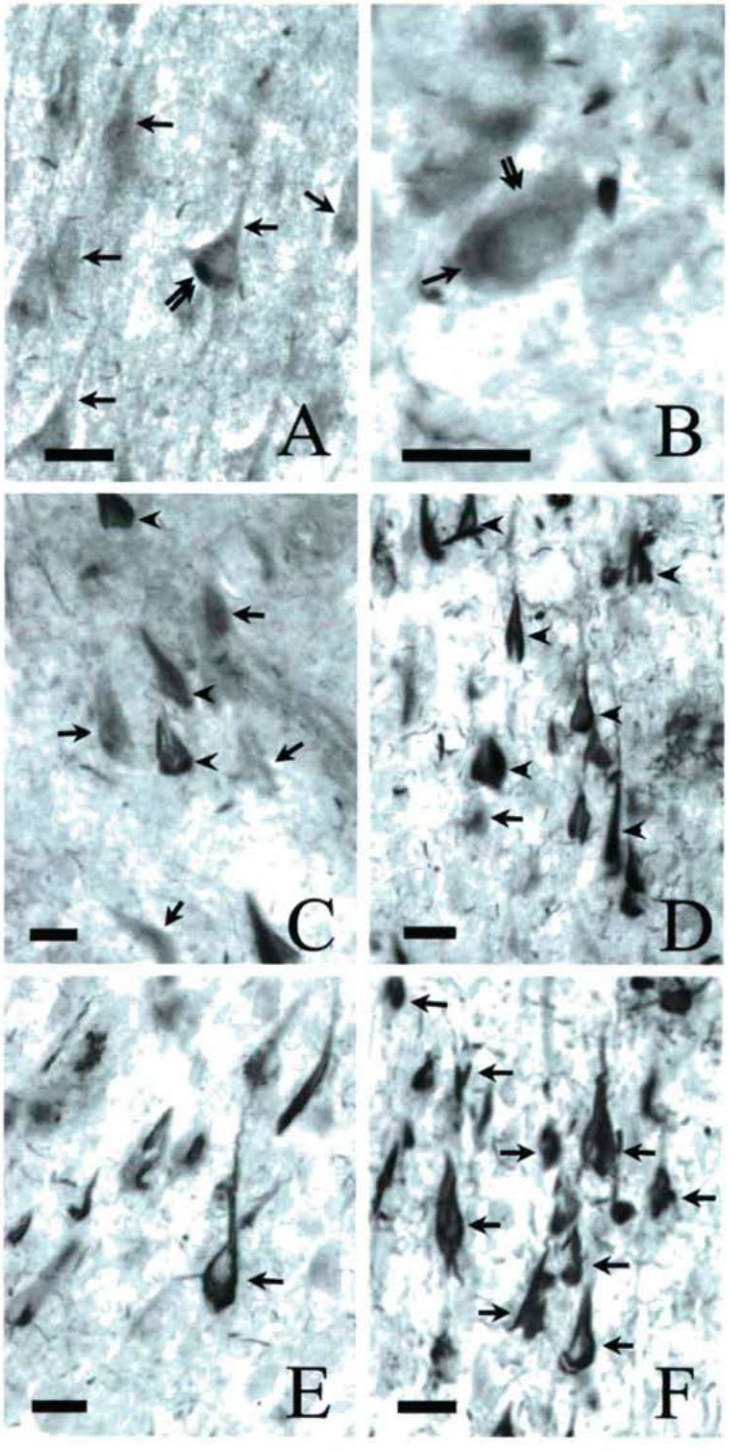

Figure 3. Activated caspase-3 labelling of tau-bearing hippocampal neurons in control samples. A: Double-labelling immunohistochemical analysis for caspase-3 (arrows) and tau (double-arrows) illustrates that only a subset of neurons are caspase-3-positive (bluish-black) and can be clearly differentiated from tau-containing neurons (brownish, double-arrows). B: Co-localization of caspase-3 (arrow) and tau (double-arrow) within a neuron. C and D: Double-immunostaining of a hippocampal tissue section from an early stage of AD (C) and a severe AD case, showing the distribution of caspase-3-positive and tau-stained neurons. In C, the caspase-3-positive neurons (arrows) seem to precede the appearance of tau-positive (arrowheads) cells. The number of tau-positive neurons (arrowheads) increases with disease severity (D), where only a few (arrow) caspase-3-positive neurons can be revealed. A similar distribution of tau-positive neurons can be demonstrated with the specific antibody for tau. In A, the number of stained neurons is lower than in the severe case of AD (F). Scale bar: 25 μm

znick et al. 1999; Slee et al. 1999); we therefore believe that in our samples some of the neurons die by apoptosis. Accordingly, our results suggest that caspase-3 activation may begin at the synapse and, after a trans-synaptic signal it propagates in the dendrite in a retrograde fashion to the neuronal cell bodies. The Aβ signal therefore induces a sequence of processes which, among others, ultimately result in caspase-3 activation, tau hyperphosphorylation, apoptosis, neurofibrillary degeneration and finally cell death. We are aware, however, that, even though we have demonstrated that activated caspase-3 and tau formation are present within the same neurons, this does not imply that they must be causally interrelated events. Indeed, we were able to detect only one subset of neurons in which caspase-3 and tau were co-localized. In another subset of nerve cells, either only caspase-3 or only tau was detected. Nevertheless this does not rule out the possibility of a causal relationship between the two processes.

It is interesting to note that, in the control brain, only scattered cells exhibited caspase-3 positivity, while in the earlier stages of AD stage I and II (Braak and Braak 1991) more activated caspase-3 neurons are present than tau-positive nerve cells. In contrast, in the advanced stages of AD stage V and VI (Braak and Braak 1991), more tau-positive structures appear than activated caspase-3 nerve cells.

In conclusion, our data support the suggestion that the presynaptic axonal Aβ may be an initiator of the death of the postsynaptic neuron. This suggestion is supported by the appearance of caspase-3 positivity in those neurons that are in close contact with Aβ-positive axon varicosities. The precise mechanisms underlying the Aβ-induced neuronal degeneration await further elucidation.

Acknowledgments

This work was supported by ETT (Hungary) Grant No 135 04/2003.

References

Bossy-Wetzel E, Schwarzenbacher R, Lipton SA (2004) Molecular pathways to neurodegeneration. Nat Med 10:S2-S9.

Braak H, Braak E (1991) Neuropathological stageing of Alzheimer-related changes. Acta Neuropathol (Berl) 82:239-259.

Chen XH, Siman R, Iwata A, Meaney DF, Trojanowski JQ, Smith DH (2004) Long-term accumulation of amyloid-β, β-secretase, presenilin-1, and caspase-3 in damaged axons following brain trauma. Am J Pathol 165:357-371.

Cotman CW (1998) Apoptosis decision cascades and neuronal degeneration in Alzheimer's disease. Neurobiol Aging 19:S29-32.

Cowan CM, Thai J, Krajewski S, Reed JC, Nicholson DW, Kaufmann SH, Roskams AJ (2001) Caspases 3 and 9 send a pro-apoptotic signal from synapse to cell body in olfactory receptor neurons. J Neurosci 21:7099-7109.

Cribbs DH, Poon WW, Rissman RA, Blurton-Jones M (2004) Caspase-mediated degeneration in Alzheimer's disease. Am J Pathol 165:353-355.

Dickson DW (2004) Apoptotic mechanisms in Alzheimer neurofibrillary degeneration: cause or effect? J Clin Invest 114:23-27.

Estus S, Tucker HM, van Rooyen C, Wright S, Brigham EF, Wogulis M, Rydel RE (1997) Aggregated amyloid-beta protein induces cortical neuronal apoptosis and concomitant "apoptotic" pattern of gene induction. J Neurosci 17:7736-7745.

Gervais FG, Xu D, Robertson GS, Vaillancourt JP, Zhu Y, Huang J, LeBlanc A, Smith D, Rigby M, Shearman MS, Clarke EE, Zheng H, Van Der Ploeg LH, Ruffolo SC, Thornberry NA, Xanthoudakis S, Zamboni RJ, Roy S, Nicholson DW (1999) Involvement of caspases in proteolytic cleavage of Alzheimer's amyloid-β precursor protein and amyloidogenic Aβ peptide formation. Cell 97:395-406.

Johnson EM Jr (1994) Possible role of neuronal apoptosis in Alzheimer's disease. Neurobiol Aging 15 Suppl 2:S187-189.

Kasa P, Papp H, Pakaski M (2001) Presenilin-1 and its N-terminal and C-terminal fragments are transported in the sciatic nerve of rat. Brain Res 909:159-169.

Rissman RA, Poon WW, Blurton-Jones M, Oddo S, Torp R, Vitek MP, LaFerla FM, Rohn TT, Cotman CW (2004) Caspase-cleavage of tau is an early event in Alzheimer disease tangle pathology. J Clin Invest 114:121-130.

Rohn TT, Head E, Su JH, Anderson AJ, Bahr BA, Cotman CW, Cribbs DH (2001) Correlation between caspase activation and neurofibrillary tangle formation in Alzheimer's disease. Am J Pathol 158:189-198.

Selkoe DJ (2002) Alzheimer's disease is a synaptic failure. Science 298:789-791.

Selznick LA, Holtzman DM, Han BH, Gokden M, Srinivasan AN, Johnson EM Jr, Roth KA (1999) In situ immunodetection of neuronal caspase-3 activation in Alzheimer disease. J Neuropathol Exp Neurol 58:1020-1026.

Slee EA, Adrain C, Martin SJ (1999) Serial killers: ordering caspase activation events in apoptosis. Cell Death Differ 6:1067-1074.

Stadelmann C, Deckwerth TL, Srinivasan A, Bancher C, Bruck W, Jellinger K, Lassmann H (1999) Activation of caspase-3 in single neurons and autophagic granules of granulovacuolar degeneration in Alzheimer's disease. Evidence for apoptotic cell death. Am J Pathol 155:1459-1466.

Su JH, Zhao M, Anderson AJ, Srinivasan A, Cotman CW (2001) Activated caspase-3 expression in Alzheimer's and aged control brain: correlation with Alzheimer pathology. Brain Res 898:350-357.

Volume 48(1-4):7-12, 2004
Acta Biologica Szegediensis
http://www.sci.u-szeged.hu/ABS

ARTICLE

Differences in distribution of the 210 kDa neurofilament subunit and the S-100 protein in the small intestine of a human fetus with trisomy 21 and in that of a normal fetus of the same age

Mária Bagyánszki[1], Mónika Krecsmarik[1], Béla E. Resch[2], Béla Á. Resch[3], János Szabó[4], Éva Fekete[1]*

[1]Department of Zoology and Cell Biology, University of Szeged, Szeged, Hungary, [2]Department of Pharmacodynamics and Biopharmacy, University of Szeged, Szeged, Hungary, [3]Department of Obstetrics and Gynecology, University of Szeged, Szeged, Hungary, [4]Department of Medical Genetics, University of Szeged, Szeged, Hungary

ABSTRACT The enteric nervous system of the small intestine of a 22-week-old male fetus with trisomy 21 was examined and compared with gut specimens from a fetus with normal karyotype at the same developmental stage. After the therapeutic termination of the pregnancies, paraffin sections and whole-mounts were prepared, which were processed for histology and immunohistochemistry, with the use of antibodies against the 210 kDA neurofilament subunit and the glial marker S-100 protein. The reduced length of the small intestine, the histologically observed fewer and shorter villi and the frequently appearing pseudostratified epithelium indicate an overall delay in the intestinal development in the trisomic fetus. Both the S-100 protein-immunopositive glial cells and the neurofilament protein-immunopositive nerve cells were distributed differentially in the gut specimens of the trisomic fetus and in the fetus with normal karyotype. While the immunohistochemical expression of the S-100 protein differed only in the circular axis of the gut wall, the distribution of the neurofilament protein-immunoreactive nerve cells also differed along the longitudinal axis of the gastrointestinal tract. Not only the distribution, but also the morphology of the neurofilament protein-immunoreactive myenteric ganglion cells differed in the trisomic fetus as compared with the normal one. The neurofilament protein-immunopositive ganglion cells of the normal fetus possessed lamellar dendrites and one long axon, while the ganglion cells of the trisomic fetus did not exhibit special morphological characteristics. These observations suggest that the enteric nervous system of the fetus with trisomy 21 is involved in the overall delay of the gut development.
Acta Biol Szeged 48(1-4):7-12 (2004)

KEY WORDS

fetal intestine
trisomy 21
neurofilament
S-100 protein

Trisomy 21 is the most common autosomal aneuploidy compatible with postnatal survival. It occurs in an average of 1 in 700 live births (Hassold et al. 1996). The presence of trisomy 21 is regarded as a significant risk factor for Hirschsprung disease (HSCR) and for a spectrum of defects in gastrointestinal motility (Epstein et al. 1991; Holschneider et al. 1994; Cohen 1999). In consequence of the wide and variable set of clinical features in a given individual, trisomy 21 is viewed as a predisposing factor, rather than as a causative factor for these diseases (Quinn et al. 1994). The gene catalog of chromosome 21 contains at least 10 kinases, 5 cell adhesion molecules and a number of transcription factors (Hattori et al. 2000). It is possible that an extra copy of these genes results in an overall delay in intestinal development as a primary disorder, and the delayed maturation of the gastrointestinal tract may then predispose or contribute to the development of disorders such as HSCR, intestinal obstruction or enterocolitis in infants with trisomy 21.

Murine trisomy 16 is accompanied by a complex genetic insult similar to that in human beings with segmental trisomy 21 (Pletcher et al. 2001). Investigations of mice with trisomy 16 have demonstrated a delayed development in the enteric nervous system (ENS) of the stomach and in the intestine (Li et al. 2000). We report here on a comparative study of a 22-week-old male fetus with prenatally diagnosed trisomy 21 and a normal fetus at the same developmental stage. Histological features typical of a younger fetal age were revealed in the fetus with trisomy 21, suggesting an overall delay in the development of the intestine. To establish whether or not the ENS was involved in the delayed development, we applied immunohistochemistry, using primary antibodies against a neurofilament (NF) subunit protein and against S-100 protein. Both antigens have been widely used to study the architecture of the ENS both in normal (Eaker 1997; Fekete et al. 1999) and in pathological (Yanagihara et al.

Accepted July 21, 2004
*Corresponding author. E-mail: efekete@bio.u-szeged.hu

1992; Deguchi et al. 1993) cases. It is well documented that cytoskeletal proteins such as NF proteins are developmentally regulated (Faussone-Pellegrini et al. 1999) and are suitable for the morphological characterization of neuronal subgroups (Román et al. 2001; Brehmer et al. 2002). These literature data indicate that NF proteins are potential markers for the study of neuronal disorders or developmental disturbances affecting morphologically distinct neuronal subgroups.

The glial marker S-100 protein furnishes information on the distribution of glial cells, which create the local microenvironment necessary for neuronal development (Bush et al. 1998; Giaroni et al. 1998; Fekete et al. 1999). The differences in the distribution and morphological appearance of the NF and S-100 protein-immunoreactive cells observed in this comparative study indicate an intestinal segment-dependent impairment in the development of the myenteric ganglion cells and the enteric glia in the ENS of the fetus with trisomy 21. To the best of our knowledge, this is the first reported case on a fetus with trisomy 21 with a developmental disorder of the ENS.

Materials and Methods

Human samples and tissue handling

The human study was approved in advance by the University Medical Ethical Committee and was performed in accordance with the ethical standards laid down in the 1964 Declaration of Helsinki. For tissue preparation, the small intestines of the fetuses with trisomy 21 or with normal karyotype were obtained immediately following therapeutic abortion performed by the laminaria plus Nalador technique after the intrauterine death of the fetuses. The crown-rump lengths of the fetuses involved in this study were 209 and 212 mm respectively, corresponding to gestational week 22.

The lengths of the unfixed small intestine along the unstretched antimesenteric border from the pylorus to the ileocecal valve were 81 and 95 cm respectively. Selected segments of the small intestine were ligated and distended, using a modified Zamboni fixative (Scheuermann et al. 1987) and fixed overnight at 4°C. The proximal, middle and distal segments were selected at 1 and 40 cm distal to the pylorus and 3 cm oral to the ileocecal junction, respectively.

Small pieces were processed for paraffin sectioning, while larger pieces were used for whole-mount preparations. Paraffin sections were stained with mucicarmine for histological observation, while unstained paraffin sections were incubated together with whole-mounts for immunostaining, using the avidin-biotin technique (Fekete et al. 1999). Anti-S-100 protein (Dakopatts Z 311, final dilution 1:400) and anti-NF 210 kDA subunit (SIGMA clone 52 mo, final dilution 1:200) were used as primary antibodies. Specimens were mounted in PBS-buffered glycerol and viewed in a Leica DMLB light microscope equipped with a Polaroid digital camera.

Results

The small intestine of the 22-week-old human fetus with karyotype 47, XY+21 (Fig. 1) was 15% shorter than the small intestine of the fetus with normal karyotype at the same developmental stage. Histologically, fewer and shorter villi were observed and pseudostratified epithelium was frequently seen on the villous and intervillous epithelium (Fig. 2).

The S-100 protein immunostaining revealed dense glial staining both in the myenteric plexus (MP) and in the submucous plexus (SP; Fig. 3A,B) throughout the whole length of the intestine. However, the S-100 protein staining was always restricted to the outer SP in the fetus with trisomy 21 (Fig. 3B). The number and distribution of the S-100 protein-immunoreactive cells differed greatly in the MP of the small intestines in the two different fetuses under investigation (Fig. 4A,B). The MP in the fetus with normal karyotype was well developed, with large, distinct ganglia (Fig. 4A). The numerous S-100 protein-immunoreactive cells were mostly located in the center of the ganglia (Fig. 4A). In the fetus with trisomy 21, the myenteric ganglia were not distinct (Fig. 4B), and the few, but intensely stained glial cells were spread throughout the MP (Fig. 4B).

The specimens from the normal fetuses exhibited intense NF immunoreactivity in both the MP and the SP throughout the whole length of the small intestine (Fig. 5A), whereas in those from the fetus with trisomy 21, the immunostaining was restricted to the MP (Fig. 5B). When the distributions of the NF-immunoreactive myenteric ganglion cells were compared along the longitudinal axis of the small intestine, a uniform distribution was revealed in the normal, and a segment-specific different distribution in the trisomic fetal intestine (Fig. 6A-D). The most proximal segments of both intestines were characterized by intense NF immunoreactivity (Fig. 6A,B). However, a semiquantitative assessment demonstrated approximately 50% more NF-immunoreactive ganglion cells in this intestinal segment of the normal fetus. The ganglion cells were not only more numerous here, but also displayed a characteristic neuronal morphology (Fig. 6A), with several lamellar dendrites and one axon.

In contrast the NF-immunoreactive ganglion cells in the fetus with trisomy 21 did not exhibit any specialized morphological character: they had only single axons differentiated. Unstained ganglion cells were seen throughout the whole length of the small intestine (Fig. 6C) both in the normal and the trisomic fetus.

Discussion

The length of the small intestine of the fetus with trisomy 21 was 81 cm, which corresponds to an 18-week-old (Weaver et al. 1991) rather than a 22-week-old fetal intestine, for which a length of 95 cm was measured. The histological features in the fetus with trisomy 21 were also characteristic of a younger

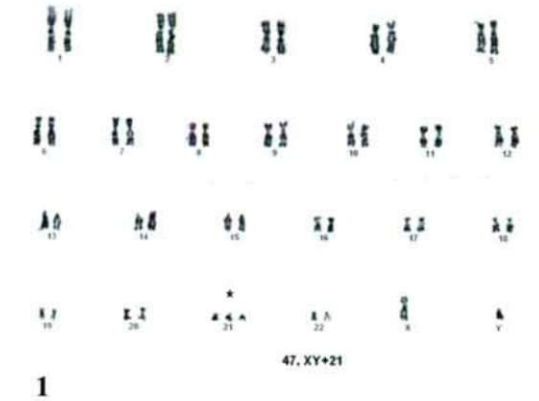

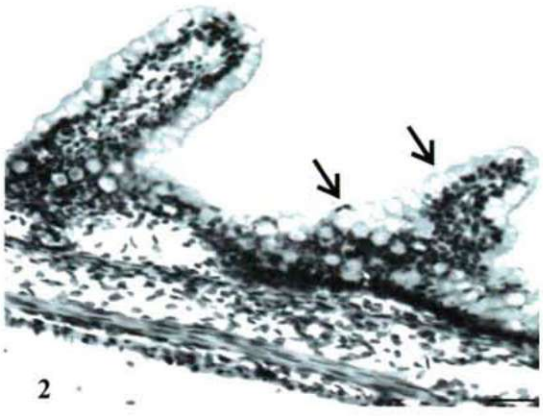

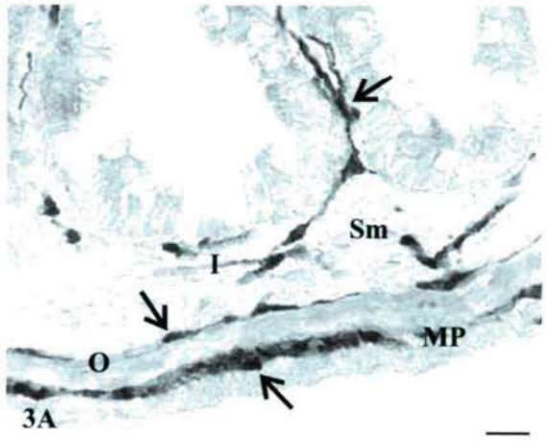

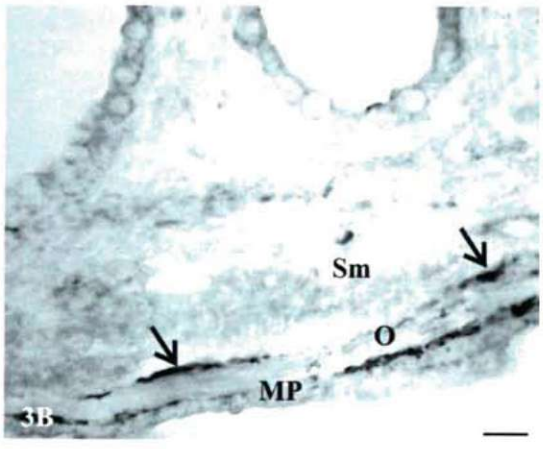

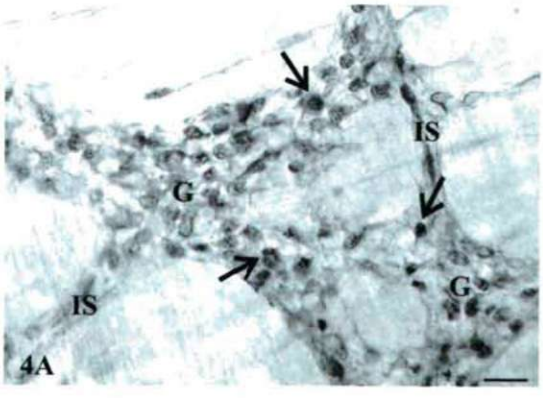

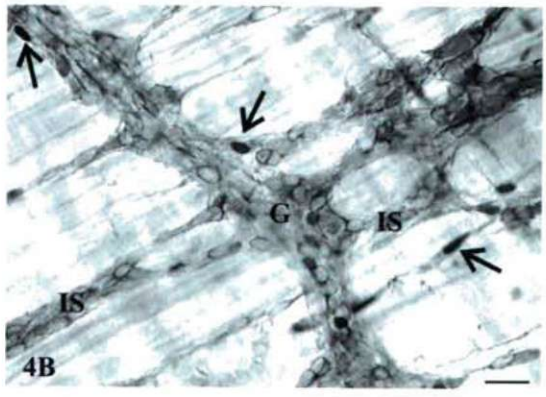

Figure 1. Karyotype of the 22-week-old fetus with trisomy 21 investigated in the present report. Trisomy 21 is indicated by an asterisk.
Figure 2. Mucicarmine-stained paraffin section of the small intestine of the 22-week-old fetus with trisomy 21. Arrows indicate stratified epithelium. Scale bar: 50 μm
Figure 3. Cross-sections of the paraffin-embedded small intestines of the 22-week-old human fetuses processed for S-100 protein immunocytochemistry. Stained glial cells (arrows) are seen in both the myenteric plexus (MP) and in the inner (I) and outer (O) submucous plexus of the normal human fetus (A). In the trisomic fetus (B), immunoreactive cells (arrows) appeared in the myenteric plexus (MP) and in the outer submucous plexus (O). Sm: the submucous layer of the intestinal wall. Scale bars: 40 μm
Figure 4. Whole-mount preparations of the myenteric plexuses from the small intestines of the 22-week-old human fetuses processed for S-100 protein immunocytochemistry. Most of the S-100 protein-immunoreactive glial cells (arrows) accumulate in the center of the large myenteric ganglia (G). Stained cells are not seen in the internodal segments (IS) of the myenteric plexus in the normal fetus (A). Stained glial cells (arrows) in the myenteric plexus of the trisomic fetus (B) are located on the periphery of the ganglia (G), which are not clearly distinct from the internodal segments (IS). Scale bars: 15 μm

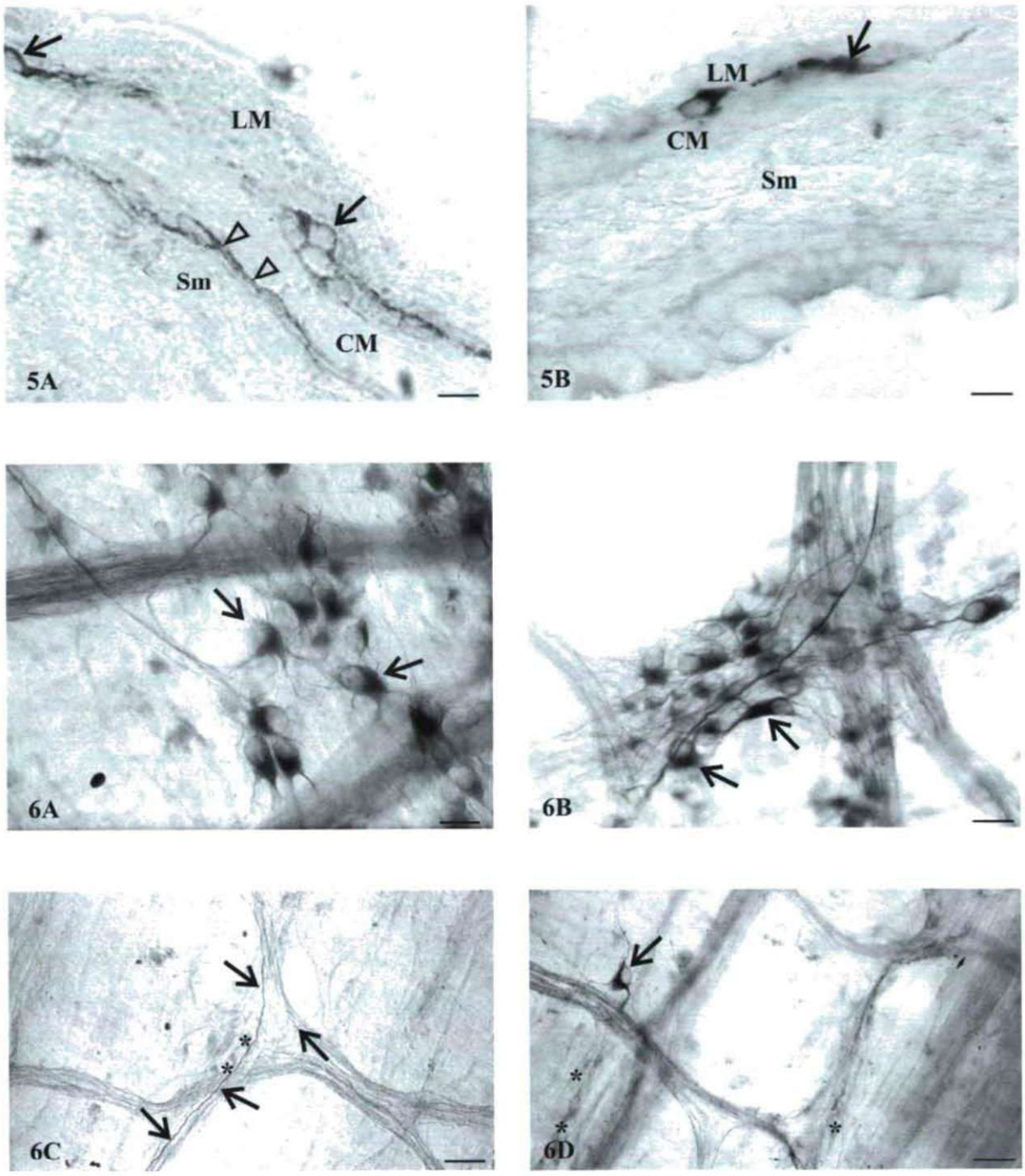

Figure 5. Cross-sections of the paraffin-embedded small intestines of the 22-week-old human fetuses stained with an antibody against the 210 kDA neurofilament subunit protein. Stained ganglion cells and fibers are seen in both the myenteric plexus (arrows) and in the submucous plexus (arrowheads) of the normal human fetus (A). In the trisomic fetus (B), intensely stained ganglion cells and fibers (arrows) were restricted to the myenteric plexus. LM: longitudinal muscle, CM: circular muscle, Sm: submucous layer of the intestinal wall Scale bars: 20 μm

Figure 6. Whole-mount preparations of the myenteric plexuses from the small intestines of the 22-week-old human fetuses stained with an antibody against the 210 kDA neurofilament subunit protein. Numerous stained ganglion cells in the most proximal segment of the small intestine of the normal fetus (A) exhibit a characteristic neuronal morphology, with lamellar dendrites and one axon. Several stained ganglion cells (arrows) are seen in the most proximal segments of the small intestine of the trisomic fetus (B); these ganglion cells did not indicate a definite morphological type. No immunoreactive neurons are seen in the middle segment of the small intestine of the trisomic fetus (C). Asterisks indicate unstained ganglion cells. Several stained cells (arrow) and fibers are seen in the most distal segment of the small intestine of the trisomic fetus. Asterisks indicate unstained ganglion cells. Scale bars represent 10 μm in A and B, 15 μm in C and D.

fetal age (Klein 1989), indicating a severe growth impairment and an overall delay in the development of the gastrointestinal system. To determine whether or not the ENS was involved in the developmental impairment revealed in the small intestine of the fetus with trisomy 21, we looked for cytoskeletal markers that indicate the degree of differentiation attained by the glial and neuronal cells by week 22 of gestation. Cytoskeletal proteins gradually accumulate in the cells in parallel with the organization of the cytoskeletal structures which mediate the important neural events, including the growth of the nerve processes and the initiation of axonal transport (Lasek et al. 1983). Immature cells in the mouse (Faussone-Pellegrini 1999) and in the human (Eaker et al. 1993) intestine express α-internexin and peripherin, while the expression of different NF subunits is related to neuronal differentiation (Bishop et al. 1985; Eaker et al. 1990). Accordingly, α–internexin may be considered a good marker for neuronal immaturity, while NF subunit proteins may be good markers for neuronal maturity. We chose the NF 210 kDA subunit protein in the present comparative study. Although, NF immunostaining demonstrates only a minority of the total enteric neuronal population (Brehmer et al. 2002), the suitability of NF immunohistochemistry for the study of morphologically defined neuron types (Román et al. 2001; Brehmer et al. 2002) makes it an appropriate tool with which to distinguish between neurons via the level of morphological maturity and hence to confirm delayed neuronal differentiation.

Our previous results (Fekete et al. 1995) led us to utilize S-100 protein immunoreactivity as a glial marker in the small intestine of the trisomic fetus and in the fetus with normal karyotype. Differences in immunohistochemical expression were revealed in both the glial marker S-100 protein and the neuronal marker NF 210kDA subunit. As concerns the circular axis of the intestine, the S-100 protein-immunoreactive glial cells were restricted to the outer SP located near the circular layer of the external muscle (Timmermans et al. 2001), whereas in the intestine of the normal fetus the S-100 protein-immunoreactive cells were widely distributed throughout the whole thickness of the submucous layer.

The NF-immunoreactive nerve cells displayed a different distribution not only in the circular axis, but also along the longitudinal axis of the small intestine. The segment-specific differences in NF subunit staining may be consequences of the close temporal and spatial interrelationship between the gut growth and neural maturation. It is well established (Bagyánszki et al. 2002) that the histodifferentiation of the human gut proceeds in an oro-anal wave that is met by an anal-oro wave, which results in a developmentally advanced environment in the foregut and in the hindgut relative to that encountered in the midgut. In the present case, in which the presence of 21 trisomy resulted in an overall growth impairment, the level of development of the middle segment was much behind that of the normal intestine, none of the ganglion cells in this part of the intestine exhibiting NF immunoreactivity. The immunohistochemical expression of NF did not reveal a difference only in the distribution of the NF-immunoreactive neurons: the stained cells in the trisomic and in the normal fetal intestine also differed in their morphology. Numerous immunoreactive ganglion cells in the most proximal segment of the small intestine of the normal fetus demonstrated the morphology of the typical type I neurons in the Stach classification (Stach 1989); in contrast, the ganglion cells in the trisomic fetus did not reach this level of morphological differentiation, and also failed to express immunoreactivity against neuronal markers such as NF protein.

These observations indicate that not only the intestinal wall, but also the ENS is involved in the overall delay of the development of the gastrointestinal tract in the fetus with trisomy 21. The delayed development of the ENS may lead to symptoms of HSCR, intestinal obstruction or enterocolitis in infants with trisomy 21.

References

Bagyánszki M, Kovács ÉG, Resch BÁ, Román V, Resch BE, Fekete É (2002) Computer-aided morphometric analysis of the developing concentric structure of the human fetal intestinal tube. Histol Histopathol 17:731-737.

Bichop AE, Carlei F, Lee V, Trojanovski J, Marangos PJ, Dahl D, Polak JM (1985) Combined immunostainig of neurofilaments, neuron specific enolase, GFAP and S-100. A possible mean for assessing the morphological and functional status of the enteric nervous system. Histochemistry 8: 293-297.

Brehmer A, Schrödl F, Neuhuber W (2002) Morphological phenotyping of enteric neurons using neurofilament immunohistochemistry renders chemical phenotyping more precise in porcine ileum. Histochem Cell Biol 117:257-263.

Bush TG, Savidge TC, Freeman TC, Cox HJ, Campbell EA, Mucke L, Johnson MH, Sofroniew MV (1998) Fulminant jejuno-ileitis following ablation of enteric glia in adult transgenic mice. Cell 93:189-201.

Deguchi E, Iwai N, Goto Y, Yanagihara J, Fushiki S (1993) An immunohistochemical study of neurofilament and microtubule-associated Tau protein in the enteric innervation in Hirschprung's disease. J Ped Surg 28:886-890.

Cohen WI (1999) Health care guidelines for individuals with Down syndrome: 1999 revision. Down Syndrome Q. 4:1-16.

Eaker EY, Shaw G, Sninsky CA (1990) Neurofilament immunoreactivity in myenteric neurons differs from that found in the central nervous system. Gastroenterology 99:1364-1371.

Eaker EZ, Sallustio JE, Harris JM, Shaw G (1993) Myenteric plexus neurons have developmentally acquired differences int he medium molecular weight subunit of neurofilament protein. Neuroscience 53:561-570.

Eaker EY (1997) Neurofilament and intermediate filament immunoreactivity in human intestinal myenteric neurons. Dig Dis Sci 42:1926-1932.

Epstein CJ (1991) Protocols to establish genotype-phenotype correlations in Down syndrome. Am J Hum Genet 49:207-235.

Faussone-Pellegrini M-S, Matini P, DeFelici M (1999) The cytoskeleton of the myenteric neurons during murine embryonic life. Anat Embriol 199:459-469.

Fekete É, Resch BÁ, Benedeczky I (1995) Histochemical and ultrastructural features of the developing enteric nervous system of the human fetal small intestine. Histol Histopathol 10:127-134.

Fekete É, Timmermans JP, Bogers JJ, Resch BA, Van Marck E, Scheuermann DW (1999) Different distribution of S-100 protein and glial fibrillary acidic protein (GFAP) immunoreactive cells and their relations with

nitrergic neurons in the human fetal small intestine. Histol Histopathol 14:785-790.

Giaroni C, De Ponti F, Cosentino M, Lecchini S, Frigo G (1999) Plasticity in the enteric nervous system. Gastroenterology 117:1438-58.

Hassold T, Merrill M, Adkins K, Freeman S (1995) Recombination and maternal age-dependent nondisjunction: Molecular studies of trisomy 16. Am J Hum Genet 57:867-874.

Hattori M (2000) The DNA sequence of human chromosome 21. The chromosome 21 mapping and sequencing consortium. Nature 405:311-319.

Holschneider AM, Meire-Ruge W, Ure BM (1994) Hirschsprung s disease and allied disorders. Eur J Pediatr Surg 4:260-266.

Klein RM (1989) Small intestinal cell proliferation during development. In: Lebenthal E, ed., Human gastrointestinal development. New York Raven Press, pp. 367-392.

Lasek RJ, Oblinger MM, Drake PF (1983) The molecular biology of neuronal geometry; the neurofilament genes influences axonal diameter. Cold Spring Harb Symp Quant Biol 48:431-444.

Li JC, Busch LC, Kuhnel W (2000) Immunohistochemical study on gastroenteric nervous system in trisomy 16 mice: an animal model of Down syndrome. World J Gastroenterol 6:793-799.

Pletcher MT, Wiltshire T, Cabin DE, Villanueva M, Reeves RH (2001) Use of comparative physical and sequence mapping to annotate mouse chromosome 16 and human chromosome 21. Genomics 74:45-54.

Quinn FMJ, Surana R, Puri P (1994) The influence of trisomy 21 on outcome in children with Hirschsprung s disease. J Pediatr Surg 29:781-783.

Román V, Krecsmarik M, Bagyánszki M, Fekete É (2001) Evaluation of the total number of myenteric neurons in the developing chicken gut using cuprolinic blue histochemical staining and neurofilament immunocytochemistry. Histochem Cell Biol 116:241-246.

Scheuermann DW, Stach W, Timmermans JP (1987) Topography, architecture and structure of the plexus submucosus internus (Meissner) of the porcin small intestine. Acta Anat 129:96-104.

Stach W (1989) A revised morphological classification of neurons in the enteric nervous system. In: Nerves and the gastrointestinal tract. Singer MV and Goebell H (eds). Kluwer Academic Publishers. Lancester p. 29.

Timmermans J-P, Hens J, Adriaensen D (2001) Outer submucous plexus: An intrinsic nerve network involved in both secretory and motility processes in the intestine of large mammals and humans. Anat Rec 262:71-78.

Yanagihara J, Shimotake T, Deguchi E, Iwai N (1992) Histological investigation of the myenteric plexus of the entire gut in an infant with hypogenesis of the intestine. Eur J Pediatr Surg 2:114-117.

Weaver LT, Austin S, Cole TJ (1991) Small intestinal length: a factor essential for gut adaptation. Gut 32:1321-1323.

Volume 48(1-4):13-17, 2004
Acta Biologica Szegediensis
http://www.sci.u-szeged.hu/ABS

ARTICLE

Ultralow-noise headstage and main amplifiers for extracellular spike recording

Dénes Budai*

Department of Biology, Juhász Gyula College, University of Szeged, Szeged, Hungary, and Kation Scientific Co., Minneapolis, MN, USA

ABSTRACT This methodological paper provides a detailed description of a novel ultralow-noise pre- and main-amplifier system designed for the extracellular recording of voltage spikes produced by neuronal action potentials. The main difficulties with extracellular recording are the unwanted electrical signals that lower the recording quality. They include destructive interferences by alternating electric or magnetic fields, in addition to thermal and other random noises resulting from the intrinsic properties of the substances from which the electrode and the electrical circuit are made. The preamplifier is placed in a specially built metal headstage probe. It is designed so that microelectrodes can be plugged directly into the probe, keeping the electrode and preamplifier in the closest possible proximity. Unique electrode holder adaptors at the same time make the probe for the electrode holder with the added benefit of extended electrical shielding. The main amplifier contains tuned circuit band pass filters optimized for metal and carbon fiber microelectrodes. Electromagnetic interference pickup is reduced by the enclosing tin-plated iron box and a built-in 50/60 Hz reject filter. In test experiments, an excellent signal-to-noise ratio and low-noise baseline recording were achieved. When carbon fiber microelectrodes were applied in the medulla of anesthetized rats, the total peak-to-peak noise level of the system was about 25 μV, *i.e.*, about 6 μV RMS, which is only a few μV higher than the theoretical random noise. It is concluded that, in combination with carbon fiber electrodes, the present amplifiers do not contribute significantly to the overall noise.
Acta Biol Szeged 48(1-4):13-17 (2004)

KEY WORDS

electromagnetic interference
random noise
grounding and shielding
band pass filtering
carbon fiber microelectrode
single-unit recording

Voltages generated by electric currents flowing in the tissue around the neurons during action potentials can be detected by means of microelectrodes as extracellular "spikes". Spike potentials recorded from the mammalian central nervous system have a duration of between 0.2 and 20 ms. The amplitudes of extracellular spikes are typically about 100 μV, although they may vary from the noise level (*vide infra*) of the electrode up to several mV, depending on the type of neuron and the quality of the recording system. The greatest advantage of extracellular recording is that the activity of neurons can be recorded without having to impale and consequently damage them. When multi-barreled microelectrode assemblies are used, extracellular recordings can easily be combined with microiontophoretic drug testing (Budai and Molnar 2001). For this and other reasons, most *in vivo* neuronal spike detection is carried out with extracellular recording. Signals picked up by an extracellular electrode are in the μV range and need to be amplified if they are to be processed in more conventional electronic devices such as oscilloscopes, analyzers or computers. The usual degree of amplitude amplification in extracellular amplifiers is around 10,000. The electrode must be connected to a specialized preamplifier (also known as a headstage) in order to work properly. The electrical properties of the headstage and main amplifiers set a limit to the smallness of signals that can be reliably measured.

The main difficulties with extracellular recording are the unwanted electrical signals or "noise" as it is popularly called. Noise in the present sense refers to unpredictable spontaneous voltage fluctuations, which appear as a thickening of the baseline when viewed on an oscilloscope at low sweep speed. An important distinction should be made, however, between the *interferences* (hum) from the mains power supply and the *random noise* that stems from the intrinsic properties of the substances from which the electrode and the electrical circuit are made (Purves 1981). Alternating electric fields give rise to capacitive coupling between the power lines and the microelectrode input circuit, and this coupling is responsible for a considerable proportion of the interference problems because of the high impedance of the microelectrode. Interference from alternating magnetic fields is another pernicious problem that can obscure microelectrode recordings. Thirdly, ground (earth) loops occur when ground leads are connected in such a way that a loop or cyclic path for current exists. A ground loop can act as a tuned circuit to pick up line frequency magnetic

Accepted Nov 16, 2004
*E-mail: kations@aol.com

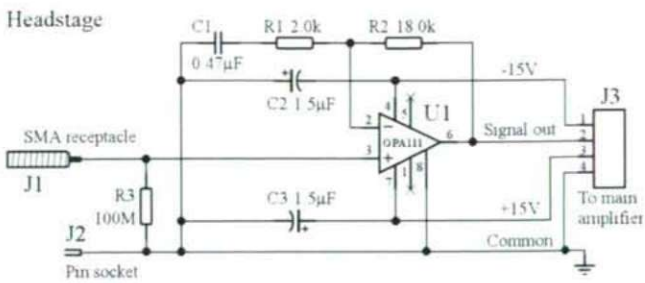

Figure 1. Schematic diagram of the headstage preamplifier. The low-noise, low bias current FET input operational amplifier (OPA111) is used as a non-inverting amplifier with a gain of 10.

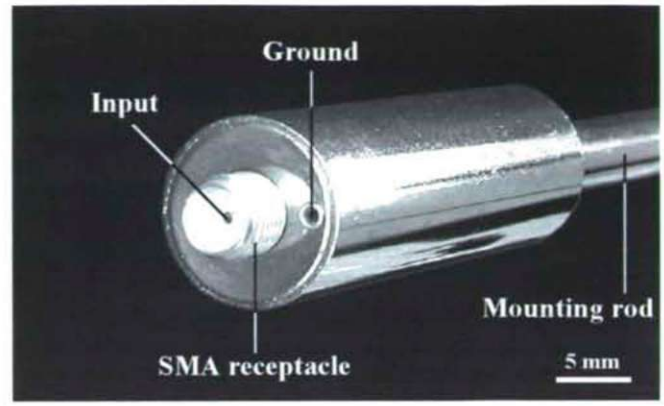

Figure 2. Physical layout of the headstage probe. The center receptacle of the SMA connector mates with the pin of the microelectrode, whereas its shell accommodates the electrode holder adaptors, as shown in Fig.3. The grounding pin is in galvanic contact with the metal parts of the headstage probe.

field radiation causing line hum interference. Transformers in line-powered equipment, microscope lamps and their associated wiring commonly cause both magnetic and electric field interference. Ground loops can form when a number of amplifiers are powered from a common direct current (DC) supply; they can be several meters in circumference if they go through ground leads to line-powered equipment.

There are four main sources of random noise in the input circuit for microelectrode recording: (1) the Johnson or thermal noise of the resistance of the microelectrode, (2) the voltage noise of the headstage preamplifier, (3) current noise of the preamplifier, and (4) "excess noise" in the microelectrode. The Johnson noise is due to the thermal motion of electrons, and sets a lower limit to the total noise. The voltage noise inherent in the preamplifier is the noise measured at the output when the input is grounded. The current noise comes from the miniature current that all operational amplifiers (op amps) have to draw in order to measure the voltage generated by the electrode. This current has a steady component (DC bias or leakage current), onto which random fluctuations are superimposed. The noise current flows through the parallel combination of electrode resistance and stray capacitance, producing a noise voltage. Microelectrodes display a noise component that is additional to their Johnson noise. This excess noise depends strongly on the voltage applied to the microelectrode, even though some excess noise is present in the absence of any applied voltage. The current noise is linearly dependent on the resistance of the electrode in contrast with the square root dependence exhibited by the Johnson noise. Both types of noise are band-limited by the low-pass filter consisting of the resistance of the electrode and the total input capacitance.

Not much can be done about the random noise, except to use electrodes with lower impedances at the frequencies necessary for spike recording. Careful selection of high-quality op amps and other parts is also of crucial importance in amplifier designs. The key specifications for the op amps are the bias current and voltage noise. Adherence to a few design rules, however, can greatly diminish the interferences resulting from alternating electric or magnetic fields and ground loops. Appropriate grounding and shielding in combination with a prudent physical layout of the experimental set-up eliminates the need for the fully enclosed Faraday cage of yesteryear. We described here a novel ultralow-noise headstage and main amplifier system for extracellular spike recording. This amplifier can be operated from batteries, totally independently from mains power. Its unique headstage probe design allows direct connection of the microelectrodes, further reducing destructive electromagnetic interferences and at the same time serves as an electrode holder.

Materials and Methods

Headstage amplifier

From an electronics viewpoint, our headstage or preamplifier is a classic non-inverting amplifier with gain (Horowitz and Winfield 1996; Fig. 1). In order to minimize interferences by alternating electromagnetic fields, microelectrodes can actually be plugged into the spark-plug type SMA receptacle of the headstage probe (J_1, Johnson Components, Part No. 142-0701-411), as shown in Figs 2 and 3. The miniature spring socket J_2 (AMP Inc., Part No. 50864) provides an input for the ground lead and mates with pin diameters ranging from 0.66 to 0.84 mm. The non-inverting input lead (pin 3) of the low-noise, low-bias current FET-input op amp, OPA111, is kept in mid-air and is directly soldered into the input pin of the SMA receptacle. The very short distance between the OPA111 and SMA connector and the PTFE (Teflon) insulation of the receptacle allows a leakage-free, low-noise connection between the microelectrode and the preamplifier. Resistors R_1 and R_2 should be of 1% tolerance or better and they provide a gain of 10, which is sufficient to bring the signal out of the amplifier noise region. The input shunt resistor R_3 should be used with

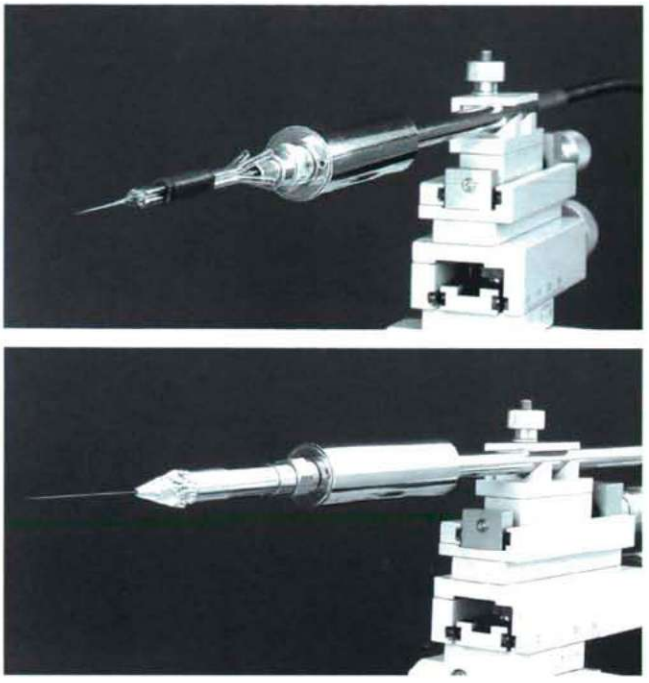

Figure 3. Use of the headstage probe in conjunction with multibarrel, carbon fiber-containing electrodes (upper panel) or with standard tungsten microelectrodes (lower panel). Note the adaptors for the two types of microelectrode. The metal electrode is held in place by copper foil with conductive adhesive, which also provides extended shielding for smooth recording.

tungsten or carbon fiber electrodes, but should be omitted for high-impedance electrodes. This resistor shunt removes DC and most low-frequency signals from the input (Millar 1992). Capacitor C_1 "rolls off" the gain to unity at low frequencies or DC to stop the amplifier saturating if DC potentials exist at the electrode (Millar and Barnett 1994). Small tantalum capacitors C_2 and C_3 bypass the ±15 V power supply leads to 0 V to prevent oscillation. The metal can of the OPA111 should be grounded (pin 8) for additional shielding of the front-end op amp.

The physical layout of the headstage probe is shown in Fig. 2 and 3. The entire circuitry is placed in a 14 mm x 50 mm (diameter x length) nickel-plated cylindrical brass container for added shielding from electromagnetic interference. Microelectrodes can be inserted directly into the center pin of the SMA connector fixed in the front-end of the probe (Fig. 2). The center pin is embedded in a PTFE insulator, whereas the grounding receptacle is in galvanic contact with the metal parts of the headstage probe. Two types of electrode holder adaptors (modified SMA plugs) can be screwed onto the SMA connector, making the headstage at the same time for an electrode holder. One is used to attach glass-insulated single or multibarrel carbon fiber electrodes (Armstrong-James and Millar 1979; Millar and Williams 1988; Budai and Molnar, 2001; Millar and Pelling 2001), as shown in Fig. 3. The other type of adaptor is used to accommodate small-diameter metal electrodes. To configure this type of electrode holder, the connector pin of the electrode is inserted first into the front of the adaptor and pulled through it so that it protrudes somewhat from the back-end of the adaptor. This is done on a flat surface before the adaptor is screwed onto the SMA connector. A small pair of tweezers is used to grasp the pin of the electrode and insert it into the input socket of the probe. The adaptor is then screwed onto the probe gently by hand. Next, an about 2.5 cm-long strip of copper foil with conductive adhesive tape (3M, Part No. 1181) is rolled cylindrically so that one-third of the 25 mm width of the tape is around

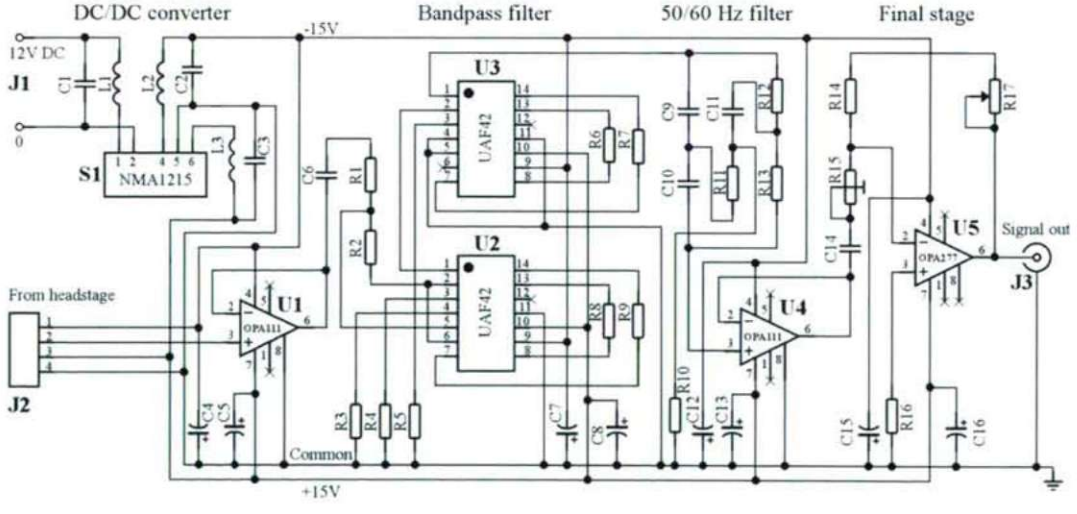

Figure 4. Schematic diagram of the main amplifier, showing details of the DC-DC converter, signal input buffer, band pass and notch filtering, as well as the final gain stages. See Table 1 for specific part values.

the front-end of the adapter and two-thirds of it is around the shank of the electrode itself. Finally, the front-end of the tape is flattened with the thumb and forefinger and the excessive parts of the foil are cut off. The copper foil has a twofold purpose: it holds the electrode in place and it provides an extended shielding for smoother recording. The end-result of this procedure is illustrated in Fig. 3. The headstage probe can be securely fixed in most micromanipulators via its 6.4 mm x 105 mm (diameter x length) mounting rod, which also serves as a cable guide. The headstage probe is connected to the main unit by a 1.5-m-long, well-shielded, high-flex cable (Belden, Part No. A3308) through the use of a four-pole, screw-on connector (Hirose, Part No. SR30-10PE-4P) placed on the free end of the cable.

Main amplifier

Miniature DC-DC converters allow a very space-saving solution to make dual ±15 V rail supplies available on board. The S_1 NMA1215S in the main amplifier can utilize almost any 12 V DC source for input, including good-quality external AC-DC converters or batteries. It is a fully encapsulated DC-DC converter, with the added benefit of galvanic isolation to reduce switching noise. The DC input and outputs are smoothed by LC filters (L_1-L_3, C_1-C_3; Fig. 4). Specific values for each part reference are given in Table 1.

Table 1. List of materials for the main amplifier

Item	Quantity	Reference	Value	Manufacturer
1	3	C1, C2, C3	1.0 µF	Panasonic
2	8	C4, C5, C7, C8, C12, C13, C15, C16	2.2 µF Ta	Panasonic
3	1	C6	0.83 µF	Panasonic
4	1	C14	3.3 µF	Panasonic
5	2	C9, C10	500 pF	Panasonic
6	1	C11	1000 pF	Panasonic
7	1	J1 DC power jack	163-1021	Kobiconn
8	1	J2 Four-pin receptacle	SR30-10R-4S	Hirose
9	1	J3 BNC jack	30-10-RFX	Amphenol
10	1	L1	47 µH	J.W. Miller
11	2	L2, L3	330 µH	J.W. Miller
12	1	R1	2 kΩ	Yageo
13	1	R2	100 kΩ	Yageo
14	2	R3, R16	10 kΩ	Yageo
15	2	R4, R5	22 kΩ	Yageo
16	2	R6, R7	68 kΩ	Yageo
17	2	R8, R9	33 kΩ	Yageo
18	1	R10	10 Ω	Yageo
19	1	R11	3.16 MΩ	Phicomp
20	2	R12, R13	6.37 MΩ	Phicomp
21	1	R14	100 Ω	Yageo
22	1	R15 Trimmer potentiometer	2 kΩ	Bourns
23	1	R17 Potentiometer	50 kΩ	Precision Electronic
24	1	S1 DC-DC converter	NMA1215S	C&D Technologies
25	1	U1	OPA111AM	TI/Burr-Brown
26	1	U4	OPA111BM	TI/Burr-Brown
27	2	U2, U3	UAF42AP	TI/Burr-Brown
28	1	U5	OPA277AP	TI/Burr-Brown

*Values for 50 Hz. For 60 Hz, use 2.67 MΩ and 5.34 MΩ, respectively

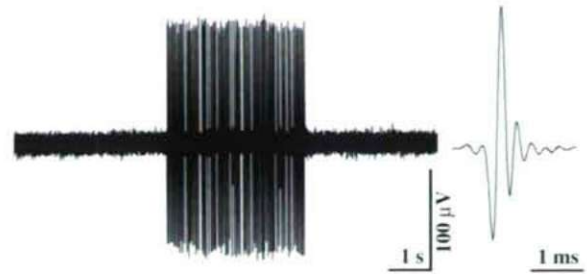

Figure 5. Single-unit recording from a medullary neuron in an anesthetized rat. Spikes were evoked by peripheral stimulation. Note the excellent signal-to-noise ratio and the low-noise baseline recording.

The U_1 op amp buffers signals arriving from the headstage preamplifier and its output are AC-coupled (C_6) to the band pass filter stage (Fig. 4). Before filtering, the signal is amplified by the uncommitted op amp of the U_2 UAF42 universal active filter(UAF42 Datasheet, 1998) and resistors R_1 and R_2. A tuned circuit band pass filter for the spike bandwidth (approximately 300 Hz to 8000 Hz) is constructed, using two UAF42 active filters (U_2 and U_3) and the network of resistors R_3-R_9 (Molina and Stitt 1993). To reduce electromagnetic interference from the mains line power, an additional 50/60 Hz reject (notch) filter is included. This is comprised of an OPA111BM op amp (U_4), resistors R_{10}-R_{13} and capacitors C_9-C_{11}. Resistors R_{11}-R_{13} define the reject frequency; different resistor values are used for 50 Hz and 60 Hz, as specified in Table 1 (OPA111 Datasheet, 1995). The notch filter stage is AC-coupled (C_{14}) to the final, variable-gain stage that consists of the op amp U_5 and resistors R_{14}, R_{15} and R_{17}. Potentiometer R_{17} is placed on the front panel to adjust the required gain during an experiment, while trimmer potentiometer R_{15} is for calibration of the overall gain in the whole system.

The layout of the circuit is not critical except for the wiring at the non-inverting input of U_1. This wiring is performed with stiff wire in mid-air. The entire circuit is placed in a tin-plated iron box in order to minimize electromagnetic interference. With the part values listed in Table 1, the main amplifier produces a max signal gain of about 1,000. During application of a 10 mV peak-to-peak sine wave signal with a frequency of 1 kHz at the input connector J_2, the trimmer R_{15} can complete fine calibration of the main amplifier. The input calibrating, signal together with the output amplified signal, should be adjusted and observed by using a calibrated two-channel oscilloscope. The signal will already have been amplified by 10 in the headstage amplifier, and thus the overall gain in the whole system is 10,000. Resistors R_1, R_2 and/or R_{14}, R_{15} or R_{17} should be replaced with the required values if a different system gain is necessary. The actual appearance of the main amplifier has been published on the Internet (Budai 2004b).

Extracellular recording *in vivo*

Sprague-Dawley rats (300-400 g) of either sex were initially anesthetized with chloral hydrate (40 mg/100 g, i.p.; supplemental doses as required). All procedures relating to animal handling and surgery followed the protocol for animal care approved by the Hungarian Health Committee and the international guidelines (EC Directives, 86/609/EEC). Experimental details have been published previously (Budai and Molnar 2001). In brief, single-unit recordings were made from neurons of the medulla located between the planes from 11 mm to 12 mm behind the bregma (Paxinos and Watson, 1998) using the headstage and main amplifiers described above. Spike potentials were recorded with a four-barreled micropipet assembly in which one of the barrels contained a 7-μm carbon fiber creating a low-impedance (0.4-0.8 MΩ at 1 kHz) recording electrode (Budai and Molnar 2001) as shown in Fig. 3. The experimental data collection was automated by means of a multifunction instrument control and data acquisition board (PC-1200, National Instruments, Austin, TX) programmed in LabView (National Instruments, Austin, TX). The LabView-based data acquisition and instrument control software was developed in-house; it has been published in part elsewhere (Budai 1994, 2004a). Analog signals were sampled and digitized at 50 kHz by the data acquisition card, and oscilloscope trace-like recordings were taken from all neurons.

Results and Discussion

If the measured noise voltages are squared and the mean square is computed, the fluctuations of both signs contribute positively. The square root of this mean (RMS) is the usual way of expressing the magnitude of noise voltages. The RMS of the Johnson noise is $(4kTR\Delta f)^{1/2}$, where k is the Boltzmann constant (1.38×10^{-23} JK^{-1}), T is the absolute temperature in Kelvin, R is the resistance of the microelectrode in ohm, and Δf is the noise bandwidth in Hz. If Δf is 5 KHz, this formula gives 5.6 μV RMS for thermal noise in the case of carbon fiber electrodes with a resistance of 0.4 MΩ, when the temperature is 20°C= 293°K. When the input of the described headstage amplifier was grounded, the voltage noise in the whole system was no more than 1 μV RMS. On the use of four-barrel, carbon-fiber containing assemblies of borosilicate glass micropipets (Fig. 3) in the medulla of anesthetized rats, the total peak-to-peak noise levels increased to about 25 μV, *i.e.,* to about 6 μV RMS. This means that our headstage and main amplifier system is very close, in terms of noise performance, to its theoretical lower limit and does not contribute significantly to the overall noise. We conclude that our preamplifier, in combination with carbon fiber electrodes, performs equally well or rather better than those described previously (Millar and Williams 1988; Millar and Barnett 1994).

Figure 5 illustrates a low-noise recording from a medullary neuron with a four-barrel carbon fiber microelectrode. Spike responses were evoked by peripheral somatosensory stimulation applied to the tail. Noteworthy features include the excellent signal-to-noise (spike-to-baseline) ratio and the very low-noise baseline recording. At times, tungsten electrodes shielded by our unique adaptor/holder (Fig. 3) produced even lower-noise recordings (data not shown). The copper foil shielding can be extended by a brushable shield through the use of silver paint or colloidal silver (Sachs 1985). By this means, the shielding could be extended very close to the tip of the microelectrode and, could possibly, further reduce interferences from electric fields as the impedance of metal or carbon fiber electrodes is largely capacitive (Robinson 1968) and only the real component of the complex impedance of the electrode contributes to thermal noise (Millar and Barnett 1994).

Acknowledgment

This work was funded by Kation Scientific Co., Minneapolis, MN 55105, USA.

References

Armstrong-James M, Millar J (1979) Carbon fibre microelectrodes. J Neurosci Methods 1:279-287.

Budai D (1994) A computer-controlled system for post-stimulus time histogram and wind-up studies. J Neurosci Methods 51:205-211.

Budai D (2004a) Software. http://www.kationscientific.com/iontophoresis/ratemeter.html

Budai D (2004b) Action potential recording. http://www.kationscientific.com/iontophoresis/spikeamps.html

Budai D, Molnar Z (2001) Novel carbon fiber microelectrodes for extracellular electrophysiology. Acta Biol Szegediensis 45:65-73.

Horowitz P, Winfield H (1996) The art of electronics. New York: Cambridge University Press.

Millar J (1992) Extracellular single and multiple unit recording with microelectrodes. In: Monitoring neuronal activity: a practical approach (Stamford JA, ed), pp 1-27. Oxford: Oxfor University Press.

Millar J, Williams GV (1988) Ultra low-noise silver-plated carbon fibre microelectrodes. J Neurosci Methods 25:59-62.

Millar J, Barnett TG (1994) A low-noise optically isolated preamplifier for use with extracellular microelectrodes. J Neurosci Methods 51:119-122.

Millar J, Pelling CW (2001) Improved methods for construction of carbon fibre electrodes for extracellular spike recording. J Neurosci Methods 110:1-8.

Molina J, Stitt RM (1993) Filter design program for the UAF42 universal active filter. http://focus.ti.com/lit/an/sbfa002/sbfa002.pdf

OPA111 Datasheet (1995) Burr-Brown Division of Texas Instruments. http://focus.ti.com/lit/ds/symlink/opa111.pdf

Paxinos G, Watson C (1998) The rat brain in stereotaxic coordinates, 4th Edition. New York, NY: Academic Press.

Purves RD (1981) Microelectrode methods for intracellular recording and iontophoresis. London: Academic Press.

Robinson DA (1968) The electrical properties of metal microelectrodes. Proc IEEE 56:1065-1071.

Sachs F (1985) Microelectrode shielding. In: Voltage and patch clamping with microelectrodes (Smith TG, Lecar H, Redman SJ, Gage PW, eds), pp 25-45. Baltimore: Waverley Press.

UAF42 Datasheet (1998) Burr-Brown Division of Texas Instruments.

Volume 48(1-4):19-23, 2004
Acta Biologica Szegediensis
http://www.sci.u-szeged.hu/ABS

ARTICLE

Calcium oxalate crystals in floral organs of *Helianthus annuus* L. and *H. tuberosus* L. (Asteraceae)

Ciler Meric*, Feruzan Dane

Department of Biology, Faculty of Arts and Sciences, Trakya University, Edirne, Turkey

ABSTRACT *Helianthus annuus* L. and *Helianthus tuberosus* L. belong to Asteraceae that is one of the greatest families of plant kingdom. Calcium oxalate crystals are found in most organs and tissues of many plant species. The type, morphology and distribution of calcium oxalate crystals in floral organs of *H. annuus* and *H. tuberosus* were studied. Crystals were investigated at light and electron microscopy levels. CaOx crystals in calyx and bracts both of *H. annuus* and *H. tuberosus* were not observed. The ligulate and tubulate corollas of *H. annuus* had styloid and prismatic crystals. Also in both of the ligulate and tubulate corollas of *H. tuberosus* were observed prismatic and styloid crystals as similar with *H. annuus*. Styloid and prismatic types of CaOx crystals in filaments of *H. annuus* and *H. tuberosus* were determined. In endothecial layer and tapetum cells of anthers of both of taxa only styloid type crystals were observed. The ovary was not contains CaOx crystals in *H. annuus* and *H. tuberosus*, Style of both of taxa had styloid shape crystals. But in stigma trichomes of *H. annuus* and *H. tuberosus* druses were found. The raphides were not observed in both of taxa. This study provides additional knowledge about the presence of CaOx crystals in Asteraceae.
Acta Biol Szeged 48(1-4):19-23 (2004)

KEY WORDS

Asteraceae
calcium oxalate crystals
floral organs
Helianthus annuus L.
Helianthus tuberosus L.

Calcium oxalate (CaOx) crystals are found in many plant species (Franceschi and Horner 1980; Prychid and Rudall 1999). They occur in different plant tissues including leaves (Horner and Zindler-Frank 1982; Lersten and Horner 2000), stems (Grimson and Arnott 1983), roots (Dane et al. 2000; Horner et al. 2000), seeds (Webb and Arnott 1982, 1983; Ilarslan et al. 1997, 2001). CaOx crystals also occur in floral organs including ovaries (Tilton and Horner 1980), anthers (Buss and Lersten 1972; Horner 1977; Horner and Wagner 1980 1992) and petals (Robertson 1978). There are not only a few taxa including Brassicaceae, Campanulaceae, Papaveraceae, Saxifragaceae and Equisetaceae (Kinzel 1989). However, their functional significance remains unclear, although various functions have been attributed them. CaOx crystals give protection against foraging animals (Molano-Flores 2001), bind toxic oxalate (Borchert 1984), involved in in-plant Ca regulation (Franceschi 1989), salt stress and homeostasis (Hurkman and Taraka 1996) and detoxification of heavy metals (Nakata 2003).

CaOx crystals are widely distributed in plant and found in over 215 plant families (Franceschi and Horner 1980; Molano-Flores 2001). The distribution and shapes of these crystals have been used as taxonomic characters for a number of plant families (Molano-Flores 2001). The shapes of CaOx crystals vary differently and they commonly described as raphides, druses, styloids, prisms and crystal sand (Ilarslan et al. 1997). Prychid and Rudall (1999) reported that there are three main types of CaOx crystal as raphids, styloids and druses in monocotyledons. Druses are relatively rare in monocotyledons than dicotiledons (Prychid and Rudall 1999).

Besides existence of CaOx crystals in long-living organs such as roots, stems and leaves, it is also notable that these crystals are present in transitory floral organs such as stamens, gynoecia and petals. They are quite prevalent in floral organs of many taxa including Dilleniaceae, Liliaceae, Palmae, Malvaceae, Cunoniaceae, Euphorbiaceae (Tilton and Horner 1980), Solanaceae (Horner and Wagner 1980, 1992), Leguminosae (Buss and Lersten 1972).

Our interest in CaOx crystals began with observations of crystals in tapetal and endothecial layers during the embriyological study on *H. annuus*. Horner have indicated also exist of CaOx crystals in tapetum cells of *H. annuus* (Horner 1977). But other floral organs of *H. annuus* were not reported. This conducted us to investigate types and distributions of CaOx crystals in floral organs of *Helianthus* species growing in Turkey. There are two species of *Helianthus* genus in Turkey: *H. annuus* and *H. tuberosus* (Kupicha 1975). We aimed to determine types and distributions of CaOx crystals in floral organs of *H. annuus* and *H. tuberosus* in the study.

Materials and Methods

Plants of *Helianthus annuus* L. and *Helianthus tuberosus* L. were grown in the Greenhouse of Department of Biology, Trakya University. The buds and opened flowers were col-

Accepted Aug 25, 2004
*Corresponding author. E-mail: cilermeric@trakya.edu.tr

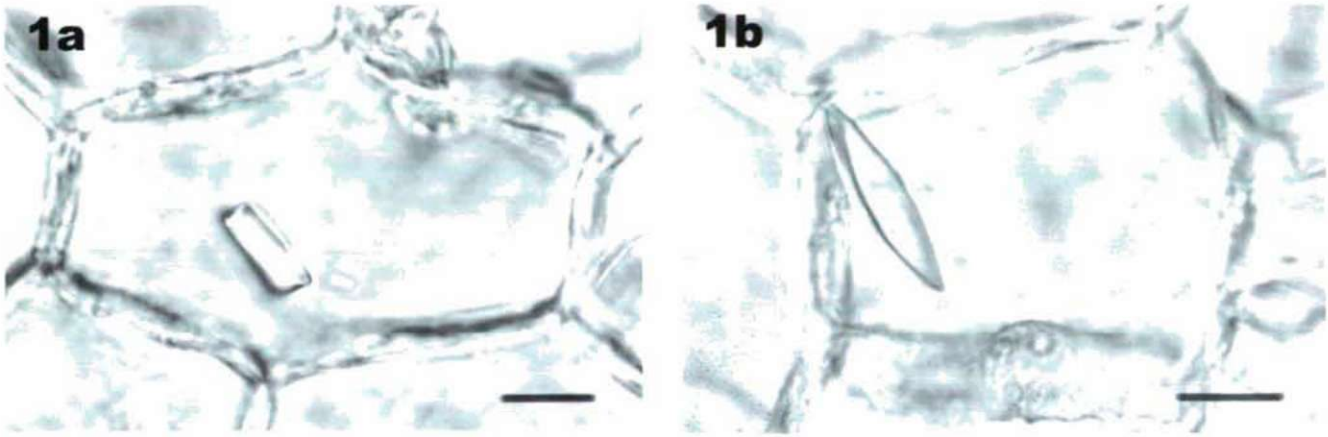

Figure 1. CaOx crystals in ligulate corolla of *H. annuus*. a, prismatic crystal; b, styloid crystal. Bar = 10 µm

lected from *H. annuus* and *H. tuberosus*.

Light Microscopy

Florets were at different development stages belonging to *H. annuus* and *H. tuberosus* were fixed in mixture ethyl alcohol and glacial acetic acid (3:1) at room temperature overnight and changed to 95% ethyl alcohol. Bracts, calyxes, corollas, stamens, ovary, style and stigma were dissected out of florets. The samples were treated with 2.5% Clorox (sodium hypochlorite) for 4 h. After graded ethyl alcohol series, the samples were infiltrated with xylene, mounted in entellan on slides, and covered with cover slips (Ilarslan et al. 1997). Photographs were taken with an Olympus Photomicroscope.

Transmission Electron Microscopy

Florets were fixed in 3% glutaraldehyde in Milloning's phosphate buffer at 4°C for 2 h. The floral organs were dissected and then placed in fresh fixative at 4°C for overnight. Fixed samples were passed though three buffer rinses, post-fixed in 1% osmium tetraoxide (OsO_4) in the same buffer for 4 h at 4°C. Then the samples are rinsed several times in the buffer, dehydrate in a graded acetone series to propylene oxide, and embedded in Epon 812. The acid tests were used to determine the chemical composition of the crystals. Control samples were immersed in turn in 5% acetic acid, 10% hydrochloric acid, 3% nitric acid and 4% sulfuric acid (Molano-Flores 2001). All these tests confirmed that the crystals were calcium oxalate.

Table 1. The types and distribution of CaOx crystals in *H. annuus* and *H. tuberosus*.

Location	Taxa	
Organs	*H. annuus*	*H. tuberosus*
bract	---	---
calyx	---	---
ligulate corolla	styloid, prismatic	styloid, prismatic
tubulate corolla	styloid, prismatic	styloid, prismatic
anther – endothecium	styloid	styloid
anther – tapetum	styloid	styloid
anther – trichome	druse	druse
filament	styloid, prismatic	styloid, prismatic
ovary	---	---
style	styloid,	styloid
stigma- trichome	druse	druse

Results

In *Helianthus* L. genus the inflorescence is a capitulum and it consist of two types flowers; ligulate flowers and tubulate flowers (Seiler 1997). The ligulate flowers have pistils, but contain no stamens. The tubulate flowers have both of pistil and stamens. Calcium oxalate crystals are displayed a similar distribution in both flower types of two taxa. Results were shown in Table 1.

Helianthus annuus L.

Calcium oxalate crystals were observed in stamen, style, stigma, ligulate petal and tubulate petal of *H. annuus*. They are not observed in sepals and bracts. Crystals in corolla of ligulate flowers were dense in basis of the corolla and exist different shapes as prismatics (Fig. 1a) and styloids (Fig. 1b). Whereas in tubulate flowers they are equally distribute in all corollas and present as prismatics and styloids. In stamens they were found in both of anthers and filaments. Also in filaments crystals were determined as prismatics and styloids. In endothecial cells (Fig. 2) and tapetal cells (Fig. 3) of anthers CaOx crystals were observed as styloid type. In these tissues no other types of crystals were observed. Epidermal cells and middle layer cells of anther contain no crystals. Only druse type of crystals was observed in glandular trichomes

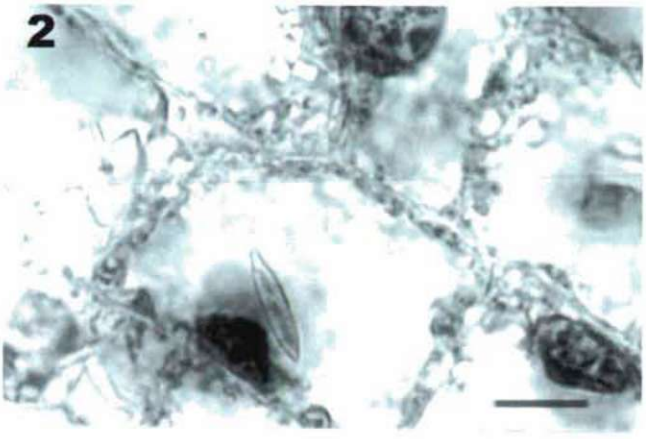

Figure 2. Styloids in endothecial cells of *H. annuus*. Bar = 10 µm

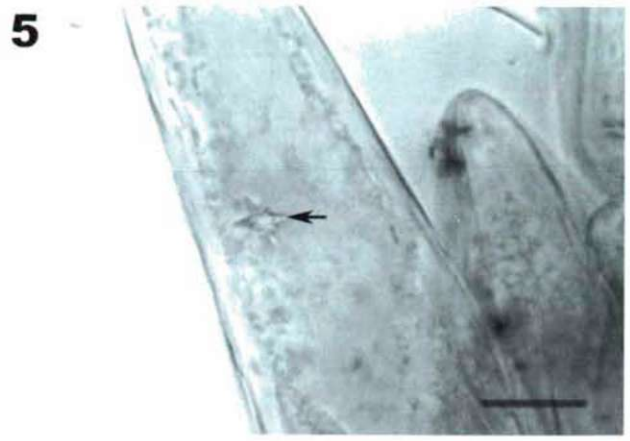

Figure 5. Druse in stigma trichomes of *H. annuus* (arrow). Bar = 10 µm

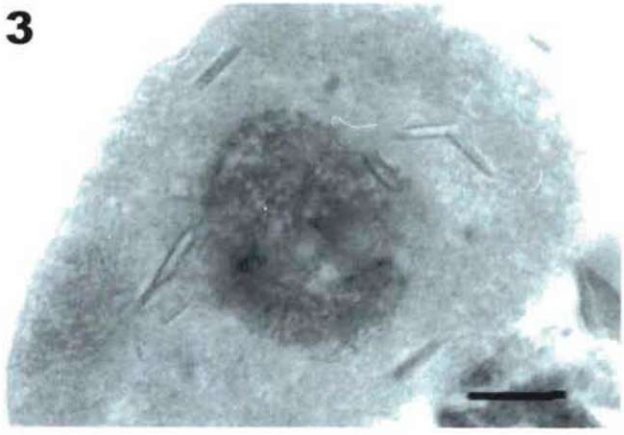

Figure 3. Styloids in tapetal cells of *H. annuus*. Bar = 10 µm

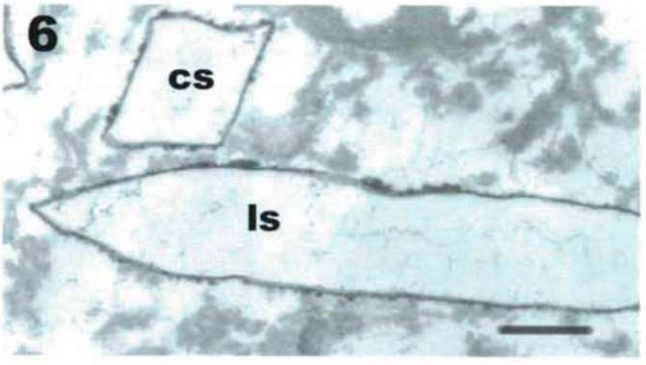

Figure 6. TEM photographs of styloids in tapetum of *H. annuus* (cs, cross section; ls, longitudinal section). Bar = 1 µm

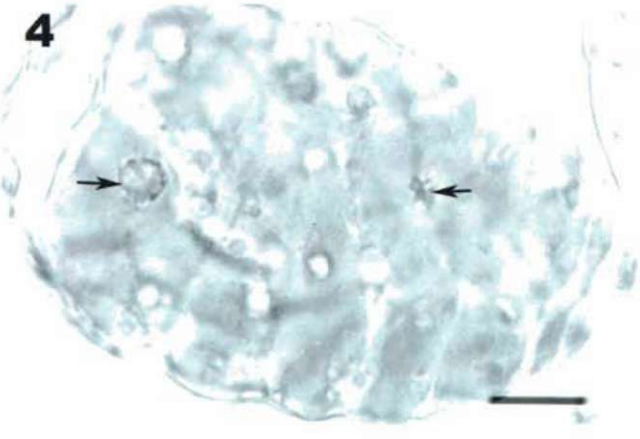

Figure 4. Druses in glandular trichomes at tip of anthers of *H. annuus* (arrows). Bar = 10 µm

at tip of anthers (Fig. 4). In style, stytoid type was found. In stigma crystals were found only in trichomes and druse shape (Fig. 5). CaOx crystals were not found in ovary of *H. annuus*. Styloids in cross sections were seemed cubical. In longitudinal section they were typically elongated and have pointed ends (Fig. 6).

Helianthus tuberosus L.

Distribution and existence of CaOx crystals in *Helianthus tuberosus* were similar with *Helianthus annuus*. Also calcium oxalate crystals were observed in stamen, style, stigma, ligulate petal and tubulate petal of *H. tuberosus* and they were not observed in sepals and bracts as *H. annuus*. Crystals in corolla of ligulate flowers were present as prismatics and styloids shapes and they are dense in basis of the corolla. In tubulate flowers they were observed as prismatics and styloids. In stamens they were found in both of anthers and filaments. In filaments crystals were determined as prismatics and styloids. Styloid type CaOx crystals were observed in endothecial cells

and tapetal cells of anthers. In epidermal cells and middle layer cells no crystals were found. In glandular trichomes at tip of anthers druse crystals were determined. In style they were observed styloid type. In stigma crystals were found only in trichomes and they were druse type. Also CaOx crystals were not found in ovary of *H. tuberosus* as *H. annuus*.

Discussion

In this study CaOx crystals in floral organs of *H. annuus* and *H. tuberosus* was revealed. Two types of the calcium oxalate crystals were common; styloids and prismatics in both of taxa. Druses were observed rarely in glandular hairs of anthers of and hair trichomes of stigmas in both of taxa. Only styloid crystals in the tapetum and endothecium cells of anthers were observed and while plasmodial tapetum degenerated they disappeared. Both of styloid and prismatic crystals in the corolla and filament were located.

In the Asteraceae crystals were shown by a few previous studies (Horner 1977; Heinrich et al. 2002). Horner (1977) reported that styloids occur in tapetal cells of *H. annuus*. Crystals is not only in tapetum cells but also in endothecial cells and in glandular hairs of anther. Heinrich et al. (2002) have observed CaOx crystals in glandular hairs of *Sigesbeckia joullensis* Kunth such as glandular hairs of anther of *H. annuus*. But researchers did not determined calcium oxalate crystal types in glandular hairs. Calcium oxalate crystals have been shown to occur within the anthers of other higher plants (Schmid 1976; Horner and Wagner 1980). Primarily researchers have suggested that CaOx crystals in the anther may supply for pollen against predators, are metabolic waste products or lead to in the anther for dehiscence (Horner and Wagner 1980). Besides CaOx crystals were suggested that they serve as a storage source for Ca (Ilarslan et al. 1997, 2001). This information is very important, because it is widely assumed that mitosis and cytokinesis are regulated by Ca^{2+} (Hepler and Wayne 1985). The existence of CaOx crystals in tapetum and endotecium cells may also affect microsporogenesis and microgametogenesis. The level of Ca^{2+} would control the assembly-disassembly of spindly microtubules and directly regulate both formation and function of the mitotic apparatus and phragmoplasts (Hepler and Wayne 1985). Besides synthesizing callose (β 1,3 glucan) during microsporogenesis is required high concentration of Ca^{2+} (Katti et al. 1994). Many studies already cited indicate the importance of Ca^{2+}, both as a structural and a physiological entity.

Tilton and Horner reported that crystals within the carpels are completely solved by the time the carpels dehisce in *Ornithogalum caudatum* Ait. They suggested that in *Ornithogalum* carpels may represent mobilization of Ca reserves from the carpels to the developing seeds.

Physical and chemical conditions such as temperature, pressure, pH, and ion concentration, may affect crystal growth, location, and properties (Franceschi and Horner 1980), however it is considered that crystal formation within the cell is under genetic control (Ilarslan et al. 2001). Although some species have different crystal types in adjacent cells, a particular taxon can have specific crystal shape (Prychid and Rudall 1999). In present study, similar results in both taxa were observed except for small differences.

In this study we aimed to determine CaOx crystals in *H. annuus* and *H. tuberosus* being a member of the Asteraceae. It is probably that also the other members may Asteraceae are contain crystals. The most comprehensive review of crystal types and distribution for a single family (Zindler-Frank 1987, Leguminosae) lacks substantial documentation (Lersten and Horner 2000). Thus additional research is needed to better determine CaOx crystals in other taxa belonging Asteraceae.

Acknowledgments

The TEM work was carried out in Istanbul University, Faculty of Medicine, Department of Histology and Embryology. We thank them for technical assistance.

References

Borchert R (1984) Functional anatomy of the calcium-excreting system of *Gleditsia triacanthos* L. Bot Gaz 145:474-482.

Buss PA, Lersten NR (1972) Crystals in tapetal cells of the Leguminosae. Bot J Linn Soc 65:81-85.

Dane F, Huseyinova G, Meric C (2000) Some ultrastructural observations on calcium oxalate raphide crystal idioblasts and meristematic cells of the adventive root tips of *Sternbergia lutea* (L.) Ker-Gawl. Ex Sprengel (Amaryllidaceae). Turk J Bot 24:71-80.

Franceschi VR (1989) Calcium oxalate formation is a rapid and reversible process in *Lemna minor*. Protoplasma 148:130-137.

Franceschi VR, Horner HT (1980) Calcium oxalate crystals in plants. Bot Rev 46:361-427.

Grimson MJ, Arnott HJ (1983) An ultrastructural study of druse crystals in the abscission zone of *Phyllanthus niruri* L. Scan Electron Micros IV: 1771-1778.

Hienrich G, Pfeifhofer HW, Stabentheiner E, Sawidis T (2002) Glandular hairs of *Sigesbeckia jorullensis* Kunth (Asteraceae): Morphology, Histochemistry and composition of essential oil. Ann Bot 89:459-469.

Hepler PK, Wayne RO (1985) Calcium and plant development. Ann Rev Plant Physio 36:397-439.

Horner HT (1977) A comparative light and electron microscopic study of microsporogenesis in male-fertile and cytoplasmic male-sterile sunflower (Helianthus annuus). Am J Bot 64:745-759.

Horner HT, Wagner BL (1980). The association of druse crystals with the developing stomium of *Capsicum annuum* (Solanaceae) anthers. Am J Bot 67:1347-1360.

Horner HT, Wagner BL (1992) Association of four different calcium crystals in the anther connective tissue and hypodermal stomium of *Capsicum annuum* (Solanaceae) during microsporogenesis. Am J Bot 67:1347-1360.

Horner HT, Zindler-Frank E (1982) Histochemical, spectroscopic, and x-ray diffraction identifications of the two hydration form of calcium oxalate crystals in three legumes and *Begonia*. Can J Bot 60:1021-1027.

Horner HT, Kausch AP, Wagner BL (2000) Ascorbic acid: a precursor of oxalate in crystal idioblasts of *Yucca torreyi* in liquid root culture. Int J Plant Sci 161:861-868.

Hurkman WJ, Tanaka CK (1996) Effect of salt stress on germin gene expression in barley roots. Plant Physiol 110:971-977.

Ilarslan H, Palmer RG, Horner HT (2001) Calcium oxalate crystals in developing seeds of soybean. Ann Bot 88:243-257.

Ilarslan H, Palmer RG, Imsande J, Horner HT (1997) Quantitative determination of calcium oxalate and oxalate in developing seeds of soybean (Leguminosae). Am J Bot 84:1042-1046.

Katti RY, Giddanavar HS, Naik S, Agadi SN, Hegde RR (1994) Persistence of callose and tapetum in the microsporogenesis of genic male sterile *Cajanus cajan* (L.) Millsp. with well formed endothecium. Cytologia 59:65-72.

Kinzel H (1989) Calcium in the vacuoles and cell walls of plant tissue. Flora 182:99-125.

Kupicha FK (1975) *Helianthus* L. In Davis PH, ed., Flora of Turkey and the East Aegean Island. Edinburgh Univ. Press, pp. 44-45.

Lersten NR, Horner HT (2000) Calcium oxalate crystals types and trends in their distribution patterns in leaves of *Prunus* (Rosaceae: Prunoideae). Plant Syst Evol 224:83-96.

Molano-Flores B (2001) Herbivory and calcium concentrations affect calcium oxalate crystal formation in leaves of *Sida* (Malvaceae). Ann Bot 88:387-391.

Nakata PA (2003) Advances in our understanding of calcium oxalate crystal formation and function in plants. Plant Sci 164:901-909.

Prychid CJ, Rudall PJ (1999) Calcium oxalate crystals in monocotyledons: a review of their structure and systematics. Ann Bot 84:725-739.

Robertson BL (1978) Raphide-sac as epidermal appendages in *Jubaeopsis caffra* Becc. (Palmae). Ann Bot 42:489-490.

Schmid R (1976) Filament histology and anther dehiscence. J Linn Soc London Bot 73:303-315.

Seiler GJ (1997) Anatomy and morphology of sunflower. In Schneiter AA, ed., Sunflower technology and production. American Society of Agronomy, Inc. Wisconsin, pp. 67-111.

Tilton VR, Horner HT (1980) Calcium oxalate raphide crystals and crystalliferous idioblasts in the carpels of *Ornithogalum caudatum*. Ann Bot 46:533-539.

Webb MA, Arnott HJ (1982) A survey of calcium oxalate crystals and other mineral inclusions in seeds. Scan Electron Micros III:1109-1131.

Webb MA, Arnott HJ (1983) Inside plant crystals: a study of the noncrystalline core in druses of *Vitis vinifera* endosperm. Scan Electron Micros IV: 1759-1770.

Zindler-Frank E (1987) Calcium oxalate crystals in legumes. In Stirton CH. ed., Advances in legume systematics, Part 3. Royal Botanic Gardens, Kew, London, pp. 279-316.

Volume 48(1-4):25-33, 2004
Acta Biologica Szegediensis
http://www.sci.u-szeged.hu/ABS

ARTICLE

Competitive binding of quinone and antibiotic stigmatellin to reaction centers of photosynthetic bacteria

László Gerencsér[1], László Rinyu[1], László Kálmán[1], Eiji Takahashi[2], Colin A. Wraight[2], Péter Maróti[1]*

[1]Department of Biophysics, University of Szeged, Szeged, Hungary, [2]Department of Biochemistry and Center for Biophysics and Computational Biology, University of Illinois at Urbana-Champaign, Urbana, IL, USA.

ABSTRACT Stigmatellin bound to the Q_B site of the reaction center of photosynthetic bacteria is one of the most potent inhibitors of interquinone electron transfer. In addition to its inhibitory effect, it can be used to model protonated semiquinone and to probe the electrostatic environment. These properties were studied by two independent methods in isolated reaction centers and in chromatophores from cytochrome c-less mutant of *Rhodobacter sphaeroides*. The binding of the stigmatellin was detected by photochemical assay (flash-induced charge recombination of the reaction center) and the protonation/deprotonation equilibrium of the phenolic group by spectral assay monitoring the band peaks at 272 nm and 340 nm of the absorption spectra of the stigmatellin ($\Delta\varepsilon_{272}$(deprot/prot) = 10 $mM^{-1}\cdot cm^{-1}$). The dissociation constant of stigmatellin binding increased by about two orders of magnitude from 4 nM (pH 8.5) to 350 nM (pH 11.0) in chromatophores indicating the difference in binding affinities between the protonated and deprotonated forms of the stigmatellin. The observed pK of the phenolic proton has proved to be very sensitive to the surroundings: 9.4 (in aqueous solution), 9.4-10.3 (in different detergents) and 10.2 (in excess to RC in detergent n-octyl-β-D-glycopyranoside). This wide range of values may indicate highly different electric fields (energetic coupling with the phenolic proton of the stigmatellin) and/or solvation energy of stigmatellin in different phases of the detergent/protein/membrane system.

KEY WORDS

photosynthesis
chromatophore
quinones
inhibitors
electron transfer
proton binding/unbinding

Ultimately all life on earth depends on the ability of photosynthetic organisms (bacteria and higher plants) to convert solar energy into other forms of free energy directly amenable to fuel energy consuming processes (ion transport, ATP production, cell growth, etc.). The photosynthetic reaction center (RC), an integral membrane protein-pigment complex, plays a central role in this process. The RCs from purple bacteria are the best characterized of these membrane protein complexes (see Blankenship et al. 1995; Wraight 2004).

The RC performs light-induced redox chemistry: upon light excitation, the RC generates and exports oxidizing and reducing equivalents in a cyclic manner. In RCs of purple bacteria and Photosystem II of oxygenic organisms, the reducing equivalents are produced and exported in pairs, as quinol (fully reduced quinone, QH_2). The reduction of quinone (Q) by two electrons and two H^+ ions requires coordinated quinone/quinol exchange, light-induced electron transfer steps and proton transfer reactions (Fig. 1 and see Gerencsér et al. 2000). The initial step of the quinone reduction cycle is the binding of quinone from the membrane pool to the Q_B binding site of the RC. While the quinone is tightly bound (as a "prosthetic group") to the Q_A site in both oxidized (Q_A) and anionic semireduced (Q_A^-) redox states in the RC, Q_B is in weak binding equilibrium when fully oxidized (Q_B) or reduced (Q_BH_2). If, however, Q_B is reduced by light generated first electron transfer, e(1), it becomes tightly bound as semiquinone (Q_B^-). The subsequent photoactivation of the RC provides a second electron, e(2) to the quinone complex ($Q_A^-Q_B^-$). The negative charges of the anionic semiquinones induce proton binding to the protein. The first proton uptake to the quinone headgroup, H(1) creates the energetically unfavorable intermediate, $Q_A^-Q_BH$. The energetic gap between the two intermediates ($Q_A^-Q_B^-$ and $Q_A^-Q_BH$) depends on the proton equilibrium constant of the Q_B^- semiquinone (pK_1'). The range of pK_1' (≈ 5 in water and 4–6 in RCs (Graige et al. 1999; Lavergne et al. 1999)) suggests that the $Q_A^-Q_BH$ state lies 60–180 meV above $Q_A^-Q_B^-$ at pH 7, and progressively more at higher pH (60 meV per pH unit). The uphill (fast) proton transfer is followed by rate-limiting and downhill interquinone electron transfer from Q_A^- to Q_BH resulting in the $Q_A(Q_BH)^-$ intermediate that is further protonated by downhill proton transfer to produce fully reduced quinone, $Q_AQ_BH_2$. The uptake of the second proton, H(2) is kinetically indistinguishable from the first proton transfer in the wild type RC and can only be resolved in the case of mutants (e.g. GluL212→Gln, where 'L' represents the L subunit of the RC),

Accepted Apr 16, 2004
*Corresponding author. E-mail: pmaroti@sol.cc.u-szeged.hu

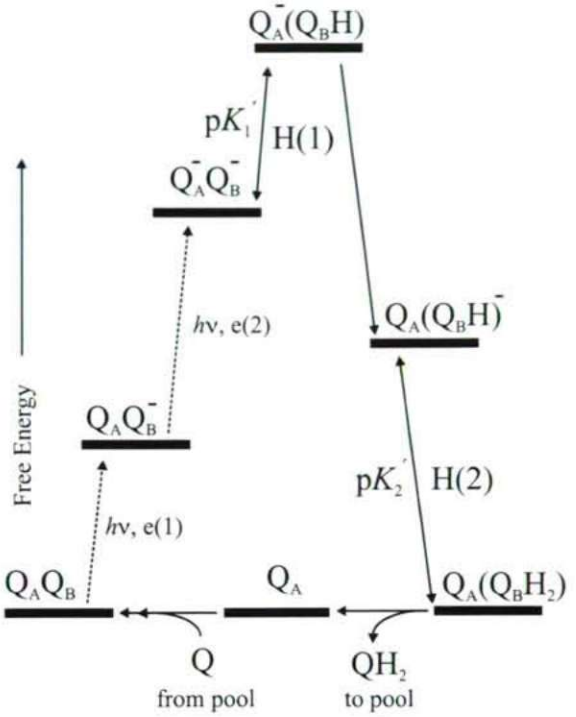

Figure 1. Relative free energy levels of the redox states of the Q_AQ_B quinone acceptor complex involved in the light-induced reduction cycle in RC of photosynthetic bacteria. Notations: *hν*: light driven reaction; e(1) and e(2): first and second electron injected to the quinone complex, respectively; H(1) and H(2): first and second H^+ ion bound to Q_B via equilibrium constants of pK_1' and pK_2' of the Q_AQ_B quinone acceptor complex, respectively.

with significantly retarded second proton uptake rates (Paddock et al. 1989; Takahashi and Wraight 1992; McPherson et al. 1994). The ubiquinol then leaves its binding site and is replaced by quinone from the membrane pool, and the turnover of the quinone complex can be started again.

The protonation and the p*K* values of the different forms of the semiquinone in the photocycle have been one of the ongoing problems of RC research. The absorption spectrum of the (first) flash-induced $Q_AQ_B^-$ state in isolated RC (with a characteristic peak at 450 nm) indicates that the semiquinone exists in fully anionic (unprotonated) redox state down to pH ≈ 3.5, a lower limit for RC protein. This means that the $pK(Q_AQ_B^-)$ should be smaller than 3.5. It is much more difficult to determine the p*K* value of Q_B^- after the second flash, when the primary quinone is in reduced state. The protonated species $Q_A^-Q_BH$ is present only at low levels (due to the low p*K* value) even at acidic pH and is short lived due to the very rapid reduction to $Q_AQ_BH^-$ (see the photocycle). Graige et al. (1999) were able to overcome this problem when they replaced the native ubiquinone at the Q_B site by rhodoquinone (RQ) that had a much higher solution p*K* (≈ 7.2) than the ubiquinone. The direct protonation of the semiquinone after the first flash could be observed and $pK(Q_ARQ^-) \approx 7.2$ value was determined. After the second flash, they observed a regular pH-dependence of the second electron transfer rate with $pK(Q_A^-RQ^-) \approx 8.0$. The upshift is $\Delta pK(Q_A^-RQ^-/Q_ARQ^-) = 0.8$. By comparing the behavior with RQ and ubiquinone, they suggested $pK(Q_A^-Q_B^-) \approx 4.5$-$5.0$ for native ubiquinone at pH 7.5. This value is very similar to the p*K* estimated for ubisemiquinone in water (p*K* = 4.9, Wraight 2004). It should be noted that, based on the pH-dependence of the rate of the second electron transfer, the $pK(Q_A^-Q_B^-)$ is not constant but is continuously modulated by interactions with changing electrostatic protein environment (different protonatable groups with different p*K* values become deprotonated upon increase of the pH).

One of the key steps of the quinone reduction photocycle is the exchange of quinone for quinol. During this process, several herbicides are able to replace the quinone by competitive binding to the Q_B site, thereby blocking the photocycle (Tischer and Strotman 1977; Wraight 1981; Stein et al. 1984; Vermaas et al. 1984; Oettmeier and Preusse 1987; Paddock et al. 1988). Over 50% of commercially available herbicides function by inhibition of higher plants at the Q_B site on the D1 polypeptide of the photosystem II RC (Percival and Baker 1991). Many herbicides are triazines (e.g. atrazine, terbutryne). The triazine binding site has been localized by X-ray crystallographic analysis of the RC-terbutryne complex at a resolution of 2.9 Å (Michel et al. 1986). High quality structural data have been collected on RC complexes with atrazine and two chiral atrazine derivatives paving the way for detailed description of the triazine type inhibitor binding (Lancaster and Michel 1996).

Other inhibitors of Q_B function more closely resemble quinones in structure. Among these compounds, the antibiotic stigmatellin is the most widely used (Fig. 2). The chromone-type stigmatellin is characterized by three unique and useful properties. a) It is a potent electron transfer inhibitor in several redox proteins of bioenergetic membranes. In addition inhibiting quinone reduction in bacterial RCs (Giangiacomo et al. 1987; Oettmeier and Preusse 1987) and in photosystem II (Oettmeier et al. 1985), stigmatellin is a very active inhibitor of quinol oxidation in the cytochrome bc_1 complex. The dissociation constants (K_S value) for stigmatellin at the Q_B site of isolated RC from *Rhodobacter sphaeroides* is reported to be ≈ 50 nM (von Jagow and Ohnishi 1985), whereas the 50% inhibition (I_{50}) value is ≈ 1.5 μM for RCs in native membranes (chromatophores; Giangiacomo et al. 1987). In chromatophores of *Rb. capsulatus*, the inhibition of the stigmatellin was found to be much greater than that of terbutryne (the K_S values are 0.37 μM and 6.0 μM, respectively) and the release time of stigmatellin from the Q_B binding site is much larger than that of terbutryne (≈ 30 s and 80 ms, respectively; Ginet and Lavergne 2001). b) The protonation state of the stigmatellin can be followed by absorption spectroscopy and the pK_a of the titrating site is estimated as 9.3 in aqueous

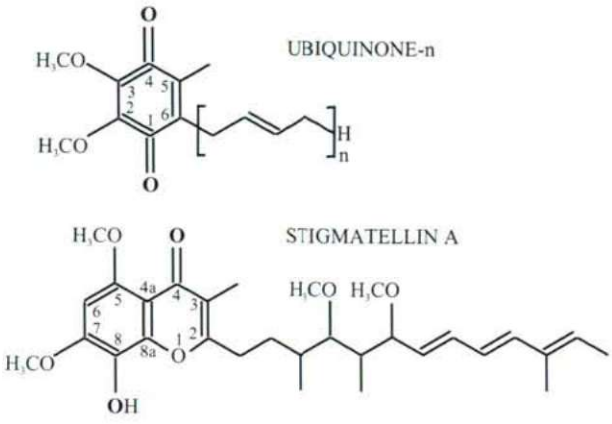

Figure 2. Chemical structures of ubiquinone and stigmatellin. Both have high binding affinity to the Q_B site of the photosynthetic RC. The native ubiquinones of *Rp. viridis* and *Rb. sphaeroides* are ubiquinone-9 and ubiquinone-10, respectively. The keto oxygens of ubiquinone can be protonated during the quinone reduction cycle and the hydroxyl group of the stigmatellin can be deprotonated in the alkaline pH region. See the structural similarity between the monoprotonated semiquinone and the stigmatellin.

solution (Graige et al. 1996). The pK_a of the phenolic proton of the stigmatellin is sensitive to the environment, and it can potentially be used as a probe of the local electrostatics. c) Comparing the chemical structures and binding positions of the quinones and the antibiotic stigmatellin, it appears that stigmatellin resembles the protonated semiquinone at lower pH (< 8) and the semiquinone anion radical at higher pH (> 10). These quinone redox states are essential intermediates in the quinone reduction photocycle (Fig. 1). However, they (especially the protonated semiquinone) are not readily accessible by direct spectroscopic and kinetics methods (Wraight 2004), and stigmatellin may provide some insight to the modes of binding and interactions of semiquinones in the photocycle of the RC. The present study addresses these three aspects of stigmatellin in bacterial RC protein both in native membrane (chromatophores) and in detergent solution.

Materials and Methods

Reagents, bacterial strains, chromatophores and RCs

The stability of the stigmatellin is limited in aqueous solution and after prolonged incubation (days) in aqueous solution, the stigmatellin looses its phenolic group: the 340 nm band gradually diminishes and disappears. To avoid this problem, fresh stigmatellin (Fluka) was always taken from a non-aqueous stock (4 mM in ethanol). To stabilize the pH of the sample solution, 2-10 mM pH buffers were used (Tris, Ches or Caps (all from Sigma) depending on the pH).

The carotenoidless R-26 strain of the photosynthetic bacterium *Rhodobacter sphaeroides* was grown under photoheterotrophic and anaerobic conditions in medium supplemented with potassium succinate. The nonphotosynthetic strain of the double mutant of *Rhodobacter sphaeroides* 2.4.1, CYCA1 (a kind gift of Prof. Donohue, Madison, Wisconsin USA) is deleted in cytochrome c_2. It was grown aerobically in darkness in Hutner medium supplemented with kanamycin corresponding to the antibiotic resistance cassette associated with the deletions.

To prepare chromatophores from CYCA1, the cells were washed, suspended in 100 mM KCl and 10 mM Tris buffer (pH 8.0) and broken by sonication. Unbroken cells were eliminated by centrifugation (17,000 g, 15 min). The supernatant was spun at 200,000g for 90 min. The chromatophore pellet was resuspended in a medium of minimum volume containing 1 mM Tris and 100 mM KCl. Samples were diluted 10-50 times for measurements.

Isolation of RC from R-26 chromatophore followed standard procedure (Maróti and Wraight 1988). The protein was solubilized by the zwitterionic detergent LDAO (N,N-dimethyldodecylamine-N-oxide, Fluka) and purified by ammonium sulfate precipitation steps followed by DEAE Sephacel (Sigma) anion exchange column chromatography. The fractions of purity (OD_{280}/OD_{802}=) 1.30 were collected. To exchange the zwitterionic detergent (LDAO) for a non-ionic one (e.g. Triton X-100), the RC preparation was dialyzed against 1 mM Tris buffer (pH 8.0) and 0.03% Triton X-100 overnight at 4°C under heavy stirring.

Optical spectroscopy

The pH-dependence of the absorption spectrum of the stigmatellin was determined (with and without RCs or chromatophores) from the steady state spectrum, measured with a dual beam absorption spectrophotometer (Unicam 4A). The relatively small absorption change of the stigmatellin ($\Delta A \approx$ 10 mOD) had to be detected in a background of large ($A \approx 1$ OD), pH-dependent and overlapping absorption of the RC (or chromatophores) in the UV and visible range where scattering could be substantial. To reduce this technical difficulty, near field (close to the photodetector) observation was applied. The reference and sample were made identical by splitting the stock solution with buffers, RC (and detergent) or chromatophores into two halves and the baseline was recorded (usually at pH 8). Then stigmatellin was added to the sample cuvette and an identical volume of ethanol to the reference cuvette. The pH values of both solutions were measured by calibrated glass electrodes immersed into the 1-1 cm cuvettes, and adjusted to the same pH value by addition of small (1-5 µl) amounts of concentrated (1 M) HCl or NaOH solutions.

Flash-induced absorption changes were detected by a single beam spectrophotometer of local design (Maróti and Wraight, 1988). The charge recombination kinetics were followed at 865 nm (isolated RC, $\Delta\varepsilon(865) = 112\ mM^{-1}\cdot cm^{-1}$) or at 603 nm (chromatophores, $\Delta\varepsilon(603) = 20\ mM^{-1}\cdot cm^{-1}$). Usu-

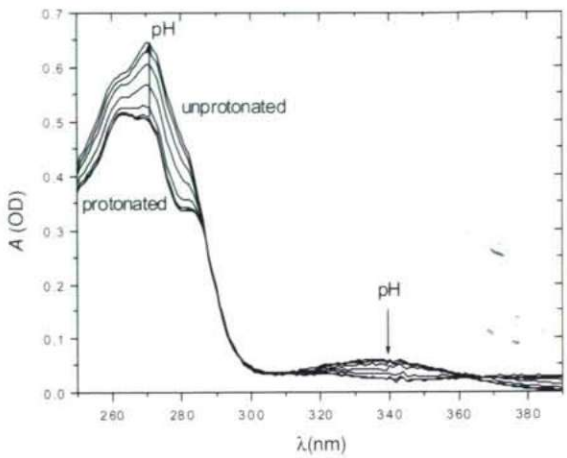

Figure 3. Absorption spectra of stigmatellin at different pH values. The arrows at two characteristic peaks (272 nm and 340 nm) indicate the direction of change of the bands upon pH increase from 6.8 to 12.05. The spectra of protonated and deprotonated forms of stigmatellin are shown at pH values much below and above the p*K* (= 10.3), respectively. Conditions: 11 µM stigmatellin, 0.03% TX-100 and 1-1 mM Tris, Ches and Caps.

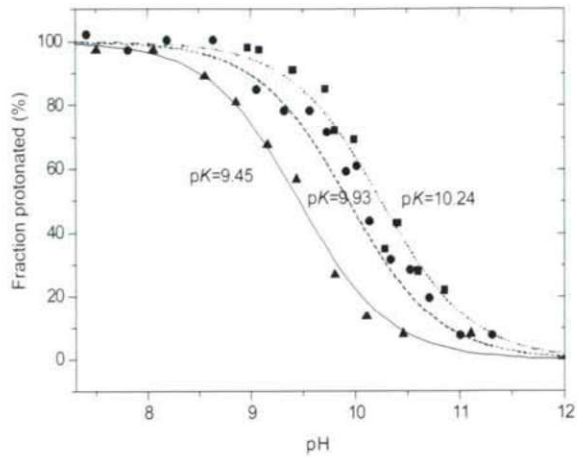

Figure 4. pH-titration of the stigmatellin based on the difference of the steady-state absorption spectra of the protonated/unprotonated forms in different environments: in water (▲), in detergent n-octyl-β-D-glycopyranoside (●) and in detergent n-octyl-β-D-glycopyranoside + RC (■). The (solid, dashes and dotted) lines indicate fits of the measured data (in water, detergent and RC, respectively) by Henderson-Hasselbalch function of characteristic of the protonation equilibrium of a single and independent protonatable group. Conditions: ▲ (5 µM stigmatellin, 2-2 mM Tris and Ches, λ = 272 nm), ● (10 µM stigmatellin, 20 mM n-octyl-β-D-glycopyranoside, 2-2 mM Tris and Caps, λ = 272 nm), ■ (10 and 13 µM stigmatellin in the reference and in the sample, respectively, 3.46 µM RC, 20 mM n-octyl-β-D-glycopyranoside and 2-2 mM Tris and Caps. The fraction of protonated stigmatellin was determined form the shape of the absorption spectrum.) The reference was identical to that of the sample except of (access) stigmatellin in the sample (the same volume of ethanol was added to the reference). The zero line of the spectrum was adjusted before addition of access stigmatellin to the sample at pH 8.4.

ally, they showed two (fast and slow) components revealed by biexponential decomposition of the trace via Levenberg-Marquardt non-linear fitting:

$$A=A_{fast}\cdot\exp(-k_{fast}t)+A_{slow}\cdot\exp(-k_{slow}t) \qquad (1)$$

Here A and k are the amplitudes and rate constants of the components, respectively. Using the firmly bound quinone (stigmatellin) model (see Appendix), the fast component is characteristic of the charge recombination from the reduced primary quinone (blocked Q_B site, $P^+Q_A^- \rightarrow PQ_A$), while the slow phase describes charge recombination from an acceptor quinone complex where the electron is shared between the two quinones: $P^+(Q_AQ_B)^- \rightarrow P(Q_AQ_B)$ (Wraight and Stein 1983; Kleinfeld et al. 1984).

Table 1. p*K* values of phenolic proton of stigmatellin dissolved in different detergents.

Detergents		p*K*
Water		9.4
LDAO (zwitterionic)		
	0.020 %	10.3
Triton X-100 (non-ionic)		
	0.005 %	9.65
	0.010 %	10.15
	0.020 %	10.3
	0.030 %	10.3
n-octyl-β-D-glycopyranoside (non-ionic)	1 mM	9.4
	5 mM	9.7
	10 mM	9.8
	20 mM (cmc)	10.0

Results

Spectral assay

Our experiments demonstrate that the steady-state absorption spectrum of the stigmatellin is pH-dependent, and indicates the distribution between its ionized (deprotonated) and protonated forms (Fig. 3). The near-UV absorption spectrum of stigmatellin shows characteristic bands at 272 nm (strong and narrow) and at 340 nm (much weaker and wider). Whereas the 272 nm band is one component of a complex UV band, the 340 nm band is a relatively isolated, single peak. Both bands are very sensitive to pH in the interval close to the p*K* value of the hydroxyl group of the molecule (Fig. 2). The absorption spectra recorded at different pH values show an isosbestic point around 300 nm, clearly indicating the interconversion of two absorbing species with maxima at 272 and 340 nm. Upon deprotonation (pH increase), the 340 nm band disappears completely, and the 272 nm band increases. By comparison of the absorption spectra of the fully protonated and unprotonated forms of the stigmatellin, the absorption peak at 272 nm can be calibrated: $\varepsilon_{272\ nm}$ (unprotonated) = 54 $mM^{-1}\cdot cm^{-1}$ and $\varepsilon_{272\ nm}$(protonated) = 44 $mM^{-1}\cdot cm^{-1}$, thus $\Delta\varepsilon_{272\ nm}$ (unprotonated – protonated) = 10 $mM^{-1}\cdot cm^{-1}$. These

values can be used for estimation of the ratio of the ionized and protonated forms.

The pK of the phenolic proton of stigmatellin is very sensitive to the environment. Figure 4 shows three pH-titrations of stigmatellin under different conditions. The pH-dependences of the fraction of protonated stigmatellin can be well approximated by a set of Henderson-Hasselbalch curves corresponding to a single protonatable group with a single pK value that changes according to the environment. We observed pK values of 9.4, 9.9 and 10.2 for the phenolic proton when stigmatellin is in aqueous solution, solubilized in detergent n-octyl-β-D-glycopyranoside or attached (is large access) to RC, respectively. Several additional pK values, measured under various conditions, are collected in Table 1. The pK values range over about 1 pH unit, indicating significant variation of interaction of the phenolic proton with the environment.

Photochemical assay

The binding of stigmatellin to the Q_B site can be probed by monitoring the absorption change of the flash-induced charge recombination. The appearance of the fast phase in the kinetics is indicative of stigmatellin binding (Fig. 5). Two criteria must be met for simple application of this, *i.e.*, without requiring major corrections: 1) the quinone occupancy at the Q_B site should be complete in the absence of stigmatellin at all pH values (full reconstitution of the Q_B activity), and 2) the lifetimes of the fast and slow components should be distinguishable at all (especially at very high) pH values. In the case of RC solubilized in detergent, the lifetimes of the two components at high pH values are rather close, but good signal-to-noise is obtained at high RC concentration and reliable decomposition of the kinetics can be achieved. The opposite case applies to chromatophores: the signal size is small compared to that of RC in detergent, but the slow component is much slower than the fast component (and the quinone occupancy remains close to 100%) even at pH 11. This is due to the larger free energy gap between the two quinones of the RC in chromatophores than in detergents.

We observed that the inhibitory effect of stigmatellin is pH-dependent, becoming less effective at high pH. The effect is more pronounced for RC in chromatophores than in detergent solution. Figure 5 shows systematic stigmatellin-titrations at low and high (fixed) pH values where the stigmatellin is largely protonated (pH 8.5) and deprotonated (pH ≥ 10.5). The data clearly show that the binding affinity of the stigmatellin to the RC decreases with increasing pH – by two orders of magnitude in chromatophores, but only a factor of 4 in micellar solution.

Discussions

The direct and separate measurements of binding and protonation state of stigmatellin provide the basis for determining the role of the phenolic group in the binding affinity to the Q_B site. Based on results obtained in this work and available in the literature, we will concentrate our discussion on structural and functional aspects of stigmatellin binding and on further possible benefits regarding the physical-chemical properties of protonated semiquinone in the RC.

Binding of stigmatellin

The titrations of Figure 5 show stigmatellin to be a very effective competitor of quinone at the Q_B site of the RC both in detergent and in native membranes (chromatophores). The effective quinone content was different in the two sets of experiments. In chromatophores, the ratio of the quinone and RC concentrations in the membrane is about 30, and the

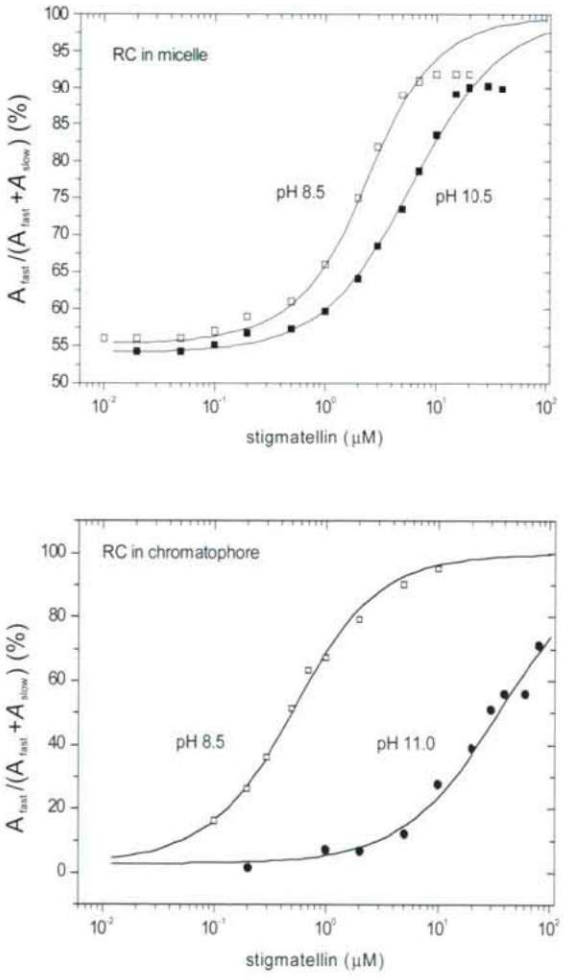

Figure 5. Concentration-dependence of the inhibitory effect of stigmatellin on photochemistry of RC in detergent Triton X-100 (top) and embedded in chromatophores of cytochrome-less mutant of *Rb. sphaeroides* (bottom). The inhibition of stigmatellin is characterized by the relative amplitude of the fast phase of the charge recombination kinetics detected at 865 nm (top) and 603 nm (bottom) after a single saturating flash excitation. Conditions: 0.03% Triton X-100, 2.21 μM RC and 5 mM Tris at pH 8.5 and 0.03% Triton X-100, 2.0 μM RC and 5 mM Caps at pH 10.5 (top), 280 nM RC, 100 mM NaCl and 10 mM Tris (bottom).

Q_B occupancy is large (only slow phase recombination can be detected even at very high pH; Fig. 5 bottom). In detergent, the quinone level was low (only endogenous Q was present, *i.e.*, no quinone was externally added) and only about half of the RC had quinone bound at the Q_B site. Somewhat surprisingly, the fraction of slow phase of the charge recombination remained unchanged upon pH increase (Fig. 5 top), even though both the quinone affinity and the interquinone one-electron equilibrium constant are strongly pH-dependent in this pH range. However, this is consistent with the low detergent concentration, in which all the quinone is present in RC-detergent mixed micelles, whether bound to the Q_B or not. Following light activation, the interquinone electron transfer equilibrium can pull unbound quinone rapidly to the Q_B site of the RC (see for details Stein et al. 1984; Shinkarev and Wraight 1997). In the presence of stigmatellin, quinone is displaced from the Q_B site, but stigmatellin unbinds very slowly so that, even after light activation, the binding pattern established in the dark (before the flash) is preserved. Thus, the titration of stigmatellin assayed by the slow recombination kinetics reflects the quinone/stigmatellin binding equilibrium in the dark-adapted state. This interpretation is supported by the slow unbinding rate of the stigmatellin (k_{off} = 0.033 s^{-1}) relative to that of the $P^+Q_A^- \rightarrow PQ_A$ charge recombination (k_{fast} = 16.4 s^{-1}) observed in *Rb. capsulatus* (Ginet and Lavergne 2001).

Based on this model of a competitive, pre-flash binding equilibrium (see the Appendix), the dissociation constants of stigmatellin can be estimated. In micellar solution, using K_Q = 1.7 μM (in 0.1 % LDAO) for the dissociation constant of ubiquinone-10 (McComb et al. 1990) and [Q] = 2.4 μM, we obtain K_S = 0.4 μM at pH 8.5 and K_S = 1.8 μM at pH 10.5 for the dissociation constant of the stigmatellin. The value of K_S = 400 nM at pH 8.5 is significantly larger than that obtained earlier (50 nM) by von Jagow and Ohnishi (1985). The reason is unclear. In chromatophores, the conditions are less defined. Assuming linear partition in the membrane, thus taking bulk concentrations for the RC (300 nM) and for the size of the quinone pool (9 μM), we get K_S = 4 nM at pH 8.5 and K_S = 350 nM at pH 11.0 if K_Q = 100 nM. (Actually, K_S/K_Q ratio can be determined from the best fit. The very low amplitude of the fast phase of the charge recombination gives only an upper limit for the quinone dissociation constant: K_Q < 200 nM.)

The protonated form of stigmatellin had much higher binding affinity to the RC than the unprotonated form. As both forms are present in the pH region around the pK of the phenolic group, the binding pattern of the Q_B site becomes more complex: in addition to the quinone (naturally present in chromatophore), the protonated and deprotonated components of the stigmatellin compete for the same binding site. The evaluation of the model and the discussion of the consequences are challenging tasks but are beyond the capacity of this work.

The observed difference in binding affinity of the unprotonated and protonated states of the stigmatellin may be partly due to changes in the H-bond network that stabilizes the bound stigmatellin to the RC (see later) and partly to the electrostatics. The RC becomes increasingly negatively charged at higher pH, which may provide a global repulsion to the unprotonated (anionic) stigmatellin. Similarly, electrostatics may play a role in the dramatically decreased binding affinity of stigmatellin at high pH in chromatophores relative to that in detergent – the negative surface charge of the membrane may greatly diminish the effective partition coefficient for the unprotonated stigmatellin. Based on our experiments, we cannot argue that the anionic stigmatellin is less likely to partition linearly than the protonated species, just mean that the anionic partition will be smaller than the neutral form. Further investigations are needed to make sharper distinctions.

Stigmatellin bound to the Q_B pocket of the RC significantly modifies not only the function of the RC by inhibiting the electron transfer, but also perturbs interactions between the donor and acceptor sides, within the protein. In chromatophores of *Rb. capsulatus*, it has been shown that stigmatellin in the Q_B site may shift the midpoint potential ($E_{m,P}$) of the bacteriochlorophyll dimer (P/P^+) (Ginet and Lavergne 2000). The shift is significant when the primary quinone is reduced (Q_A^-): $E_{m,P}(Q_A^-\ldots)$ = 507 mV and $E_{m,P}(Q_A^-$ stig) = 449 mV, thus the shift is $\Delta E_{m,P}(Q_A^-$ stig) = 58 mV. In case of terbutryne, the shift is insignificant: $\Delta E_{m,P}(Q_A^-$ terb) = 4 mV. Thus, stigmatellin stabilizes the oxidized state of the dimer if Q_A is reduced. The interactions between P/P^+ and Q_A/Q_A^- are markedly modified by the condition of the Q_B binding pocket (empty or occupied by ubiquinone, terbutryne or stigmatellin).

Structural view of stigmatellin binding to the RC

Lancaster and Michel (1997) determined the crystal structures of RCs from *Rhodopseudomonas viridis* with ubiquinone-2 (refined at 2.45 Å resolution, PDB entry code 2PRC) and stigmatellin (refined at 2.4 Å resolution, PDB entry code 4PRC) at the Q_B binding site (Fig. 6). The geometry and the stabilizing interactions of the quinone and stigmatellin binding are similar. The quinone ring and the chromone ring of the stigmatellin are in the same plane. The stigmatellin is bound to the Q_B site with the titratable hydroxyl group at essentially the same position as a keto oxygen of the ubiquinone, the same keto oxygen that is believed to become protonated during the second electron reduction (the first protonation event) of Q_B. It appeared that the pK of stigmatellin was above 11 in native RC but decreased to 9.5 in L213Asp → Asn mutant RC that is very close to the value observed for stigmatellin in solution (Graige et al. 1996). Although this is a promising result to use stigmatellin as electrostatic probe of the Q_B binding site,

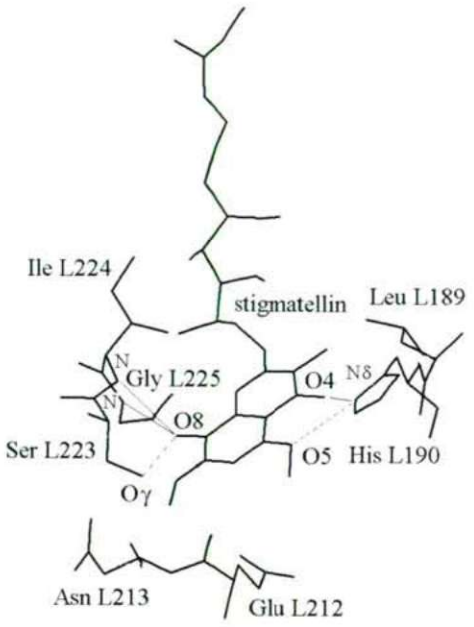

Figure 6. Stigmatellin in Q_B binding site of RC from *Rhodopseudomonas viridis* (the coordinates were taken from Protein Data Bank with accession code 4PRC). Thin solid lines: H-bond interactions present also if the binding domain is occupied by ubiquinone (His L190 Nδ – stig O4, Ile L224 N – stig O8 and Gly L225 N – stig O8) and dashed lines: extra hydrogen bonds for further stabilization of stigmatellin binding (His L190 Nδ – stig O5 and stig O8 – Ser L223 Oγ).

further investigations are needed (see below).

All of the interactions implicated in the binding of the ubiquinone headgroup are also implicated in the binding of the stigmatellin headgroup: the hydrogen bonds for quinone binding (His L190 Nδ – O4, Ile L224 N – O1 and Gly L225 N – O1) are also associated with stigmatellin binding (His L190 Nδ – O4, Ile L224 N – O8 and Gly L225 N – O8). However, two additional hydrogen bonds stabilize the binding of stigmatellin over that of ubiquinone. First, the stigmatellin proximal methoxy oxygen atom (O5) can act as a second acceptor of a hydrogen bond from the His L190 Nδ atom. Second, the Ser L223 Oγ atom accepts a hydrogen bond from the stigmatellin hydroxyl group (O8). These two additional hydrogen bonding interactions may explain the higher affinity of stigmatellin to the Q_B site as compared to quinone in RCs from *Rb. sphaeroides* (Giangiacomo et al. 1987). The hydrogen bond interaction with Ser L223 Oγ seems to be crucial in stigmatellin binding, as mutation of Ser L223 to Ala made the RC of *Rb. sphaeroides* resistant to stigmatellin (Paddock et al. 1995). The distances between H-bonding donors and acceptors can be derived from the *Rp. viridis* RC-stigmatellin structure data (PDB code 4PRC) and are listed in Table 2. The distances are short enough (average of 3.0 Å) to assure relatively strong H-bonds. The Oγ atom of Ser L223 is closest to the hydroxyl group (O8) of the stigmatellin (2.8 Å), and most likely makes the strongest H-bond.

If the ambient pH exceeds pK, the level of anionic stigmatellin becomes significant. Deprotonation of the hydroxyl group of the stigmatellin weakens the binding affinity via loss of H-bond donation from the stigmatellin to Ser L223 Oγ (stigmatellin is the proton donor) and by straightforward coulombic forces. On the other hand, deprotonation of the stigmatellin strengthens H-bond donation from the Ile L224 N and Gly L225 peptide NH groups (they are hydrogen-binding donors). These effects together will cause pH-dependent change of the binding affinity of stigmatellin to the Q_B binding site as was observed in our experiments. We might expect that the relatively small distinction between the affinity for protonated and unprotonated stigmatellin seen in isolated RCs more closely reflects the purely structural influences of the Q_B site, whereas the much greater distinction seen in chromatophores includes more extensive electrostatic influences in the membrane phase.

Stigmatellin as possible electrostatic probe

The measured pK values of the OH group of the stigmatellin showed large variation in different environments indicating sensitive changes of the interactions (Fig. 4 and Table 1). The interaction energy between the stigmatellin and the environment can include solvation energy of the stigmatellin in different (aqueous, detergent, membrane) phases, loose association (nonspecific binding, Kálmán et al. 1997) with the RC protein or electrostatic energy. If the last term dominates the interaction (or the other terms can be separated) then the stigmatellin may work like a molecular probe of the environment. The observed pK shift of the phenolic proton, ΔpK, is a direct indicator of the change in the prevailing electrostatic potential, $\Delta\psi$:

$$\Delta pK = -\frac{\Delta\psi}{60\ \text{mV}} \qquad (2)$$

Here, the proportionality factor 60 mV is calculated from the Boltzmann expression for the thermal energy ($2.303k_BT$) at room temperature. One unit of pK shift corresponds to –60 mV change in electrostatic potential. $\Delta pK \approx 0.3$ pH unit

Table 2. Distances between hydrogen-bonding donors (D) and acceptors (A) in the Q_B site for *Rp. viridis* RC-stigmatellin crystals (Protein Data Bank with accession code 4PRC).

D	A	D-A (Å)
His L190 Nδ	Stig O4	2.7
His L190 Nδ	Stig O5	3.1
Ile L224 N	Stig O8	3.0
Gly L225 N	Stig O8	3.1
Stig O8	Ser L223 Oγ	2.8

upshift is observed in RC relative to that in detergent (n-octyl-β-D-glycopyranoside) that might be a consequence of negative surface potential of the protein ($\Delta\psi \approx -20$ mV).

It would be more interesting and important to probe inside the binding pocket. Preliminary experiments indicate that no major changes can be observed between pK values of stigmatellin inside (added in stoichiometric quantity to the RC) and outside (added in large access to the RC). However, we can predict significant changes if the electrostatics of the binding pocket is artificially modified by site-directed mutagenesis of key amino acids. Graige et al. (1996) removed a negative charge from the vicinity of the bound stigmatellin by mutation of Asp for Asn at position L213 (AspL213 → Asn) and the pK downshifted from an unidentified high value (pK >> 10.6) to about 10, a value closer to the "solutional" pK. Assuming that this pK downshift comes from a single strong Coulombic interaction between the negative charges on the carboxylate of AspL213 and carbonyl oxygen of the stigmatellin, the effective potential at O8 can be calculated:

$$\Delta\psi = \frac{1}{4\pi\varepsilon_0} \cdot \frac{e}{\varepsilon_r \cdot r} \qquad (3)$$

where e is the elementary charge ($e = 1.6 \cdot 10^{-19}$ C), ε_0 (= $8.854 \cdot 10^{-12}$ As/Vm) and ε_r are the absolute and relative dielectric constants, respectively, and r is the (average) distance between O8 of the stigmatellin and the carboxylic oxygens of AspL213. Using $\Delta pK \geq -1.5$, *i.e.* based on Eq. (2) $\Delta\psi \geq +90$ mV and $r = 7$ Å (obtained from the 4PRC crystal structure), we obtain rather small value for the effective dielectric constant: $\varepsilon_r < 20$. This indicates that the interaction is only moderately screened by polarizable molecules. The stigmatellin (and also the native ubiquinone) is bound to a highly hydrophobic region of the Q_B binding pocket and the X-ray structures reveal only very few water molecules in the immediate vicinity.

Appendix

Scheme of binding equilibrium between quinone (Q) and stigmatellin (S) to the Q_B site of the RC in the oxidized state of the primary quinone Q_A (in the dark or under pre-flash conditions):

$$Q_A S \xleftarrow{K_S} Q_A \xleftarrow{K_Q} Q_A Q_B$$

Here K_S and K_Q are the dissociation constants of the stigmatellin and quinone, respectively. The RC, the quinone and the stigmatellin can be found either in free or in bound forms, thus their total amounts (concentrations, denoted by [..]) can be expressed as

$$[RC_{total}] = [Q_A S] + [Q_A] + [Q_A Q_B] \qquad (A1)$$
$$[Q_{total}] = [Q_{free}] + [Q_A Q_B] \qquad (A2)$$
$$[S_{total}] = [S_{free}] + [Q_A S] \qquad (A3)$$

Under steady-state conditions

$$[Q_A] \cdot [S_{free}] = K_S \cdot [Q_A S] \qquad (A4)$$
$$[Q_A] \cdot [Q_{free}] = K_Q \cdot [Q_A Q_B] \qquad (A5)$$

There are 5 unknown quantities ($[Q_A]$, $[Q_{free}]$, $[S_{free}]$, $[Q_A S]$ and $[Q_A Q_B]$) and 5 equations which are solved numerically using MatCad 4.0 (Fig. 5)

Acknowledgments

This work was supported by OTKA (T-42680), TéT (I-46/99 and F-34/02), NSF (MCB 03-44449) and MTA-NSF (042/2000).

References

Blankenship RE, Madigan MT, Bauer CE (1995) *Anoxygenic Photosynthetic Bacteria.* Kluwer Academic Publishers, Dordrecht, The Netherlands.

Gerencsér L, Jánosi T, Laczkó G, Maróti P (2000) Kinetic limitations in turnover of photosynthetic bacterial reaction center protein. Acta Biol Szeged 44:45-52.

Giangiacomo KM, Robertson DE, Gunner MR, Dutton PL (1987) Stigmatellin and other Electron Transfer Inhibitors as Probes for the Q_B Binding Site in the Reaction Center of Photosynthetic Bacteria. In Biggins J ed., Progress in Photosynthesis Research. Martinus Nijhoff Publishers, Dordrecht, The Netherlands, pp. 409-412.

Ginet N, Lavergne J (2000) Interactions between the Donor and Acceptor Sides in Bacterial Reaction Centers. Biochemistry 39:16252-16262.

Ginet N, Lavergne J (2001) Equilibrium and Kinetic Parameters for the Binding of Inhibitors to the Q_B Pocket in Bacterial Chromatophores: Dependence on the State of Q_A. Biochemistry 40:1812-1823.

Graige MS, Paddock ML, Feher G, Okamura MY (1996) Using Stigmatellin to Probe the Electrostatic Environment of the Q_B Site in Bacterial RCs. Biophys J (Abstracts) 70: A11 (Abstr. # Su-AM-G7, 40th Annual Meeting of the Biophysical Society, in Baltimore, MD, February 17-21, 1996).

Graige MS, Paddock ML, Feher G, Okamura MY (1999) Observation of the Protonated Semiquinone Intermediate in Isolated Reaction Centers from *Rhodobacter sphaeroides:* Implications for the Mechanism of Electron and Proton Transfer in Proteins. Biochemistry 38:11465-11473.

Kálmán L, Gajda T, Sebban P, Maróti P (1997) pH-metric study of reaction centers from photosynthetic bacteria in micellar solutions: protonatable groups equilibrate with the aqueous bulk phase. Biochemistry 36:4489-4496.

Kleinfeld D, Okamura MY, Feher G (1984) Electron transfer in reaction centers of *Rhodopseudomonas sphaeroides* I. Determination of the charge recombination pathway of $D^+Q_A Q_B^-$ and free energy and kinetic relations between $Q_A^- Q_B$ and $Q_A Q_B^-$. Biochim Biophys Acta 766:126-140.

Lancaster CR, Michel H (1996) New insights into the X-ray structure of the reaction center from *Rhodopseudomonas viridis*. In: Reaction Centers of Photosynthetic Bacteria. Structure and Dynamics. Michel-Beyerle ME ed. Springer Verlag, Berlin, pp. 23-35.

Lancaster CR, Michel H (1997) The coupling of light-induced electron transfer and proton uptake as derived from crystal structures of reaction centres from *Rhodopseudomonas viridis* modified at the binding site of the secondary quinone, Q_B. Structure 5:1339-1359.

Lavergne J, Matthews C, Ginet N (1999) Electron and Proton Transfer on the Acceptor Side of the Reaction Center in Chromatophores of *Rhodobacter capsulatus:* Evidence for Direct Protonation of the Semiquinone State of Q_B. Biochemistry 38:4542-4552.

Maróti P, Wraight CA (1988) Flash-induced H^+ binding by bacterial photosynthetic reaction centers: Comparison of spectrophotometric and conductimetric methods. Biochim Biophys Acta 934:314-328.

McComb JC, Stein RR, Wraight CA (1990) Investigations on the influence of headgroup substitution and isoprene side-chain length in the function of primary and secondary quinines of bacterial reaction centers. Biochim Biophys Acta 1015:156-171.

McPherson PH, Schönfeld M, Paddock ML, Okamura MY, Feher G (1994) Protonation and free energy changes associated with formation of Q_BH_2 in native and Glu-L212→Gln mutant reaction centers from *Rhodobacter sphaeroides*. Biochemistry 33:1181-1193.

Michel H, Epp O, Deisenhofer J (1986) Pigment protein interactions in the photosynthetic reaction centre from *Rhodopseudomonas viridis*. EMBO J 5:2445-2451.

Oettmeier W, Godde D, Kunze B, Höfle G (1985) Stigmatellin. A dual type inhibitor of photosynthetic electron transport. Biochim Biophys Acta 807:216-219.

Oettmeier W, Preusse S (1987) Herbicide and quinone binding to chromatophores and reaction centers from *Rhodobacter sphaeroides*. Z Naturforsch 42c:690-692.

Paddock ML, Rongey SH, Abresch EC, Feher G, Okamura MY (1988) Reaction centers from three herbicide-resistant mutants of *Rhodobacter sphaeroides* 2.4.1: sequence analysis and preliminary characterization. Photosynth Res 17:75-96.

Paddock ML, Rongey SH, Feher G, Okamura MY (1989) Pathway of proton transfer in bacterial reaction centers: Replacement of glutamic acid 212 in the L subunit by glutamine inhibits quinone (secondary acceptor) turnover. Proc Natl Acad Sci USA 86:6602-6606.

Paddock ML, Feher G, Okamura MY (1995) Pathway of proton transfer in bacterial reaction centers: further investigations on the role of Ser L223 studied by site-directed mutagenesis. Biochemistry 34:15742-15750.

Percival MP, Baker NR (1991) Herbicides and photosynthesis. In: Baker NR, Percival MP eds. Herbicides pp. 1-26. Elsevier Science Publishers, Amsterdam, The Netherlands.

Shinkarev VP, Wraight CA (1997) The interaction of quinone and detergent with reaction centers of purple bacteria. 1. Slow quinone exchange between reaction center micelles and pure detergent micelles. Biophys J 72:2304-2319.

Stein RR, Castellvi AL, Bogacz JP, Wraight CA (1984) Herbicide-Quinone Competition in the Acceptor Complex of Photosynthetic Reaction Centers From *Rhodopseudomonas sphaeroides*: A Bacterial Model for PS-II-Herbicide Activity in Plants. J Cell Biochem 24:243-259.

Takahashi E, Wraight CA (1992) Proton and Electron Transfer in the Acceptor Quinone Complex of *Rhodobacter sphaeroides* Reaction Centers: Characterization of Site-Directed Mutants of the Two Ionizable Residues, Glu^{L212} and Asp^{L213}, in the Q_B Binding Site. Biochemistry 31(3):855-866.

Tischer W, Srotman H (1977) Relationship between inhibitor binding by chloroplasts and inhibition of photosynthetic electron transport. Biochim Biophys Acta 460:113-125.

Von Jagow G, Ohnishi T (1985) The chromone inhibitor stigmatellin-binding to the ubiquinol oxidation center at the C-side of the mitochondrial membrane. FEBS Lett 185:311-315.

Vermaas WFJ, Renger G, Arntzen CJ (1984) Herbicide/quinone binding interactions in photosystem II. Z Naturforsch 39c:368-373.

Wraight CA (1981) Oxidation-Reduction Physical Chemistry of the Acceptor Quinone Complex in Bacterial Photosynthetic Reaction Centers: Evidence for a New Model of Herbicide Activity. Israel J Chem 21:348-354.

Wraight CA, Stein RR (1983) Bacterial reaction centers as a model for photosystem II: turnover of the secondary acceptor quinone. In: Inoue Y, Crofts AR, Govindjee, Murata N, Renger G, Satoh K eds. The Oxygen Evolving System of Photosynthesis pp. 383-397. Academic Press, New York.

Wraight CA (2004) Proton and Electron Transfer in the Acceptor Quinone Complex of Bacterial Reaction Centers. Front Biosci 9:309-337.

Volume 48(1-4):35-38, 2004
Acta Biologica Szegediensis
http://www.sci.u-szeged.hu/ABS

ARTICLE

Genetic variability of astaxanthin-producing yeasts: random amplified polymorphic DNA (RAPD) analysis of *Phaffia rhodozyma* and *Xanthopyllomyces dendrorhous*

Zsuzsanna Palágyi[1], Tamás Papp[1], Miklós Takó[1], Ágnes Nagy[2], Miklós Pesti[2], Csaba Vágvölgyi[1]*

[1]Department of Microbiology, Faculty of Sciences, University of Szeged, Szeged, Hungary, and [2]Department of General and Environmental Microbiology, Faculty of Sciences, University of Pécs, Pécs, Hungary

ABSTRACT Astaxanthin (3,3'-dihydroxy-β,β-carotene-4,4'-dione)-accumulating yeasts are of great biotechnological interest. Random amplified polymorphic DNA (RAPD) analysis involving 5 primers and 13 astaxanthin-producing yeast strains was performed. Cluster analysis based on RAPD markers differentiated isolates of *Xanthopyllomyces dendrorhous* (self-sporulating) and *Phaffia rhodozyma* (asexual) at an intraspecific level. Strains considered to be derived from the same isolate, but which had had different strain histories, revealed significant differences in their RAPD patterns. The applicability of RAPD analysis for the species-level differentiation of these yeasts is discussed.

Acta Biol Szeged 48(1-4):35-38 (2004)

KEY WORDS

astaxanthin
genetic variability
Phaffia rhodozyma
RAPD
Xanthopyllomyces dendrorhous

Phaffia rhodozyma was described by Miller et al. (1976). The accumulation of astaxanthin (3,3'-dihydroxy-β,β-carotene-4,4'-dione) as primary pigment in this red yeast created considerable biotechnological interest (Johnson and An 1991; Johnson and Schroeder 1996). Although astaxanthin is found in nature in several organisms (e.g. certain marine fish, crustaceans and birds), the number of natural sources of practical value is very limited. At the same time, both the aquaculture industry (as a feed supplement for salmon and trout) and various other applications connected with the excellent antioxidant properties of astaxanthin (Schroeder and Johnson 1993) demand substantial amounts of this carotenoid.

Golubev (1995) described the sexual cycle of this yeast and of the teleomorph *Xanthopyllomyces dendrorhous*, proposed to be con-specific with the anamorph *P. rhodozyma*. However, a number of data have accumulated that contradict this assumption. Kucsera et al. (1998) studied 6 isolates and suggested that *X. dendrorhous* and *P. rhodozyma* are different yeast species: the type strain of *P. rhodozyma* (CBS 5905) differed from all the other investigated isolates as it was able to reproduce only asexually and it produced respiratory-deficient petite mutants. Similarly, when the same 6 isolates were screened for the presence of extrachromosomal genetic elements, all proved to harbour double-stranded DNA plasmids, with the exception of *P. rhodozyma* type strain CBS 5905 (Pfeiffer et al. 1994). The most convincing evidence for the separation of the two proposed yeast species has been obtained through the analysis of their rDNA IGS (intergenic spacer) and ITS (internal transcribed spacer) sequences (Fell and Blatt 1999). The phylogentic trees based on these data suggested the species-level separation of the CBS 5905 isolates (*P. rhodozyma*) and 4 other isolates (*X. dendrorhous*).

Random amplified polymorphic DNA (RAPD) analysis has proved to be a rapid and very sensitive molecular method when genetic polymorphism is to be detected (Williams et al. 1990). This assay has been employed for the characterization of many fungi, e.g. *Rhizomucor* (Vastag et al. 2000), *Gilbertella* (Papp et al. 2003) and *Rhizopus* (Vágvölgyi et al. 2004).

The aim of the present study was to investigate the utility of DNA polymorphisms detected by RAPD analysis for astaxanthin-producing yeasts. Five random primers were tested for their ability to detect variability among 13 yeast strains, and cluster analysis was performed on the basis of these data.

Materials and Methods

Microorganisms, media and culture conditions

The names and origins of the 13 yeast strains examined are listed in Table 1. On the basis of their collection codes, some of the strains (1, 7, 8 and 10; 2 and 4) were regarded as originating from the same isolate, but they were obtained independently from different culture collections. Three strains of *Cryptococcus sp.* (designated Cr1, Cr69 and Cr76) were used as outgroups for numerical analysis. The strains were maintained on yeast-malt extract agar (YM: 0.5% malt extract, 0.25% yeast extract, 1% glucose, 0.25% peptone and 1.5% agar) slants at 4°C. For nucleic acid extractions, the strains were cultivated in liquid YM medium at 18°C with continuous shaking (200 rpm).

Accepted Sept 10, 2004
*Corresponding author. E-mail: csaba@bio.u-szeged.hu

Table 1. List of the astaxanthin-producing yeast strains investigated.

	Original code[a]	Other code[b]	Source[c,d]
1	CBS 5905	ATCC24202	ex *Fagus crenata*, Japan
2	CBS 5908	ATCC24203	ex *Alnus japonica*, Kiso, Japan
3	CBS 6938	CCRC22365	ex sap on stump of *Betula* sp., Finland
4	ATCC 24203	CBS 5908	ex *Alnus japonica*, Kiso, Japan
5	ATCC 24229	-	ex *Cornus brachypoda*, Hiroshima, Japan
6	ATCC 24261	-	ex *Betula maximowicyiana*, Yamagata, Japan
7	CBS 5905	ATCC24202	ex *Fagus crenata*, Japan
8	CBS 5905	ATCC24202	ex *Fagus crenata*, Japan
9	ATCC 24228	-	ex *Betula papyrifera*, Rainbow Lake, Alaska
10	CCY 77-1-1	CBS 5905	ex *Fagus crenata*, Japan
11	ATCC 24230	UCD 67-385	ex *Betula tauschii*, Kiso, Japan
12	W/IMP-UB	-	u.s., Norway
13	Z/IMP-UB	-	u.s., Norway

[a]The code which is used throughout this paper for clarity.
[b]Abbreviations: ATCC: American Type Culture Collection, Manassas, VA, USA. CBS: Centralalbureau voor Schimmelcultures, Utrecht, The Netherlands. CCRC: Culture Collection and Research Center, Food Industry Research and Development Institute, Hsinchu, Taiwan. CCY: Czechoslovak Collection of Yeasts, Bratislava, Slovakia. IMP-UB: Institute of Microbiology and Plant Physiology, University of Bergen, Norway. UCD: H. J. Phaff Yeast Culture Collection, University of California Davis, Davis, CA, USA.
[c]Strains regarded as the same, but obtained independently from different sources: 1, 7, 8 and 10; 2 and 4.

RAPD analysis

Total DNA was isolated by a modification of the method of Leach et al. (1986). Yeast DNA sequences were amplified by the 10-mer primers OPC-02 (5′-GTGAGGCGTC-3′), OPC-04 (5′-CCGCATCTAC-3′), OPC-05 (5′-GATGACCGCC-3′), OPC-07 (5′-GTCCCGACGA-3′) and OPC-08 (5′-TGGACC-GGTG-3′) from Operon Kit C (QIAGEN Operon, Alameda, CA, USA).

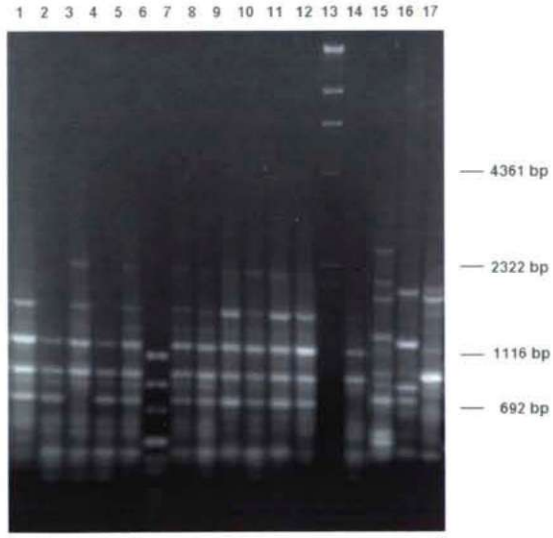

Figure 1. Representative amplification patterns of *Phaffia*, *Xanthophyllomyces* and *Cryptococcus* strains obtained with OPC-02 used as primer. Lane 6, pUC Mix Marker DNA as size standard (Fermentas). Lane 13, *Hind*III-digested λ DNA as size standard (Fermentas). Lanes 1-5, strains 1, 2, 3, 4 and 5, respectively. Lanes 7-12, strains 6, 8, 9, 10, 11 and 12, respectively. Lane 14, strain 13. Lanes 15-17, *Cryptococcus* strains Cr1, Cr69 and Cr76, respectively.

Amplifications were performed as described earlier (Vastag et al. 2000), with slight modifications. The reaction mixtures (25 µl) contained 1 x PCR buffer (10 mM Tris-HCl, pH 9.0, 50 mM KCl, 1.5 mM $MgCl_2$ and 0.1% Triton X-100), 200 µM each of the dNTPs (Pharmacia, Peapack, NJ, USA), 2.5 mM $MgCl_2$, 0.2 µM primer, 0.5 U of Taq DNA polymerase (Zenon, Oakville, ON, Canada) and 125 ng of genomic DNA. Samples were overlayered with 40 µl of sterile mineral oil (Sigma, Budapest, Hungary). Control reactions, without genomic DNA extract, were also run.

PCR was carried out with a PTC-100-60 DNA programmable thermal controller (MJ Research, Waltham, MA, USA) set for a denaturation step at 93°C for 1 min, followed by 45 cycles at 92°C for 1 min, at 37°C for 1 min and at 72°C for 1 min. An extension step at 72°C for 6 min was applied after the final amplification cycle.

The amplification products (10 µl of each reaction) were analysed by electrophoresis on 0.9% agarose gels in TAE

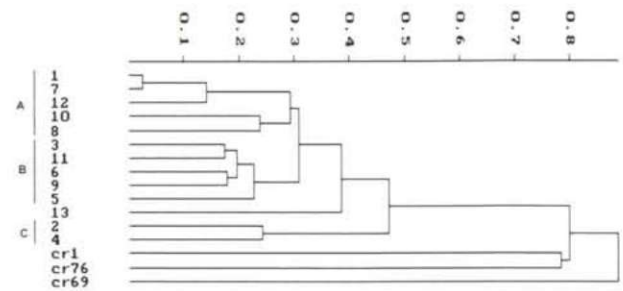

Figure 2. Dendogram obtained by UPGMA linkage with clustering of Jaccard coefficients calculated from RAPD data. The scale represents dissimilarity (squared distance). The strain numbers on the left are those listed in Table 1. The cophenetic correlation coefficient of the similarity matrix and the resulting dendogram was 0.9825.

buffer (40 mM Tris-acetic acid pH 7.6, plus 1 mM Na_2EDTA) containing 0.5 μg/ml ethidium bromide. Banding patterns were visualized by UV fluorescence. *Hind*III-digested λ DNA (Fermentas, Vilnius, Lithuania) and pUC Mix Marker (Fermentas) were used as size standards. Each isolate was analysed by RAPD-PCR at least 3 times.

Numerical analysis of the RAPD patterns

The RAPD banding patterns were analysed in order to determine the genetic relatedness of the isolates. A matrix based on the presence or absence of amplicons observed after electrophoretic separation was created. From these data, similarity matrix of Jaccard coefficients were calculated and used with the UPGMA (unweighted pair-group method using arithmetic averages) linkage (Sneath and Sokal 1973) to produce a dendogram. Numerical analysis was performed with the SYNTAX 5.0 software package (Podani 1993).

Results and Discussion

All 5 primers used efficiently amplified various regions of the investigated yeast genomes. They revealed different levels of variability, but in general a substantial level of polymorphism was detected among the 13 strains. As an example, results of the RAPD experiment with the OPC-02 primer are shown in Figure 1.

The data derived from the RAPD experiments were used for cluster analysis. A dendrogram was generated by using unweighted pair group average linkage clustering of the Jaccard coefficients. The dendrogram obtained is shown in Figure 2. Three *Cryptococcus* strains were used as outgroups during this analysis. The dendrogram revealed 3 clusters (A, B and C) and 4 unclustered strains. Among these, we found the 3 *Cryptococcus* strains used as outgroups. They differed at a high level both from all *Phaffia* and *Xanthophyllomyces* strains and from each other. Cluster A contains 5 *P. rhodozyma* strains (strain 1 is the type strain of *P. rhodozyma*). Among them, 4 strains (1, 7, 10 and 8) are known to be the same origin, but had undergone prolonged maintenance in different culture collections. Suprisingly, their RAPD patterns displayed characteristic differences. Members of this cluster are not able to sporulate, but are able to produce a respiratory-deficient petite mutant (Kucsera et al. 1998) and have a genome size higher than 20 Mbp (Nagy et al. 1994). In contrast, cluster B involves *Xanthophyllomyces* strains with sporulation capability, a petite-negative character and a genome size around 16 Mbp (Nagy et al. 1994). Cluster C contains 2 *Xanthophyllomyces* strains with a common origin (ATCC and CBS maintenance), but with several different RAPD markers. Strain 13 was situated as an unclustered strain in the dendrogram.

These results prove the applicability of the RAPD method for investigations of intraspecific variability and for determinations of strain-specific markers (*Phaffia* and *Xanthophyllomyces* strains separate well when RAPD markers are evaluated), but they also demonstrate some limits of this approach. Particularly as concerns culture collection strains which have undergone prolonged maintenance, special care is required in assessments of natural genetic variability. Interestingly, some of the *Xanthophyllomyces* strains (strains 2, 4 and 13) also revealed very high, nearly species-level differences from the other *Xanthophyllomyces* strains in this RAPD analysis.

This rather high intraspecific genetic variability might originate from the aneuploid or polyploid state of these yeasts. An earlier study relating to the electrophoretic karyotyping of some wild-type and mutagenized strains of *Xanthophyllomyces* raised questions concerning their haploid character (Nagy et al. 1997). A recent investigation (Hermosilla et al. 2003) concluded that *X. dendrorhous* is diploid. A similar result was obtained when the ploidy of the *P. rhodozyma* type strain (ATCC 24202) was evaluated via flow cytometric analyses of propidium iodide-stained cells and mutagenic inactivation kinetics (Medwid 1998): the findings suggested that *P. rhodozyma* is polyploid.

The results of the present study provide further information concerning the genetic make-up of the two astaxanthin-producing yeasts *P. rhodozyma* and *X. dendrorhous*, and help to identify genetic markers for the species delimitation which is not allowed by simple morphological traits.

Acknowledgments

This work was supported in part by the Hungarian Scientific Research Fund (OTKA) grants T37471 and F46658.

References

Fell JW, Blatt GM (1999) Separation of the strains of the yeasts *Xanthophyllomyces dendrorhous* and *Phaffia rhodozyma* based on rDNA IGS and ITS sequence analysis. J Ind Microbiol Biotechnol 23:677-681.

Golubev WI (1995) Perfect state of *Rhodomyces dendrorhous* (*Phaffia rhodozyma*). Yeast 11:101-110.

Hermosilla G, Martínez C, Retamales P, León R, Cifuentes V (2003) Genetic determination of ploidy level in *Xanthophyllomyces dendrorhous*. Anton Leeuw Int J G 84:279-287.

Johnson EA, An G-H (1991) Astaxanthin from microbial sources. CRC Crit Rev Biotechnol 11:297-326.

Johnson EA, Schroeder W (1996) Astaxanthin from the yeast *Phaffia rhodozyma*. Stud Mycol 38:81-90.

Kucsera J, Pfeiffer I, Ferenczy L (1998) Homothallic life cycle in the diploid red yeast *Xanthophyllomyces dendrorhous* (*Phaffia rhodozyma*). Anton Leeuw Int J G 73:163-168.

Leach J, Finkelstein DB, Rambosek JA (1986) Rapid miniprep of DNA from filamentous fungi. Fung Genet Newslett 33:32-33.

Medwid RD (1998) *Phaffia rhodozyma* is polyploid. J Ind Microbiol Biotechnol 21:228-232.

Nagy Á, Garamszegi N, Vágvölgyi Cs, Ferenczy L (1994) Electrophoretic karyotypes of *Phaffia rhodozyma* strains. FEMS Microbiol Lett 123:315-318.

Nagy Á, Palágyi Zs, Ferenczy L, Vágvölgyi Cs (1997) Radiation-induced chromosomal rearrangement as an aid to analysis of the genetic constitution of *Phaffia rhodozyma*. FEMS Microbiol Lett 152:249-254.

Palágyi Zs, Ferenczy L, Vágvölgyi Cs (2001) Carbon-source assimilation pattern of the astaxanthin producing yeast *Phaffia rhodozyma*. World J Microbiol Biotechnol 17:95-97.

Papp T, Vastag M, Nagy Á, Michailides TJ, Vágvölgyi Cs (2001) Genetic variability of the postharvest pathogen *Gilbertella persicaria*: identification of randomly amplified polymorphic DNA (RAPD) markers correlating with (+) and (-) mating types. Anton Leeuw Int J G 80:301-309.

Pfeiffer I, Kucsera J, Varga J, Ferenczy L (1994) Regulatory effect of linear DNA plasmids in *Phaffia rhodozyma*. 7th Int Congr Mycol Div IUMS, Prague, Abstracts p 364.

Podani J (1993) SYN-TAX-pc. Computer programs for multivariate data analysis in ecology and systematics. Version 5.0. User's Guide. Sciencia Publishing, Budapest, Hungary.

Schroeder WA, Johnson EA (1993) Antioxidant role of carotenoids in *Phaffia rhodozyma*. J Gen Microbiol 139:907-912.

Sneath PHA, Sokal RR (1973) Numerical Taxonomy. W.H. Freeman, San Francisco, CA, USA.

Vágvölgyi Cs, Heinrich H, Ács K, Papp T (2004) Genetic variability in the species *Rhizopus stolonifer*, assessed by random amplified polymorphic DNA analysis. Anton Leeuw Int J G 86:181-188.

Varga J, Vágvölgyi Cs, Nagy Á, Pfeiffer I, Ferenczy L (1995) Isoenzyme, restriction fragment length polymorphism and random amplified polymorphic DNA characterization of *Phaffia rhodozyma* Miller et al. Int J Syst Bacteriol 45:173-177.

Vastag M, Papp T, Kasza Zs, Vágvölgyi Cs (2000) Intraspecific variation in two species of *Rhizomucor* assessed by random amplified polymorphic DNA analysis. J Basic Microbiol 40:269-277.

Williams JGK, Kubelik AR Livak KJ, Rafalsky JA, Tingey SV (1990) DNA polymorphisms amplified by arbitrary primers are useful as genetic markers. Nucleic Acids Res 18:6531-6535.

Volume 48(1-4):39-42, 2004
Acta Biologica Szegediensis
http://www.sci.u-szeged.hu/ABS

ARTICLE

Developmental anomalies and other pathological lesions of the sternum in a medieval osteological sample

Gyula L. Farkas[1]*, László Józsa[2], László Paja[1]

[1]Department of Anthropology, University of Szeged, Szeged, Hungary, [2] Department of Morphology, National Institute of Traumatology, Budapest, Hungary

ABSTRACT We cannot often read about the developmental anomalies of the sternum in paleopathological literature (Brothwell 1965; Tóth and Buda 2001); medical publications on anomalies resulting in chest deformity based on recent population are also rare (Keszler and Szabó 1996). Fractures and inflammation of the sternum are fairly infrequent, and the symptoms of porotic hyperostosis caused by increased red blood cell production are seldom detected in osteological samples. Some developmental anomalies (e. g. sternum fenestratum, alterations of the xiphoid process) do not influence the function or physiological form of the chest, while others may change the shape and diameter of the chest causing difficulties in breathing and in heart function. Some genetic diseases, through the malfunction of the production of the connecting tissues' basic substantia and fibres, necessarily entail changes in the shape of the sternum. In individuals suffering from Marfan syndrome, sternum excavatum, while in individuals suffering from Hurler- and Morqio-syndrome (and other mucopolysaccharidosis cases), pectus gallinaceum can be observed. Other sternum anomalies resulting from non-genetic factors also seem to run in the family, though how they are inherited is not yet known. An anomaly called synchondrosis sternii develops during postnatal life, and means that the originally cartilaginous sternebrea do not become ossified, there remain synchondrosis between the parts even through the whole lifetime. This, however, does not cause abnormal chest movement. In some cases, the fracture of the sternum may lead to serious respiratory disfunction, and the healing of these injuries without any surgical intervention is not guaranteed. The development of pseudo-articulations may also cause abnormal chest movement. Osteomyelitis spreading to other organs may prove to be dangerous, even fatal.

KEY WORDS

14-15th century
paleopathological finds
sternum
developmental anomalies

Acta Biol Szeged 48(1-4):39-42 (2004)

It was in 1966, when 103 graves were dug out by archaeologist Mihály Kőhegyi at the site of Bátmonostor-Pusztafalu (15 km from Baja southward, Southern Hungary; Kőhegyi 1967). Later, between 1977 and 1986, Piroska Biczó continued the excavation: 2543 further graves were excavated. In Biczó's opinion, the cemetery dates back to the 14th-15th century, and 80% of the graves have been excavated (Biczó 1978-1986). We have to note, however, that this is the biggest medieval cemetery found in Hungary so far.

Materials and Methods

The age determination of the infant and adolescent individuals was carried out on the basis of the diaphyseal length of long bones (Stloukal and Hanáková 1978), the sequence of tooth formation and eruption (Ubekaler 1978) and the ossification of the epihyses based on X-ray examination (Schinz et al 1952). The age determination of adults was based on the method of Nemeskéri et al. (1960).

Sex determination of the skeletons was carried out on the basis of 24 metric and non-metric morphological characteristics of the skull and post-cranial bones showing sexual differences, which was possible only in case of adult and some juvenile individuals (Éry et al. 1963). Anatomic variations were detected in a large number of cases (827), while further 868 cases of other pathological lesions were observed (often several different kinds in one individual). The above shows the finds' anthropological importance. During the paleopathological analysis the sternal length and its possible alterations were measured in millimetres. In case of sternums of irregular shape, the angular deviation was recorded, the angle between the two distal parts was measured.

Anthropological data

3782 individuals' skeletal remains were found in 2646 graves; more than one individual was found in 444 graves. A considerable part of skeletons (1510 cases, 39.9%) belongs to the Infantia I and II categories, while the Juvenis age category includes 153 skeletons (4.05 %). Among skeletal remains of adults (>21 years of age; Adultus, Maturus and Senium categories) 1342 males (35.48%) were determined, while in

Accepted Jan 29, 2004
*Corresponding author. E-mail: farlgy@bio.u-szeged.hu

Figure 1. Bifurcation of the xiphoid process (grave 2114, Mat., male).

Figure 2. Sternum bifidum (grave 1774, adult, male).

719 cases characteristics of females can be seen. During the excavation, as a result of the careful rescue, the remains of 39 foetuses were rescued (included in the Infantia category). Unfortunately, in case of 123 (3.18%) skeletons, neither the sex, nor the age at death was determinable.

Results

Developmental alterations

Anomalies were detected in 40 breast-bones, among which the co-existence of two alterations can be seen in only two cases, in the rest of cases only one lesion was observed. In four cases the change of the xiphoid process was found, in one of them the two branches of the splitted process were at right angles. In two further cases the distal two-third of the breastbone showed a V-shaped bifurcation, the branches closed at an angle of 35 and 60 degrees, respectively (Fig. 1). Sternum bifidum was determined in five cases (Fig. 2). Synchondrosis sternii (incomplete ossification of the sternum) was recorded in 7 cases. Other anomalies in the shape of the sternum (wedge-shaped or asymmetrical bone) were found in two cases (Table 1).

The large number of sternum gallinaceum cases must be noted. The anomaly both occured in small children (Infantia

Table 1. Developmental anomalies of the sternum at the finds from Bátmonostor.

Grave No.	Age at death	Sex	Grave No.	Age at death	Sex
	Fenestratio			Synchondrosis	
814	Juv.	male	182	Mat.	female
1107	Sen.	male	259	Mat.	female
1456	Sen.	male	355	Mat.	female
1740	Mat.	female	747	Mat.	female
1992	Ad.	female	1278	Ad.-Mat.	male
2126.	Sen.	male	1383	Mat.	male
2148.	Juv.	?	2431	Mat.	male
2382	Ad.	male		Sternum bifidum	
2551.	Mat.-Sen.	female	1278	Ad.-Mat.	male
2557	Mat.-Sen.	male	1774	adult	male
B/XXIII.	?	?	1814	Ad.	male
	Anomalies of the xiphoid process		2518	Mat.	male
767	Ad.	male	2567	Inf. II	?
1217	Ad.	male		Other morphological anomalies	
1941	Mat.	male	898	Mat.	female
2114	Mat.	male	137/b	?	?

Figure 3. Pectus gallinaceum (grave 1414, Mat., female).

I) and old individuals, mostly affected males (as all other anomalies). The deviation ranged from 10 degrees to 46. (Table 2, Fig. 3).

Other pathological anomalies

Other pathological anomalies were detected on 13 sternums. Osteomyelitis of the sternum in two cases, periostitis in four cases was recorded. Three sternums were broken, all partially ossified. Two cases of purulent arthritis of the sternoclavicular joint were observed, which went together with the fracture of the clavicle and osteomyelitis. On two sternums traces of porotic hyperostosis can be seen. (Table 3).

Discussion

The body of the sternum and the xiphoid process are originally formed of cartilaginous tissue, the fusion and ossification of the bone becomes complete in postnatal life. Sternum fenestratum indicates abnormal ossification (Ashley 1956).

Perforated sternum is the most common abnormality (Tóth et al. 2001), but bears no pathological significance. The mechanism of the formation of pectus gallinaceum is not yet understood. In such cases the length and shape of the ribs are affected. Pectus gallinaceum often occurs with serious curvature of the spine (kyphoscoliosis), though we did not find any such cases.

Although we seldom had the opportunity to examine all the bones of the chest, it is supposed that there was no major chest deformity in this sample. Most individuals suffering from pectus gallinaceum were adults at death (Adultus or

Table 2. The occurence of pectus gallinaceum.

Grave No.	Age at death	Sex	Angle of deviation	Sternal length (mm)	Other pathological alterations
767	Ad.	male	30°	-	Anomaly of xiphoid process
858	adult	male	46°	80	
1028	?	?	38°	130	
1107	Sen.	male	30°	140	
1383	Mat.	male	10°	130	
1414	Mat.	female	32°	140	
1473/a	Inf.I.	?	-	-	
2125	Mat.	female	39°	160	
2264	Ad.-Mat.	female	28°	150	
2372	Mat.	male	20°	160	
2395/a	adult	male	12°	170	Hyperostosis porotica
2567	Inf.II.	?	14°	80	
B/X.	?	?	20°	170	

Table 3. The pathological alterations of the sternum.

Grave No.	Age at death	Sex	Symptoms
1435	Inf.I.	?	Osteomyelitis pur.sterni
2607	Sen.	male	Ostitis et periostitis sterni
2148	Juv.	?	Fractura sterni
2330	Ad.	male	Fractura sterni
1440	Mat.	male	Fractura sterni
747	Mat.-Sen.	female	Periostitis sterni
1278	Ad.-Mat.	male	Periostitis sterni
1480/a	Ad.-Mat.	male	Periostitis sterni
2645	Sen.	male	Periostitis sterni
1134/a	Mat.	male	Arthritis pur.sternoclav.
1305	Sen.	male	Arthritis pur.sternoclav
814	Juv.	male	Hyperostosis porotica
2395/a	adult	male	Hyperostosis porotica

Maturus age categories), but we found some elderly persons (Senilis) as well. There seems to be male predominance in all congenital pathological cases. Sex could not be determined in 6 cases, taking into consideration the rest, male-female ratio is 2.4:1. The result must necessarily seen in the light that there were twice as many men than women in the sample. We can therefore say that congenital anomalies of the sternum are not sex-dependent.

Other pathological lesions (fracture, osteomyelitis, periostitis) also affected mostly males. Fractura sternii and osteomyelitis may prove fatal, but there is no evidence of that in our sample. Most pathological anomalies of the sternum we found were congenital, fractures and inflammations were quite rare.

Acknowledgments

Present study was supported by the Hungarian Science Foundation (OTKA No. TO 32824).

References

Ashley GT (1956) The relationship between the pattern of ossification and the definitive shape of the mesosternum in man. J Anat 90:87-105.

Biczó P (1978-1986) Bátmonostor-Pusztafalu (Bács-Kiskun m.). Régészeti Füzetek 31:93-94, 32:108-109, 33:90, 34:86, 35:100, 36:90, 37:101, 38:89, 39:79.

Brothwell DR (1965) Digging up bones. London. pp. 167-169.

Éry K, Kralovánszky A, Nemeskéry J (1963) Történeti népességek rekonstrukciójának reprezentációja. Anthrop Közl. 7:41-90.

Keszler P, Szabó Gy.J (1996) Veleszületett mellkasi deformitások. Pathologia és sebészet. Akadémiai kiadó. Budapest. pp. 1-24.

Kőhegyi M (1967) Bátmonostor-Pusztafalu (Bács-Kiskun megye, bajai járás). Régészeti Füzetek 20:71-72.

Nemeskéri J, Harsányi L, Acsádi Gy (1960) Methoden zur Diagnose des Lebensalters von Skelettfunden. Anthrop Anz 24:71-88.

Schinz H, Baensch W, Friedl E, Uehlinger E (1952) Ossifikationstable. In: Lehrbuch der Röntgen-Diagnostik. 5, Aufl.–Thieme, Stuttgart.

Stloukal M, Hanáková H (1978) Die Lange der Langsknochen altslawischer Bevölkerungen. - Unter besonder Berücksichtigung von Wachstumsfragen. Homo 29:53-69.

Tóth G, Buda BL (2001) Funnel chest (pectus excavatum) in 10-16th century fossil material. J Paleopath 13:63-66.

Ubelaker AM (1978) Human skeletal remains. Excavation, analysis, interpretation. Taraxacum, Washington.

Volume 48(1-4):43-45, 2004
Acta Biologica Szegediensis
http://www.sci.u-szeged.hu/ABS

ARTICLE

The frequency of enthesopathies in the 14-15th century series of Bátmonostor-Pusztafalu

László Józsa[1], Gyula L Farkas[2]*, László Paja[2]

[1]Department of Morphology, National Institute of Traumatology, Budapest, Hungary, [2]Department of Anthropology, University of Szeged, Szeged, Hungary

ABSTRACT This study presents the frequency of enthesopathies in the osteological material of a medieval cemetery. The development of the phenomenon is explained as a result of the exerting way of living. The bony outgrows appear in the patellae and the calcanei the most frequently, and twice as much males are involved than females. The appearence of the lesions may be single, but in some cases multiple changes may also be seen on a skeleton.
Acta Biol Szeged 48(1-4):43-45 (2004)

KEY WORDS

paleopathology
enthesopathy
activity-dependent changes
14-15th century

Enthesopathy (synonyms: insertion tendinopathy, hyperostosis circumscripta, insertion osteopathy) is a bony alteration at the site of tendon and muscle insertions, the area known as enthesis. Enthesopathy develops as an adaptation to repeated traumatic effects or increased burden. The burden-dependent adaptation develops slowly. The symptoms depend on the range of burden, and if the burden stops, the alterations may regress. On the basis of our previous investigations (Józsa and Kannus 1997; Józsa and Pap 1997), comparing the normal and enthesopathic bony areas, there is no difference in the structure of the cortical and spongious parts.

The frequency of enthesopathy is 2-4% in recent populations. The lesions appear mainly at sportsmen, e.g. long-distance runners, walkers, ski-runners (Smart et al. 1980; Józsa et al. 1989; Porter et al. 1995). Contrary to this fact, enthesopathy could be recognized more frequently in osteoarcheological samples, where its incidence may reach 50% in certain populations (Dutour 1986). The development and localisation of enthesopathy may inform us about the way of life and the activities of the examined population. Alterations in the upper limbs may refer to physical labour of the trunk (e.g. smiths, fishermen or oarsmen), while the changes of the lower limbs and girdle may develop in walkers, runners and certain agricultural workers. As a curiosity, Rosenthal (1965) and His (1895) observed some alterations in the skeletal remains of Johann Sebastian Bach: well-developed enthesopathies can be seen in the hip-bones, the femora and the tibiae's posterior surface of the composer. In the opinion of Geyrot (2000), these changes were caused by exhausting movements; these lesions called to „organ-player disease" by Rosenthal. In addition, similar alterations could be seen in the X-ray pictures of Günther Raminn (he was also a choir-master at the Thomas Church between 1940 and 1956) as a result of the overburden of leg movement during organ playing (Geyrot 2000).

Enthesopathy can develop in any age category; we have described it in a 12-year-old individual (Józsa et al. 1991)– but it's frequency is higher in skeletons belonging to adult individuals.

In contrast to present populations, the individuals of Medieval Age walked more, their everyday life was not facilitated by engines, so the higher incidence of enthesopathies is not surprising. The well-preserved osteological series of Bátmonostor-Pusztafalu seemed to be well suited for the examination of the population's lifestyle from this point of view.

Materials and Methods

Bátmonostor-Pusztafalu, which is the largest medieval cemetery in Hungary, is situated in the Great Hungarian Plain, 15 km southward from Baja. As a result of the first excavation carried out by Mihály Kőhegyi in 1966, 103 graves were dug out. Later, during the second session of the excavation, made by Piroska Biczó resulted further 2543 graves.

The total number of individuals found in graves and reduction areas is 3783; among them 1510 skeletons belong to the infantia I and infantia II age categories. The number of juvenis individuals is 153, while the number of adult males is 1342, which is almost twice the number of adult female skeletons (719). In 123 cases neither the sex nor the precise age at death could be determined.

Our sample for analysis constituted 864 well-preserved skeletons showing pathological lesions.

The sex and age at death were determined by classical physical anthropological methods (Nemeskéri et al. 1960; Éry et al. 1963; Strouhal and Hanaková 1978; Ubelaker 1978).

Symptoms of enthesopathy are observable easily, as

Accepted June 4, 2004
*Corresponding author. E-mail: farlgy@bio.u-szeged.hu

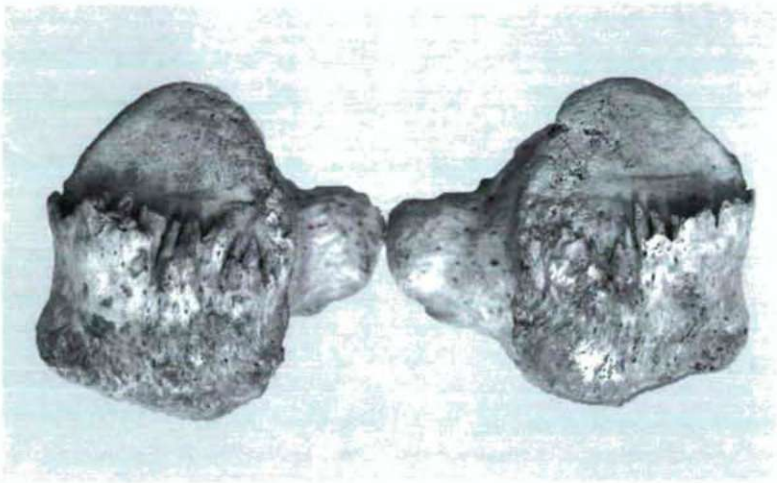

Figure 1. Bony outgrowths on the posterior surface of both calcaneus at the site of tendo calcaneus (Achilles tendon; grave XXXVII).

they could be seen macroscopically. The attached bones, the localisation and the degree of enthesopathic lesions were estimated by two examiners. In some interesting or particular cases, X-ray pictures were also taken.

Results

Entesopathy was not observable in infants' skeletal remains, and it was seen in only one juvenile individual. The frequency increased among the adultus age category, and the lesions were particularly frequent in individuals aged 41-60 years. The fact that advanced age individuals' skeletons are also involved refers to hard and permanent activity in older age.

The sex distribution of the 267 cases found in the sample showed strong male predominance, as only 54 cases occurred in female skeletons (20.2%).

Concerning localisation, the lesions occurred in calcanei the most frequently (238 cases; Fig. 1), the alterations in the patellas could be seen more rarely: 3 unilateral and 18 bilateral cases were found (Fig. 2). In six male skeletons the bony outgrows of the two sites appeared together. In another case the calcaneus and the ischial tuberosity were also affected. The lesions appeared in the tibia and in the femur together, in 3 skeletons the femoral changes could be seen mainly on the posterior surface. In another two cases, joint appearence of enthesopathies were observed. In the first case the femoral shaft and the ischial tuberosity, while in the second case, the

Figure 2. Bilateral enthesopathy of calcanei (grave 2126).

Table 1. Localisation, sex and age distribution of enthesopathies in the series of Bátmonostor-Pusztafalu.

Localisation	Age category	Male	Female	Total
Calcaneus l.d.	Adultus	3	2	5
	Maturus	15	2	17
	Senium	11	-	11
	?	9	-	9
Calcaneus l.s.	Juvenis	1	-	1
	Adultus	5	2	7
	Maturus	11	5	16
	Senium	5	4	9
	?	4	-	4
Calcaneus l..u.	Adultus	21	2	23
	Maturus	50	15	65
	Senium	33	17	50
	?	21	-	21
Patella l.d.	Maturus	2	-	2
	Senium	-	1	1
Patella l.u.	Adultus	2	-	2
	Maturus	12	-	12
	Senium	1	3	4
Humerus l.d.	Maturus	1	-	1
	Senium	-	1	1
Femur l.d.	Maturus	1	-	1
	Senium	1	-	1
Radius l.d.	Senium	1	-	1
Radius l..u.	Maturus	1	-	1
	Senium	1	-	1
Ulna l.u.	Maturus	1	-	1
Total		213	54	267

femur and the radius were affected. Humeral lesions related to enthesopathy could be seen in two cases, in one of them (grave 2249), the alteration was seen in the sulcus tendinis longi musculi bicipitis brachii. In a complex case (grave 1799) , the femori, the tibiae, the radii and the ulnae were affected.

Some of the authors interprete the symptoms of the DISH (Forestier's disease) as enthesopathy, but in our opinion the diffuse diopathic skeletal hyperostosis is a separate disease. So, the eight DISH cases found in the series will be published later.

Conclusions

The scientific study of osseous alterations produced by habitual patterns of activity is an important approach to get new information on the examined population. The results of our investigation correspond to earlier studies found in paleopathological literature: the alterations appear more frequently among adults, and they could also be seen in advanced age skeletal remains. More males than females were affected, this fact refers to the difference between the two sexes: males had harder activity. Concerning localisation, the most common sites were the calcanei and the patellae.

Acknowledgments

This study was supported by the Hungarian Science Foundation (OTKA No. TO 32824).

References

Dutour O (1986) Enthesopathies (lesions of muscular insertions) as indicators of the activities of Neolithic Saharan populations. Am J Phys Anthrop 71:221-224.

Éry K, Kralovánszky A, Nemeskéri J (1963) Történeti népessége rekonstrukciójának reprezentációja. Anthropol Közl 7:41-90.

Gejrot T (2000) Johann Sebastian Bachs kvarlevor hittades och identifierades efter ett idogt detektivarbete. Läkartidningen 97:3520-3521.

His W (1895) Johann Sebastian Bach. Forschungen über dessen Grabstätte, Gebeine und Anlitz. Bericht an der Stadt Leipzig. Vogel Verl. Leipzig.

Józsa L, Kannus P (1997) Human tendons. Anatomy, physiology and pathology. Human Kinetics Champaign III.

Józsa L, Pap I (1997) A sarokcsonti enthesopathia gyakorisága és morfológiája a középkorban és napjainkban. Osteológiai Közl 5:187-191.

Józsa L, Kvist M, Bálint BJ (1986) The role of recreational sport activity in Achiles tendon rupture. A clinical, pathological and sociological study of 292 cases. Am J Sports Med 17:338-343.

Józsa L, Pap I, Fóthi E (1991) Enthesopathies (insertion tendinopathies) as indicators of overuse of tendons and muscles in ancient Hungarian population. Annales Historico-Natur Mus Nat Hung 83:269-276.

Nemeskéri J, Harsányi L, Acsádi Gy (1960) Methoden und Diagnose des Lebensalters von Skelettfunden. Anthrop Anz 24:71-88.

Porter HH, Vandervoot HH, Lexell J (1995) Aging of human muscle, structure, function and adaptability. Scand J Med Sci Sports 5:129-142.

Rosenthal W (1965) Die Identifierung der Gebeine Johann Sebastian Bachs. Mit Bemerkungen über die „Organistkrankheit". Nova Acta Leopoldina Reiche 3. Halle/Saale.

Smart GW, Taunton JE, Clement DB (1980) Achilles tendon disorders in runners. Med Sci Sports Exerc 12:231-243.

Strouhal M, Hanakova H (1978) Die Lange der Langsknochen altslawischer Bevölkerungen unter besonder Berücksichtigung von Wachstumfragen. Homo 29:53-69.

Ubelaker AM (1978) Human skeletal remains. Excavation, analysis, interpretation. Taraxacum, Washington.

Volume 48(1-4):47, 2004
Acta Biologica Szegediensis
http://www.sci.u-szeged.hu/ABS

DISSERTATION SUMMARY

Towards an efficient and integrated biogas technology

Zoltán Bagi

Department of Biotechnology, University of Szeged, Szeged, Hungary, and Institute of Biophysics, Biological Research Center, Hungarian Academy of Sciences, Szeged, Hungary

Among the significant recent advances in understanding the ecology of anaerobic biodegradation of organic wastes is the recognition of the close syntropic relationship among the three distinct microbe populations and the importance of H2 in process control. (Dolfing et al. 1992; Shi-yi et al. 1992; Shima et al. 2002) The regulatory roles of hydrogen levels and interspecies hydrogen transfer optimize the concerted action of the entire population. The concentration of either acetate or hydrogen, or both together, can be reduced sufficiently to provide a favorable free-energy change for proportionate oxidation.

During anaerobic biodegradation hydrogen concentration is reduced to a much lower level than that of acetate. In addition, the hydrogen partial pressure can change rapidly, varying by an order of magnitude or more within a few minutes. This is related to its rapid turnover rate. The energy available to the acetate-using methanogens is independent of hydrogen partial pressure, whereas that of the hydrogen-producing and hydrogen-consuming species is very much a function of it.

We have shown that under these circumstances addition of hydrogen producers to the system and thereby shifting the population balance brings about advantageous effects for the entire methanogenic cascade (Kovács et al. 1987). The decomposition rate of the organic substrate increases and both the acetogenic and methanogenic activities are remarkably amplified. In laboratory experiments some 2.6-fold intensification of biogas productivity has been routinely observed and the same results were obtained in scale-up experiments.

Proper management of the bacterial population is expected to facilitate the start-up of the fermentation. In order to reduce the costs of this treatment supplemented bacteria are grown in diluted industrial wastewater.

In contrast to the commonly used factor of 0.6-0.8 that is used to estimate biogas yields, the integrated technology, using intensified microbiological biomass decomposition, should yield a two-three fold increase when using 15% solid content biomass. The integrated technology uses sugar accumulating energy plants (e.g., sweet sorghum, Jerusalem artichoke) to increase the biodegradable biomass density.

References

Kovács K, Bagyinka Cs, Verebély I (1989) Eljárás kevert baktériumpopulációt alkalmazó fermentációs rendszer biogázt termelőképességének fokozására. Szabadalom, lajstromszám: 195 978, 1987.

Dolfing J (1992) The energetic consequences of hydrogen gradients in methanogenic ecosystems. FEMS Microb Lett 101:183-187.

Shi-yi L, Jian C (1992) The contribution of interspecies hydrogen transfer to the substrate removal in methanogenesis. Proc Biochem 27:285-289.

Shima S, Warkentin E, Thauer RK, Ermler U (2002) Structure and function of enzymes involved in the methanogenic pathway utilizing carbon dioxide and molecular hydrogen. J Bios Bioengine 93:519-530.

Supervisor: Kornél Kovács
E-mail: bagiz@nucleus.szbk.u-szeged.hu

Volume 48(1-4):49, 2004
Acta Biologica Szegediensis
http://www.sci.u-szeged.hu/ABS

DISSERTATION SUMMARY

In vivo ROS detection in UV-stressed leaves

Csengele Barta

Laboratory of Molecular Stress and Photobiology, Institute of Plant Biology, Biological Research Center, Hungarian Academy of Sciences, Szeged, Hungary

During their life cycle plants are daily exposed to adverse environmental impacts, since light, temperature or water conditions are often far from optimal. Various stress conditions affect a number of metabolic functions in plants through the generation of reactive oxygen species (ROS). Under field conditions, plants are often exposed to high PAR irradiances as well as to ultraviolet (UV) radiation. The solar radiation reaching the Earth's surface is divided into UV-B (280-320 nm), UV-A (320-400 nm) and visible (PAR: 400-700 nm) radiation, the latter one being used for photosynthesis by the vegetation. ROS induction is known to be the early plant response to UV exposure. Previous studies showed, that high levels of UV-B radiation induce lipid peroxidation and oxidative membrane damage (Cen et al. 1994; Takeuchi et al. 1995). In isolated thylakoid membranes UV-B exposure triggered hydroxyl radical generation, but the presence of carbon centred (methyl-like), and peroxyl radicals were also reported (Hideg et al. 1996; Hideg et al. 1999). Singlet oxygen was not found in the same preparation. The difference in the action site of UV-A and UV-B in photosynthesis has been intensely discussed, attributing smaller damaging effect to the UV-A irradiation, than to the UV-B (Turcsányi et al. 2000; Flint et al. 2003).

Since the ROS generating abilities of various UV energies have not been compared yet, our goal was to study the nature of ROS involved in the stress by both UV-A and UV-B radiation *in vivo*, in leaves.

In order to understand the physiological functions of ROS generated under oxidative stress by UV radiation, their direct measurement in leaves is of special importance. Therefore, the short-lived ROS were detected by fluorescent sensors: the fluorescence of the sensors decreased upon their reaction with ROS. Spinach leaves were infiltrated with either the singlet oxygen sensitive DanePy or with the singlet oxygen and superoxide reactive HO-1889NH, then exposed to $2x10^{22}$ photons of quasi-monochromatic (±8 nm around central wavelength) UV radiation in the 280-390 nm range, corresponding to 18-36 μmol m^{-2} s^{-1}. The effect of UV radiation on the photosynthesis of various leaves was estimated from the relative decrease in their variable chlorophyll fluorescence.

We have found, that reactive oxygen production in leaves exposed to UV radiation was heterogeneous. Superoxide production was characteristic to the UV-B wavelength region but not to UV-A. The correlation between the UV-induced superoxide production and photosynthetic activity decrease of the leaves indicated, that the superoxide yielding primary reaction is localized in the chloroplasts, possibly in the thylakoid membranes. Singlet oxygen evolution was a characteristic UV-A induced physiological response, which we identified in plants for the first time. It was typical for irradiation by 340-390 nm, however its source is probably not localized inside the chloroplasts, since no correlation was found between the damage of the photosynthetic apparatus and the singlet oxygen production (Barta et al. 2004).

In summary, we have shown, that UV stress is a complex oxidative stress, inducing the production of various reactive oxygen species in plants.

References

Barta Cs, Kálai T, Vass I, Hideg K, Hideg É (2002) Dansyl- and rhodamine-based fluorescent sensors for detecting singlet oxygen and superoxide production in plants *in vivo*. Acta Biol Szeged 46:149-150.

Cen YP, Björn LO (1994) Action spectra from enhancement of ultraweak light emission by ultraviolet radiation (270-340 nm) in leaves of *Brassica napus*. J Photochem Photobiol B 22:125-129.

Takeuchi Y, Fukumoto R, Kasahra H, Sakaki T, Kitao M (1995) Peroxidation of lipids and growth inhibition induced by UV-B irradiation. Plant Cell Rep 14:566–570.

Turcsányi E, Vass I (2000) Inhibition of photosynthetic electron transport by UV-A radiation targets the photosystem II complex. Photochem Photobiol 72:513–520.

Flint SD, Caldwell MM (2003) A biological spectral weighting function for ozone depletion research with higher plants. Physiol Plant 117:137-144.

Supervisor: Éva Hideg
E-mail: csengele@nucleus.szbk.u-szeged.hu

Volume 48(1-4):51, 2004
Acta Biologica Szegediensis
http://www.sci.u-szeged.hu/ABS

DISSERTATION SUMMARY

Construction of a linkage map for *Medicago truncatula* RIL population and its comparative analysis with other *Medicago* genetic maps

Andrea Borbola

Institute of Genetics, Biological Research Center, Hungarian Academy of Sciences, Szeged, Hungary

The Fabaceae, better known as the legume family, is the second most important family of crop plants. From agronomical point of view, legume crops are valuable source of vegetable protein for humans and livestock, and as green manure in the field. It is mostly due to the special capacity of legumes to form symbiotic relationship with nitrogen-fixing bacteria.

Medicago truncatula (M.t.) species is an important model system for legume molecular biology, which is closely related with alfalfa (*Medicago sativa, M.s.*). There is a multilateral international Medicago Genome project that encompasses four general categories of activities: cDNA sequencing and hybridization arrays for gene-expression studies, knock-out mutant collections and categorizing plant phenotypes, structural genomics with a goal of reconciling physical and genetic maps, and comparative and evolutionary analysis of gene families or genomes.

Our work is closely related to the last two activities of the genome program. A detailed genetic map of the diploid *M.s.* has been constructed by our laboratory (Kaló et al. 2000, Kiss et al. 1993). Based on the expertise of our lab in genetic mapping, one of our aims was to develop an improved genetic map for a *M. t.* RIL (Recombinant Inbred Line) population in cooperation with a French laboratory. The second aim was to compare the genetic maps of the *M. t.* and alfalfa. The individuals of the RIL population are the seventh generation of the cross between Jemalong 6 and DZA 315 lines (Thoquet et al. 2002). Other two *M. t.* populations, resulted from the cross of A17xA20 (D. Cook's laboratory) and J6xDZA (T. Huguet's group), were also used for the comparative mapping analysis.

PCR based markers were used for mapping. Gene-specific primers were designed by intron targeting method or single sequence repeats were taken into consideration. The genotypes of the individuals in the mapping populations were determined after agarose gel electrophoresis for those markers that showed either length polymorphism or dominant inheritance. The non polymorphic PCR fragments in agarose gels were subjected for further analysis to detect polymorphism; either SSCP experiments were performed or the sequence of the amplified products were determined for different alleles. Based on the sequence information, restriction enzyme digestion (CAPS) was performed to identify polymorphism, where it was possible.The genotypes of the individuals of the RIL population were determined for 250 genetic markers. Newly and previously mapped RFLP and PCR based markers corresponding to genes with known functions or sequences were used for the comparison. The comparative analysis of linkage maps revealed high level of correlation of the marker order between the two *Medicago* species. Only a few differences in the marker position and allele numbers were detected between the maps. The results of this syntenic analysis allow us to create an integrated *Medicago* map and to use the mapping data mutually for further genetic experiments.

References

Kaló P, Endre G, Zimányi L, Csanádi G, Kiss GB (2000) Construction of an improved linkage map of diploid alfalfa (*Medicago sativa*). Theor Appl Genet 100:641-657.

Kiss GB, Csanádi G, Kálmán K, Kaló P, Ökrész L (1993) Construction of a basic genetic map for alfalfa using RFLP, RAPD, isozyme and morphological markers. Mol Gen Genet 238:129-137.

Thoquet P, Ghérardi M, Journet EP, Kereszt A, Ané JM, Prosperi JM, Huguet T (2002) The molecular genetic linkage map of the model *Medicago trunctula*: an essential tool for comparative legume genetics and isolation of agronomically important genes. BMC Plant Biology 2:1.

Supervisor: Gabriella Endre
E-mail: borbola@brc.hu

Volume 48(1-4):53, 2004
Acta Biologica Szegediensis
http://www.sci.u-szeged.hu/ABS

DISSERTATION SUMMARY

Analysis of Y-chromosomal microsatellites on archaeological and modern samples

Bernadett Csányi

Institute of Genetics, Biological Research Center, Hungarian Academy of Sciences, Szeged, Hungary

The special properties of the Y chromosome, which include haploidy, paternal inheritance and absence of recombination through most of its length (95%), make this chromosome a powerful tool for tracing and comparing paternal lineages of human populations.

Among its markers microsatellites or short tandem repeat loci (STR) are marked by tandemly repeated sequences of 2-5 bp. The specific number of repeats (or allele) is the same in men who belong to the same paternal lineage and usually remains unchanged from generation to generation but changes sometimes occur and the number of repeats may increase or decrease by one unit (Kimura and Ohta 1978).

Y-chromosomal STRs show sufficient variability among individuals in a population and high degree of geographical differentiation (Jobling and Tyler-Smith 1995). Thus, their polymorphic character makes them especially suited for forensic, genealogical and population genetic studies (Schultes et al. 1999).

According to these features 4 microsatellite markers were selected for reconstruction of paternal lineages of ancient Hungarians, originated from 10th century. These markers have simple structures, they are highly variable and short in length which qualifies them as an investigate tool in the study of ancient DNA (aDNA). Due to degradation and low amounts of aDNA the first attempts were unsuccessful. Therefore several methods have been introduced to enhance the efficiency of our analyses. We tried to repair the highly fragmented and heavily damaged aDNA with different enzymes (Bernardo et al. 2002) and to increase the amount of aDNA with random primers (Zhang et al. 1992). These trials supported the notion that the bones did not preserve any amplifiable Y-chromosomal DNA or our detection system does not have enough sensitivity.

Then the examinations were continued on a fully automated, highly accurate and very sensitive system (Automated Laser Fluorescent DNA Sequencer). Its function relies on the detection of laser-induced fluorescence of the carbocyanine dye (Cy5) with which the DNA fragments are labelled. Using appropriate internal molecular size markers it can detect as small as one basepair difference. So it appeared to be a good system to investigate Y-chromosomal length polymorphisms.

This method proved to be successful. In the case of 3 ancient bone samples Y-chromosomal STR markers have been revealed. Among the 4 selected markers we could examine 2 STRs, which yield amplification products in shorter ranges (108-140 bp and 147-179 bp). The markers, which characterize the human remains, occur mainly in the Asian continent in our Y chromosome STR database, but they can be found in European populations also.

The Y-chromosomal DNA analysis was extended to modern Hungarians and Szeklers too. We have data from 137 Hungarian and 115 Szekler men.

Comparing the allele frequency distributions of these two modern populations for 4 STR markers it was established that there is no significant genetic difference between the modern Hungarian and Szekler men and they contain Asian genetic elements beside the European ones. The statistical evaluation of the results confirmed the small genetic distances between Hungarians, Szeklers and Albanian, Greek, Romanian, Bulgarian, Bulgarian-Turkish, Turkish, Estonian, Iranian, Syrian, German, Austrian and Italian populations, while both modern ethnic groups differ significantly from Portuguese, Spanish, British, Basque, Finnish, Lithuanian and Japanese populations.

References

Di Bernardo G, Del Gaudio S, Cammarota M, Galderisi U, Cascino A, Cipollaro M (2002) Enzymatic repair of selected cross-linked homoduplex molecules enhances nuclear genes rescue from Pompeii and Herculaneum remains. Nucleic Acids Res 30:e16.

Jobling MA, Tyler-Smith C (1995) Fathers and sons: the Y chromosome and human evolution. Trends Genet 11:449-456.

Kimura M, Ohta T (1978) Stepwise mutation model and distribution of allelic frequencies in a finite population. Proc Natl Acad Sci USA 75:2868-2872.

Schultes T, Hummel S, Herrmann B (1999) Amplification of Y-chromosomal STRs from ancient skeletal material. Hum Genet 104:164-166.

Zhang L, Cui X, Schmitt K, Hubert R, Navidi W, Arnheim N (1992) Whole genome amplification from a single cell: Implications for genetic analysis. Proc Natl Acad Sci USA 89:5847-5851.

Supervisor: István Raskó
E-mail: csanyib@nucleus.szbk.u-szeged.hu

Volume 48(1-4):55, 2004
Acta Biologica Szegediensis
http://www.sci.u-szeged.hu/ABS

DISSERTATION SUMMARY

Isolation and characterization of redlip, a novel circadian clock mutant in *Arabidopsis*

Balázs Fehér

Institute of Plant Biology, Biological Research Center, Hungarian Academy of Sciences, Szeged, Hungary

Many physiological and biochemical processes in plants exhibit endogenous rhythms with a period of about 24 hours. These rhythms are generated and maintained by an internal timing mechanism, the circadian clock, which enables plants to anticipate the forthcoming rhythmic changes in the environment and to temporally coordinate their internal processes. In model organisms, such as *Neurospora*, *Drosophila*, mice and cyanobacteria, several key components of the circadian clock have been identified and their functions in the clock mechanism have been well described. In plants, however, only few elements of the central oscillator have been characterized and little is known about their functional interactions.

In order to learn more about the molecular structure and function of the circadian clock in *Arabidopsis*, a luciferase imaging-based mutant screen (Millar et al. 1992) has been carried out and several mutants showing aberrant rhythmic expression of the CAB gene (coding for the chlorophyll a/b-binding protein) have been identified. As a result of this screen we have identified several previously described clock genes: 11 allels of zeitlupe (ZTL), an early flowering 3 (ELF3), a timing of CAB (TOC) and a completely new mutation, red light insensitive period (redlip), that shortens the period length of CAB expression under constant darkness (DD) and constant light (LL). All other clock-controlled processes examined, including the expression of the cold-circadian rhythm-RNA-binding 2 (CCR2) gene (Carpenter et al. 1994) and the rhythm of leaf movement, showed similar period shortening under free-running conditions. To investigate which part of the circadian system is affected by the mutation, fluence rate curves (FRCs; Covington et al. 2001) have been created by determining the effect of different light intensities on period length. In contrast to wild type, the free running period length in the mutant does not change significantly under varying red light intensities, suggesting a role for REDLIP in the regulation of the light sensitivity of the central oscillator. To determine whether REDLIP's action is phase dependent, we examined clock resetting by using light pulses and constructed phase response curves (PRCs; Covington et al. 2001). Mutation causes a significant alteration of the phase response curve end of the subjective day and early phase of the subjective night, suggesting that REDLIP has important role in light input to the clock during this time. The mutation is mapped to a region of chromosome 5 where already known clock genes are localized. However, comparative sequencing of the already known clock genes revealed that they are unchanged in the mutant, which means that REDLIP is a novel component of the *Arabidopsis* circadian clock.

References

Millar AJ, Short SR, Chua NH, Kay SA (1992) A novel circadian phenotype based on firefly luciferase expression in transgenic plants. The Plant Cell 4:1075-1087.

Carpenter CD, Kreps JA, Simon AE (1994) Genes encoding glycine-rich *Arabidopsis* thaliana proteins with RNA-binding motifs are influenced by cold treatment and an endogenous circadian rhythm. Plant Physiol 104:1015-1025.

Covington MF, Panda S, Liu XL, Strayer CA, Wagner DR, Kay SA (2001) ELF3 modulates resetting of the circadian clock in *Arabidopsis*. The Plant Cell 13:1305-1315.

Supervisor: Ferenc Nagy
E-mail: feherb@nucleus.szbk.u-szeged.hu

Volume 48(1-4):57, 2004
Acta Biologica Szegediensis
http://www.sci.u-szeged.hu/ABS

DISSERTATION SUMMARY

Construction and characterization of a multi-deletional *Escherichia coli* strain

Tamás Fehér

Department of Biochemistry, Biological Research Center, Hungarian Academy of Sciences, Szeged, Hungary

In the past decade, among the first genomes to be sequenced were those of *Escherichia coli* K-12 and *E. coli* O157:H7. Comparison of the data revealed that approximately 70% of their genomes are highly conserved. This is called the backbone sequence, which is interrupted by many strain-specific islands (Perna et al. 2001). Our group's goal was to delete as many strain-specific islands in the K-12 strain as possible, for two main reasons: as a basic scientific research goal, we wanted to see how far we can go with the deletions without impairing the viability of the bacterium under laboratory conditions. Second, we wished to develop a strain that is more useful for DNA-cloning experiments or other biotechnological purposes. Our deletion method is based on a λ-Red type recombination of a PCR-generated linear DNA fragment into the genome, followed by a specific double stranded break-induced intramolecular recombination event. The deletion process leaves no extrachromosomal sequences behind, and can be repeated in the same cell in an unlimited number (Kolisnychenko et al. 2002).

So far we have accumulated 42 deletions in the K-12 strain. Among the deleted sequences were all the mobile genetic elements (IS elements, prophages, Rhs sequences), some damaged genes, putative virulence genes and many genes of unknown function. The DNA-microarray tests made with the multi-deletional strain showed that, although all known IS's were removed, further IS elements were present in the genome. We located three IS1's, one IS2 and one IS5 using inverse PCR, and deleted all five extra insertional sequences.

We compared the growth rates of wild type and multi-deletional strains, and found them to be equal in minimal medium, with the latter growing slightly slower in rich medium. The multi-deletional strain showed elevated electroporation efficiencies in the case of 100 kbp-large BACs, but showed no elevation in the efficiency of small plasmid-electroporation. We compared the mutation rates of the two strains by measuring the inactivation frequencies of the *cycA* gene during growth, and the activation frequency of the *bgl* operon in the absence of growth. Our experiments showed that the inactivation of the *cycA* gene in the wild type strain is caused by IS element-insertions in 20-25% of the cases. We measured the overall inactivation frequency of this gene in the multi-deletional strain to be 20-25% lower than in the wild type. The difference among the two strains can thus be explained by the deletion of IS elements. Also, the *bgl* operon is activated in wild type in 90% of the cases by IS element-insertions into the regulatory region of the operon. The multi-deletional strain has a 90% lower overall activation frequency of this operon, which can also be explained by the lack of IS elements.

The results listed above demonstrate that, by careful planning, 14.1% of the genome of *E. coli* can be deleted without impairing the viability of the bacterial cell. Moreover, our work resulted in a strain that, due to its elevated electroporation efficiency and lower mutation rate, is advantageous for experiments involving téhe cloning of DNA fragments.

References

Kolisnychenko V, Fehér T, Herring CD, Plunkett G 3rd, Pósfai J, Blattner FR, Pósfai G (2002) Engineering a reduced *E. coli* genome. Genome Res 12:640-647.

Perna NT, Plunkett G 3rd, Burland V, Mau B, Glasner JD, Rose DJ, Mayhew GF, Evans PS, Gregor J, Kirkpatrick HA, Posfai G, Hackett J, Klink S, Boutin A, Shao Y, Miller L, Grotbeck EJ, Davis NW, Lim A, Dimalanta ET, Potamousis KD, Apodaca J, Anantharaman TS, Lin J, Yen G, Schwartz DC, Welch RA, Blattner FR (2001) Genome sequence of enterohaemorrhagic *Escherichia coli*. O157:H7. Nature 409:529-533.

Supervisor: György Pósfai
E-mail: fehert@nucleus.szbk.u-szeged.hu

Volume 48(1-4):59, 2004
Acta Biologica Szegediensis
http://www.sci.u-szeged.hu/ABS

DISSERTATION SUMMARY

Genetic analysis of a *Medicago truncatula* mutation causing variegated leaf phenotype

Katalin Kontár

Institute of Genetics, Biological Research Center, Hungarian Academy of Sciences, Szeged, Hungary

In plants, as in animals, normal cellular differentiation depends on coordinated interactions between the nuclear and organellar genomes. A genetic dissection of plant variegation mutants is a powerful means to gain insight into these poorly understood interactions.

The leaves of the variegation mutant plants typically have green and white sectors. Whereas the cells in the green sectors contain normal chloroplasts, the cells in the white sectors have plastids that lack chlorophyll and/or carotenoid pigments. This indicates that these cells are perturbed in the nuclear-chloroplast communication that is manifested in pigment-deficient plastids (Wetzel et al. 1994).

A common mechanism of variegation is the induction of defective chloroplasts by mutation in nuclear genes for organelle proteins. This is sometimes due to transposable element activity, in which case the green and white cells have different genotypes. In other cases, the two types of cells have the same (mutant) genotype, indicating that the gene defined by the mutation codes for a product that is required for organelle biogenesis in some, but not all, cells of the mutant (Aluru et al. 2001).

The *Medicago truncatula (M.t.)* variegated mutant, identified in our group, has green and white stripes on its leaves. The mutant individual has other morphological differences compared to the wild type as well: they are usually dwarf and have small and narrow leaves the arrangement of leaves also differs. In some cases revertant lateral shoots with full-green leaves appear on mutant plants. Our aim is to identify the mutant gene by map-based cloning. For genetic mapping we constructed an F2 segregating population. In this population 36 individuals out of 148 have the variegated phenotype. Based on the segregation ratio the mutation resulted in a recessive allele of a nuclear gene.

We determined the position of the mutant gene on the genetic map of *M.t.*, which consists of eight linkage groups (LG). We chose two to three microsatellite markers from each LG to seek for molecular marker showing linkage with the mutant gene. The genotypes of the mutant plants were determined for these markers and analyzed by color-map (Kiss et al. 1998). This resulted in the identification of a microsatellite marker closely linked to the mutation on the LG2.

Having this result we determined the genotype of more length-polymorphic and CAPS markers on the LG2 in the population segregating the mutation to assign more precise position of the mutation. Our aim was to determine two bordering molecular markers with which we could identify BAC clones for chromosome-walking.

We identified a gene-specific marker showing tight linkage to the mutation with no recombination detected in the mapping population. Based on available sequence data of *M.t.* we could identify the BAC clone that carries this gene-specific marker at one end of the clone. A new SSR marker was generated at the other end of the BAC clone (in 115 kbp distance), which also did not show recombination with the mutation.

Using different homology searches we found that this *M.t.* BAC clone carries a 2500 bp long sequence (between the two BAC-end markers), which is highly homologue to the *Arabidopsis thaliana IMMUTANS* gene. Based on published data it is known that a mutation in that gene also leads to variegated phenotype. Further experiments are in progress to determine whether the *M.t.* ortholog of the *IMMUTANS* gene was mutated in our variegated mutant.

References

Aluru MR, Bae H, Wu D, Rodermel SR (2001) The *Arabidopsis immutans* mutation affects plastid differentiation and the morphogenesis of white and green sectors in variegated plants. Plant Phys 127:67-77.

Kiss GB, Kereszt A, Kiss P, Endre G (1998) Colormapping: a non-mathematical procedure for genetic mapping. Acta Biol Hun 49:125-142.

Wetzel CM, Jiang CZ, Meehan LJ, Voytas DF, Rodermel SR (1994) Nuclear-organelle interactions: the *immutans* variegation mutant of *Arabidopsis* is plastid autonomous and impaired in carotenoid biosynthesis. Plant J 6:161-175.

Supervisor: Gabriella Endre
E-mail: kontark@brc.hu

Volume 48(1-4):61, 2004
Acta Biologica Szegediensis
http://www.sci.u-szeged.hu/ABS

DISSERTATION SUMMARY

Analysis of the mitochondrial genome of the human pathogenic yeast *Cryptococcus neoformans*

Judit Litter

Department of Microbiology, University of Szeged, Szeged, Hungary

Cryptococcus neoformans is an encapsulated basidiomycetous yeast. This opportunistic pathogen primarily infects immunosuppressed and immunodeficient patients. The disease is most frequently manifested as meningitis.

Well functioning respiratory system assured by well functioning mitochondria is one of the most important factors of the yeast's successful survival in the body. To date only a few data are available about the organization of the mitochondrial genome of basidiomycetous fungi. Varma and Kwon-Chung (1989) have demonstrated extensive polymorphism among the strains of *Cryptococcus neoformans* regardless of their serotype or varietal status by analysis of restriction fragment length polymorphisms (RFLP) in mitochondrial DNA.

The aim of the present work was the characterization of the structure and organization of the mitochondrial genome in *C. neoformans var. grubii* IFO 410 (serotype A) and *C. neoformans var. neoformans* α IFM 5844 (serotype D) strains. Physical and functional maps were constucted by *Eco*RI and *Eco*RV restriction enzymes using a reciprocal digestion technique (Hamari et al. 1999). Several genes could be localised to some fragments by Southern hybridizations using heterologous *Aspergillus nidulans* primers working on *Cryptococcus hungaricus* (Gácser et al. 2002). Additional genes were localised by cloning the majority of *Eco*RI and *Eco*RV fragments into pSK vector, and sequencing.

The correct order of several mitochondrial genes important in the respiration (*nad*1, *nad*2, *nad*3, *nad*4, *nad*4L, *nad*5, *nad*6, *atp*6, *atp*9, *cox*1, *cox*2, *cob*) and *rns* gene important in protein synthesis was determined. We did not find any differences in the order of the genes between the strains. However, they differed significantly in the sizes of their mt DNAs, measuring 32.6 kb and 24.1 kb for *C. n. var. neoformans* and *C. n. var. grubii*, respectively.

Comparing the maps it was found that two large regions, altogether of 8.5 kb, could give rise to this variance. The presence of introns and alteration of the length of intergenic regions was investigated in both regions.The greatest difference was observed in the size and number of introns of *cox*1 and *cob* genes. The size of *cox*1 gene in *C. n. var. grubii* was 1587 bp without any introns, while in *C. n. var. neoformans* it was 6004 bp and contained five introns. LAGLI-DADG motifs were found in several introns and there were also differences in the *rns-atp*6, *atp*6-*atp*9 and *atp*9-*cox*1 intergenic regions between the two strains.

Primer pairs for *cox*3, *rnl* and *nad*5 genes were designed using the *C. neoformans* mitochondrial genome database to execute detailed comparison. Using these primers in PCR reactions we found that there were some differences in the size of the *nad*5 and *rnl* genes, too. The PCR products of *rnl* genes were sequenced and concluded the presence of intron in *C. n. var. neoformans*. A 0.2 kb diffrence from the 8.5 kb size was revealed.

References

Gácser A, Hamari Zs, Pfeiffer I, Litter J, Kevei F, Kucsera J (2002) Organization of mitochondrial DNA in the basidiomycetous *Dioszegia hungarica* (*Cryptococcus hungaricus*) species. FEMS Microbiol Lett 212:1-6.

Hamari Zs, Pfeiffer I, Ferenczy L, Kevei F (1999) Interpretation of variability of mitochondrial genomes in the species *Aspergillus carbonarius*. Antonie van Leeuwenhoek 75:225-231.

Varma A, Kwon-Chung KJ (1989) Restriction fragment polymorphism in mitochondrial DNA of *Cryptococcus neoformans*. J Gen Microbiol 135:3353-3362.

Supervisor: Judit Kucsera
E-mail: liju@bio.u-szeged.hu

Volume 48(1-4):63, 2004
Acta Biologica Szegediensis
http://www.sci.u-szeged.hu/ABS

DISSERTATION SUMMARY

Characterization of the nodulation receptor kinase (NORK) protein in *Medicago truncatula*

Anita Lózsa

Institue of Genetics, Biological Research Center, Hungarian Academy of Sciences, Szeged, Hungary

Legumes are able to establish root endosymbioses with rhizobial bacteria and arbuscular mycorrhizal fungi. These relationships enable these plants to fix atmospheric nitrogen and acquire phosphorus from the soil, respectively. The legume-rhizobia relationship begins with a molecular dialog in the rhizosphere. Plant exudates (flavonoids) induce the production of the so-called Nod factor (NF) in the bacteria (Dénarié et al. 1996). NFs induce nodule formation on roots and they are the major determinant of host specificity of the interaction. Since responses are induced in the plant by NF concentrations in a nano- to picomolar range, it has been postulated that NFs are recognized by specific receptor(s). Recently, several genes have been identified and characterized that are involved in the perception and early signal transduction of the NF thereby in the nodulation process.

The nodulation receptor kinase (*NORK*) gene was the first symbiotic legume gene isolated via map-based cloning from *Medicago* (Endre et al. 2002). It is predicted to play a key role in the NF signal transduction pathway in the plant. The gene encodes for a receptor-like kinase that contains a unique (NORK extacellular-sequence-like - NSL) motif and three leucine-rich repeats (LRRs) in the extracellular domain, a transmembrane domain (TM) and an intracellular serine/threonin kinase domain.

In order to elucidate the role of the NORK protein in nodulation we designed different chimaeric and truncated *NORK* constructs to test their activity in transgenic roots with mutant background. The transformation experiments were carried out by the *Agrobacterium rhizogenes* system. The plant material used for transformation is a NORK mutant, non-nodulating *Medicago truncatula (Mt)* line TR25. In order to assess the effects of transgenes the transgenic roots were observed by light microscopy after 3-9, 14, 21 days post inoculation (dpi) with *Sinorhizobium meliloti (Sm)* carrying a plasmid containing the *lacZ* gene. For infection studies the roots were fixed and stained for β-galactosidase activity (Oldroyd and Long 2003).

In the case of the chimaeric constructs, the extracellular domain (NSL + LRR) of the *Mt NORK* gene was replaced with the extracellular domains of other legume species, *Melilotus albus (Ma)* or *Vicia hirsuta (Vh)*, respectively. Both constructs complemented the *Mt* NORK mutant plants, pink, nitrogen fixing nodules appeared on the transformed roots 21 dpi with *Sm*. We could observe the different early plant responses (root hair deformations, infection thread and nodule primordia formation) normally induced by the bacteria. The nodulation process did not show any delay compared to the control transformed roots. The truncated constructs did not contain the NSL domain or the NSL and the LRR domains from the extracellular part. These constructs did not complement the non-nodulating phenotype of the mutant plants, no nodules on the transformed roots were detected.

Vh is a more distant relative of *Mt* than *Ma*, and it has another symbiotic partner, *Rhizobium leguminosarum* bv. *viciae*, which produces NF with a structure different from that of *Sm*. From these experiments we concluded that the NORK protein does not take part in the NF binding directly, but the whole protein is necessary for the activation of the signal transduction pathway.

References

Dénarié J, Debellé F, Promé JC (1996) *Rhizobium* lipo-chitooligosaccharide nodulation factors: signaling molecules mediating recognition and morphogenesis. Annu Rev Biochem 65:503-535.

Endre G, Kereszt A, Kevei Z, Mihacea S, Kaló P, Kiss GB (2002) A receptor kinase gene regulating symbiotic nodule development. Nature 417:962-966.

Oldroyd GED, Long SR (2003) Identification and characterization of *Nodulation Signaling Pathway 2*, a gene of *Medicago truncatula* involved in Nod factor signalling. Plant Physiol 131:1027-1032.

Supervisors: Gabriella Endre, Attila Kereszt
E-mail: lozsa@brc.hu

Volume 48(1-4):65, 2004
Acta Biologica Szegediensis
http://www.sci.u-szeged.hu/ABS

DISSERTATION SUMMARY

Characterization of the biodegradation patways of sulfanilic acid and catechol derviatives in *Sphingomonas subarctica*

Mónika Magony

Department of Biotechnology, University of Szeged, Szeged, Hungary, and Institute of Biophysics, Biological Research Center, Hungarian Academy of Sciences, Szeged, Hungary

The appearance of man-made chemicals in the world are generally incompatible with the life and their natural degradation is very slow or it does not take place at all. Sulfanilic acid (or p-amino-benzenesulfonate), a typical representative of aromatic sulfonated amines, is widely used as an important intermediate in production of azo-dyes, plant protectives and pharmaceuticals.

So far, efficient decomposition of sulfanilic acid has been reported for a bacterial consortium consisted of a *Hydrogenophaga palleronii* and an *Agrobacterium radiobacter* strain (Dangmann et al. 1996). A dioxygenase, capable to oxidize sulfocatechuate was characterized from both strains (Hammer et al. 1996), but the other components involved in the sulfanilic acid degradation are still unknown.

Recently, a single strain capable to use sulfanilic acid as sole carbon, nitrogen and sulfur source has been isolated (Perei et al. 2001). The isolate was identified taxonomically as *Sphingomonas subarctica*.

Screening the substrate specificity of our strain disclosed its capability to completely degrade six analogue aromatic compounds: sulfanilic acid, protocatechuate, p-aminobenzoic acid, 4-sulfocatechuate, 4-hydroxybenzoate, 3,5-dihydroxybenzoate and oil contaminations.

S. subarctica seemed to express distinct enzyme cascades to utilize these molecules, since alternative enzymes were induced in cells grown on various substrates. Similar protein patterns were observed in the case of sulfanilic acid and sulfocatechol indicating that the latter compound was an intermedier in the degradation of sulfanilic acid.

The sulfanilic acid could only be converted with either intact cells or spheroplasts, but the disrupted cells were unable to convert sulfanilic acid. Hence, we analyzed proteins exclusively expressed in cells grown in the presence of the substrates. Two such proteins were sequenced and the corresponding genes were identified. We found a locus containing genes encoding aminotransferase type and ring hydroxylating dioxygenase enzymes, which likely participated in the conversion of sulfanilic acid to sulfocatechol. Other genes encoding proteins possibly involved in the degradation of aromatics were also found, their functional characterization is in progress.

The product of the first step is sulfocatechol, which is further oxidized by a ring cleaving dioxygenase. The sulfocatechol dioxygenase of *S. subarctica* was partially purified and sequenced by mass spectrometry. On the basis of the protein sequence data, a genomic region was isolated, which contained genes coding for sulfocatechol dioxygenase (SCD), sulfomuconate cycloisomerase (SMC), sulfolactone hydrolase (SLH), an oxidoreductase and a permease.

The *S. subarctica* cells have two types of protocatechol dioxygenase enzymes: type I (PCD) degrades to only protocatechol, but type II (SCD) degrades both to sulfo- and protocatechol. Protocatechol and sulfocatechol pathways are overlapped by sulfocatechol dioxygenase, but the next ring connecting steps require different cycloisomerase enzymes.

Finally, three enzymes, SCD, SMC, SLH, were overexpressed in E. coli, and the pathway of sulfanilic acid degradation was demostrated by recombinant proteins.

References

Dangmann E, Stolz A, Kuhm AE, Hammer A, Feigel B, Noisommit-Rizzi N, Rizzi M, Reuss M, Knackmuss H-J (1996) Degradation of 4-aminobenzenesulfonate by a two-species bacterial coculture. Biodegradation 7:223-229.

Hammer A, Stolz A, Knackmuss H-J (1996) Purification and characterization of novel type of protocatechuate 3,4-dioxygenase with the ability to oxydase 4-sulfocatechol. Arch Microbiol 166:92-100.

Perei K, Rákhely G, Kiss I, Polyák B, Kovács KL (2001) Biodegradation of sulfanilic acid by Pseudomonas paucimobilis. Appl Microbiol Biotechnol 55:101-107.

Supervisors: Gábor Rákhely, Kornél L. Kovács
E-mail: magonym@nucleus.szbk.u-szeged.hu

Volume 48(1-4):67, 2004
Acta Biologica Szegediensis
http://www.sci.u-szeged.hu/ABS

DISSERTATION SUMMARY

Maturation of hydrogenase enzymes in *Thiocapsa roseopersicina*

Gergely Maróti

Department of Biotechnology, University of Szeged, Szeged, Hungary, and Institute of Biophysics, Biological Research Center, Hungarian Academy of Sciences, Szeged, Hungary

T. roseopersicina is a purple photosynthetic sulfur bacterium, which harbours at least two membrane-bound (HynSL and HupSL) and one soluble (HoxEFUYH) [NiFe] hydrogenases (Rákhely et al. 2004). The maturation of these enzymes requires several accessory proteins, which are involved, among others, in metal incorporation, formation of the active centre, the proteolytic cleavage of the large subunit. In *T. roseopersicina* only few accessory genes could be found downstream from the *hupSL* genes. Using transposon-based random mutagenesis six independent hydrogenase minus mutants were isolated, and Southern analysis of these mutants indicated that they are scattered along the genome (Fodor et al. 2001).

Molecular analysis of three different mutant strains led to the identification of the Orf-s showing similarity to the [HupK (HoxV), HypC1, HypD, HypE], [HypC2, HynD] proteins of various bacteria. The genes are found in two distinct locuses, and transposon inserted into the *hypD*, *hypE* and *hynD* genes in the various mutants. The detailed analysis was executed to establish the role and the specificity of the *hupK*, $hypC_1$, $hypC_2$ and *hynD* genes (Maróti et al. 2003).

The localization of *hupK* gene is unusual: it is adjacent to the $hypC_1$, it occured generally with the hup genes. In frame deletion of *hupK* resulted around 90% loss of the membrane-bound activities (both Hup and Hyn), although the activity of the soluble hydrogenase was almost unaltered. RT-PCR experiments showed that the *hupK* and the $hypC_1$ were on the same transcript, although alternative transcripts and promoters could not be excluded.

The presence of at least two *hypC* genes in the genome was also surprising. None of the *HypC* proteins seemed to be strongly specific for any [NiFe] hydrogenases. The activity of each enzyme was affected by the mutation of both *hypC* genes.

In one hydrogenase mutant strain, the transposon inserted into the *hynD* gene resulting the loss of thermostable but not the heat labile hydrogenase activities. Carefully performed activity measurements on various mutants proved that the HynD protein being similar to the hydrogenase specific endoproteases was responsible for the maturation of the HynSL enzyme.

Homologous complementations with the appropriate genes proved the responsibility of these genes for the observed affects.

An expression vector-system was created in order to examine the maturation process of the hydrogenases in our host organism (Fodor et al. 2004). These vectors are useful for protein purification and for studying protein-protein interactions in a range of bacterial species.

References

Fodor B, Rákhely G, Kovács ÁT, Kovács KL (2001) Transposon mutagenesis in purple sulfur photosynthetic bacteria: identification of *hypF*, encoding a protein capable of processing [NiFe] hydrogenases in alpha, beta, and gamma subdivisions of the proteobacteria. Appl Env Microbiol 67:2476-2483.

Fodor BD, Kovács AT, Csáki R, Hunyadi-Gulyás É, Klement É, Maróti G, Mészáros LS, Medzihradszky KF, Rákhely, Kovács KL (2004) Modular broad-host-range expression vectors for single protein and protein complex purification. Appl Env Microbiol 70:712-721.

Maróti G, Fodor BD, Rákhely G, Kovács ÁT, Arvani S, Kovács KL (2003) Accessory proteins functioning selectively and pleiotropically in the biosynthesis of [NiFe] hydrogenases in *Thiocapsa roseopersicina*. Eur J Biochem 270:2218-2227.

Rákhely G, Kovács ÁT, Maróti G, Fodor BD, Csanádi G, Latinovics D Kovács KL (2004) Cyanobacterial type, heteropentameric, NAD+ reducing [NiFe] hydrogenase in the purple sulfur photosynthetic bacterium, *Thiocapsa roseopersicina*. Appl Env Microbiol 70:722-728.

Supervisors: Kornél L. Kovács, Gábor Rákhely
E-mail: marotig@nucleus.szbk.u-szeged.hu

Volume 48(1-4):69, 2004
Acta Biologica Szegediensis
http://www.sci.u-szeged.hu/ABS

DISSERTATION SUMMARY

Demographical studies on the Late Roman Limes between Szöny (Brigetio) and Visegrád (Pone Navata)

Mónika Merczi

Department of Anthropology, Univesity of Szeged, Szeged, Hungary, and Balassa Bálint Museum, Esztergom, Hungary

In the cemeteries along the Limes, frontier of the Roman province of Pannonia, soldiers and civilian were buried. Only the anthropological analysis of the Late-Roman population (4^{th}–5^{th} century) can be fullfilled because of the differences in the funeral habits. The anthropological studies payed little attention to this period and area.

The age determination between 0–22 years is based on the method of Schour-Massler (1941), Stloukal-Hanáková (1978), Schinz et al. (1952) and Ferembach et al. (1979); above 23 years, we followed the method of Nemeskéri et al. (1960). Sex determination was based on the work of Éry et al. (1963). The number of newborns was corrected after Coale and Demény (1966). The following cemeteries have been examined: Tokod–Erzsébet Shaft (Éry 1981), Esztergom–Kossuth Street, Esztergom–Bánom Lane, Visegrád–Diós (Merczi 2001).

In the cemeteries, the proportion of children, especially that of newborns, is very low. After correction of the number of newborns, the proportion of children/adults stands near to the hypothetical distribution. Within the population above 15 years of age in Visegrád and Esztergom-Kossuth Street, there is a lot more men then women, while in Tokod and in Esztergom-Bánom Lane, the proportion of the sexes is balanced.

In Visegrád the most men and women died in the adult age group, between 35–39 years. Between 15–39 years the mortality of men is higher. In Esztergom–Bánom Lane, the most men died between the age of 45–49, while the most women died between 35–39 years of age. Between 15–29 years, the mortality rate of women is higher. In Esztergom–Kossuth Street the most men died between 50–54 years. Almost half of the women died between 45–49 years. Between 15–24 years the mortality of men, between 25–34 years that of women is more unfavourable. In Tokod, the peak mortality rate of men is between 50–54, that of women 50–54 years; between 20–49 years, more men died than women.

The peak mortality rate of men can be found only in Visegrád in the adult age group, in the other cemeteries in the matured age group. The most women died in the adult age group not only in Visegrád, but in Esztergom–Bánom Lane too. The more unfavourable mortality of women in the adult age group, which can be attributed to the pregnancy and to the complications during the childbearing, cannot be noticed in Visegrád.

References

Coale AJ, Demény P (1966) Regional model life tables and stable populations. Princeton.

Éry K, Kralovánszky A, Nemeskéri J (1963) Történeti népességek rekonstrukciójának reprezentációja. Anthrop Közl 7:41–90.

Éry K (1981) Anthropologische Analyse der Population von Tokod aus dem 5. Jahrhundert. in: Mócsy A: Die Spätrömische Festung und das Gräberfeld von Tokod. pp. 223–263.

Ferembach D, Schwidetzky I, Stloukal M (1979) Empfehlungen für die Alters- und Geschlechtdiagnose am Skelett. Homo 30:1–32.

Merczi M (2001) Embertani adatok a Dunakanyar (Visegrád–Diós) késő római kori népességéhez. Anthrop Közl 42:33–41.

Nemeskéri J, Harsányi L, Acsádi Gy (1960) Methoden zur Diagnose des Lebensalters von Skelettfunden. Anthrop Anz 24:103–115.

Schinz H, Baensch W, Friedl E, Uehlinger E (1952) Ossifikationstabelle. in: Lehrbuch der Röntgen–Diagnostik.

Schour J, Massler M (1941) The development of the human dentition. J Amer Dent Assoc 28:1153–1160.

Stloukal M, Hanáková H (1978) Die Länge der Längsknochen altslavischer Bevölkerungen unter besonderer Berücksichtigung von Wachstumsfragen. Homo 29:53–69.

Supervisors: Antónia Marcsik, Kinga Éry
E-mail: balassamuz.e@vnet.hu

Volume 48(1-4):71, 2004
Acta Biologica Szegediensis
http://www.sci.u-szeged.hu/ABS

DISSERTATION SUMMARY

Connection between membrane physical state and heat shock response

Enikö Nagy

Institute of Biochemistry, Biological Research Center, Hungarian Academy of Sciences, Szeged, Hungary

The classical model on the sensing/signaling of heat shock proposes that primarily the accumulation of denatured proteins triggers the activation of the stress-response. Our alternative, but not exclusive, view is that the mechanism of temperature sensing is associated also with the alterations of the physical state of membranes (Horváth et al. 1998; Vígh et al. 1998; Vígh and Maresca 2002).

In our recent study the membrane fluidizing agent benzyl alcohol (BA) was used to test the role of proteootoxicity and membrane perturbation separately, in generation of HS response (Balogh et al. 2002). Mammalian cells treated with BA at their growth temperature showed an elevated synthesis of the major stress protein, HSP70. By monitoring the enzymatic activity of luciferase expressed in mammalian cells we have demonstrated that unlike heat stress, BA treatment does not result in protein denaturation. Furthermore, it was also evidenced that the non-toxic cytoprotective drug candidate bimoclomol, which is a coinducer of HSPs, does not affect protein denaturation *in vivo*. Bimoclomol, however, interacts specifically with and increases significantly the fluidity of negatively charged membrane lipids even at normal temperatures (Török et al. 2003). Based on these results we can hypothesize that there are signaling cascades at least with two origins leading to the expression of heat shock genes. One is linked to the formation of denaturated proteins and the other is derived from the lipid phase changes of the membranes. In order to further understanding the mostly unknown regulatory mechanisms acting in response to different stressors, an extensive structural and functional analysis of the promoter region of the hsp70i gene was performed by using B16 melanoma cells. Series of plasmids containing the bacterial chloramphenicol acetyltransferase (CAT) as a reporter gene under the control of different fragments of the rat hsp70.1 promoter were used: namely, each of three HSEs alone, combination of two HSEs, all three HSEs or only proximal promoter sequences without any HSE. These promoter regions directed variable expression of the reporter, however, the induction pattern was similar by mild heat or BA treatment. Our data further supports the hypothesis that subtle alterations of membrane physical state is involved in the conversion of heat stress into sequential processes culminating in the transcriptional activation of stress regulated genes. In order to reveal and analyse the hypothetical heat sensing elements and the connected signalling pathways, different metabolic inhibitors have been introduced. Our preliminary results on the role of intracellular Ca^{2+} and the possible involvement of p38 MAP kinase will be discussed.

References

Horváth I, Glatz A, Varvasovszki V, Török Z, Páli T, Balogh G, Kovács E, Nádasdi L, Benkő S, Joó F, Vígh L (1998) Membrane physical state controls the signaling mechanism of the heat shock response in *Synechocystis* PCC 6803: Identification of *hsp17* as a "fluidity gene". Proc Natl Acad Sci USA 95:3513-3518.

Vígh L, Maresca B, Harwood J (1998) Does the membrane's physical state control the expression of heat shock and other genes? Trends Biochem Sci 23:369-374.

Vígh L, Maresca B (2002) Dual role of membranes in heat stress: As thermosensors modulate the expression of stress genes and, by interacting with stress proteins, re-organize their own lipid order and functionality. Cell and Molecular Responses to Stresses, Eds. KB Storey and JM Storey, Elsevier Science, pp. 173-188.

Balogh G, Horváth I, Nagy E, Török Z, Győrfy Z, Hoyk Z, Benkő S, Bensaude O, Vígh L (2002) Membrane as thermosensor modulates the expression of stress genes. Chem Phys Lipids 118:84.

Török Zs, Tsvetkova NM, Balogh G, Horváth I, Nagy E, Pénzes Z, Hargitai J, Bensaude O, Csermely P, Crowe JH, Maresca B, Vígh L (2003) Heat shock protein co-inducers with no effect on protein denaturation specifically modulate the membrane lipid phase. Proc Natl Acad Sci USA 100:3131-3136.

Supervisors: László Vígh, Imre Boros
E-mail: loti@brc.hu

Volume 48(1-4):73, 2004
Acta Biologica Szegediensis
http://www.sci.u-szeged.hu/ABS

DISSERTATION SUMMARY

Investigation of the applicability of the *Agrobacterium*-mediated transformation in Zygomycetes

Ildikó Nyilasi

Department of Microbiology, University of Szeged, Szeged, Hungary

Fungi belonging to the Zygomycetes can cause serious post-harvest losses in various agricultural products; they are well known as opportunistic human and animal pathogens. Among them, *Mucor circinelloides* is frequently studied, e.g. due to its dimorphic nature, the ability of fungus to produce extracellular enzymes and the unique sex pheromones of its mating system. Transformation approaches, based on the complementation of auxotroph markers, have been worked out for *Mucor*. However, in these experiments foreign DNA was maintained exclusively in an autonomously replicating form in the cells and the transformation required the construction of auxotroph strains. *Agrobacterium tumefaciens* is a Gram-negative plant pathogenic bacterium, which is able to transfer a part of its tumour-inducing plasmid (T-DNA) into the genome of the infected cell. *A. tumefaciens*-mediated transformation (ATMT) proved to be efficient tool of gene transfer to a wide variety of plants. Recently, this approach was successfully applied also to transform some fungal species (de Groot et al. 1998).

The aims of the present study were: (i) to adapt the *Agrobacterium*-mediated transformation method to *Mucor* and other zygomycetous fungi and to develop a protocol which can be applied routinely to obtain integrative transformants, and (ii) to elaborate a direct selection method for the transformants which does not require the usage of auxotroph markers.

We have worked out the conditions of ATMT for *M. circinelloides*. The usage of antibiotics, such as hygromycin B, which inhibits fungal growth, would make possible the direct transformation of wild-type isolates, so the need for mutagenesis to obtain auxotroph strains could be avoided. *Agrobacterium* transfers T-DNA to the host cell, which integrates into the nuclear genome at a random position. This method can integrate heterologous sequences (as the *hph* gene in this study) into the *Mucor* genome, without the need for flanking homologous regions in the transforming vector to direct the homologous recombination.

Experiments revealed that media supplemented with the combination of dichloran and rose bengal not only reduces the colony size of transformants, but also increases the sensitivity of these fungi to hygromycin B. Transformation was performed with different plasmids containing the hygromycin B resistance gene controlled by the *Aspergillus nidulans trpC* promoter (Mullins et al. 2001) or *M. circinelloides gpd* promoter (Ács et al. 2002). The transformation event, the presence of the *hph* gene in the genomic DNA of transformed isolates was verified by PCR reaction with *hph* specific primer pair (Ács et al. 2003; Nyilasi et al. 2003). Other experiments (e.g. the hybridization of transformant DNA with *hph* specific probe) also verified the successful transformation event.

References

Ács K, Kasza Zs, Lukács Gy, Schwab H, Vágvölgyi Cs (2002) Cloning and sequence analysis of *Mucor circinelloides* glyceraldehyde-3-phosphate dehydrogenase gene. Acta Microbiol Immunol Hung 49:305-312.

Ács K, Nyilasi I, Papp T, Vágvölgyi Cs (2003) Development of new vector systems for transformation of Zygomycetes. 1st FEMS Congress Eur Microbiol Ljubljana, Abstracts.

de Groot MJA, Bundock P, Hooykaas PJJ, Beijersbergen AGM (1998) *Agrobacterium tumefaciens*-mediated transformation of filamentous fungi. Nat Biotechnol 16:839-842.

Mullins ED, Chen X, Romaine P, Raina R, Geiser DM, Kang S (2001) *Agrobacterium*-mediated transformation of *Fusarium oxysporum*: An efficient tool for insertional mutagenesis and gene transfer. Phytopathology 91:173-180.

Nyilasi I, Ács K, Lukács Gy, Papp T, Kasza Zs, Vágvölgyi Cs (2003) *Agrobacterium tumefaciens*-mediated transformation of *Mucor circinelloides*. 1st FEMS Congress Eur Microbiol Ljubljana, Abstracts.

Supervisor: Csaba Vágvölgyi
E-mail: nyilasii@freemail.hu

Volume 48(1-4):75, 2004
Acta Biologica Szegediensis
http://www.sci.u-szeged.hu/ABS

DISSERTATION SUMMARY

Qualitative and quantitative analysis of the developing enteric nervous system

Viktor Román

Department of Zoology and Cell Biology, University of Szeged, Szeged, Hungary

The enteric nervous system (ENS) is an anatomically and neurochemically complex division of the peripheral nervous system (Furness and Costa 1987) with unique embryonical origins (Doyle et al. 2004). In the present studies, chicken embryos, hatched chicks, and human embryonal tissue samples were used. The human studies always fulfilled the requirements of the declaration of the Medical World Federation proclaimed in Helsinki in1964. From the gut samples whole-mount preparations were made in each study. NADPH-diaphorase histochemistry was used to visualize nitrergic neurons in the developing chicken gut on embronic days 12, 13, 14, and 19 (Bagyánszki et al. 2000). Between the examined time points, both the desity of ganglia and nitrergic neurons decreased significantly, the later showing a delay in the colon. At the first three examined time points, the neurons/ganglion ratio showed a wave-like pattern with higher values in the proximal part of the small intestine and the colon. This pattern changed into a more balanced one by embryonal week 19. In our next study we attempted to develop a staining method to label the entire population of myenteric neurons in the intestine of developing chickens (Román et al. 2001). Histochemical staining with cuprolinic blue and immunostaining against neurofilament (NF) were used to stain the total number of neurons. Cuprolinic blue stained a huge number of neurons in the myenteric plexus. Double-staining with cuprolinic blue and NF revealed that NF staining labelled only approximately 35% of the total myenteric neuronal population. Double-staining made it possible to intensify both stainings, which allowed a more accurate morphological classification of NF-labelled neurons. Further on, the spatial distribution of nitrergic neurons was investigated in the developing human fetal myenteric plexus (Román et al. 2004). NADPH-diaphorase-stained segments of human fetal intestine were photographed, and the borders of the myenteric plexus and nuclei were digitalized. Plexus Pattern Analysis programme designed in our laboratory was used to perform randomization analyses. The results showed that nitrergic neurons were aggregated within the ganglia. The developmental dynamics of changes in the pattern of nitrergic neurons exhibited regional differences. These results suggest that, in addition to the gut wall and the plexus, intraganglionic constituents might also contribute to the spatial distribution of nitrergic neurons.

References

Bagyánszki M, Román V, É Fekete (2000) Qualitative distribution of NADPH-diaphorase-positive myenteric neurons in different segments of the developing chicken small intestine and colon. Histochem J 32:679-684.

Doyle AM, Roberts DJ, Goldstein AM (2004) Enteric nervous system patterning in the avian hindgut. Dev Dyn 229:708-712.

Furness JB, Costa M (1987) The enteric nervous system. Churchill Livingstone, London.

Román V, Krecsmarik M, Bagyánszki M, Fekete É (2001) Evalution of the total number of myenteric neurons in the developing chicken gut using cuprolinic blue histochemical staining and neurofilament immunocytochemistry. Histochem Cell Biol 116:241-246.

Román V, Bagyánszki M, Krecsmarik M, Horváth A, Resch BÁ, Fekete É (2004) Spatial pattern analysis of nitrergic neurons in the developing myenteric plexus of the human fetal intestine. Cytometry 57A:108-112.

Supervisor: Éva Fekete
E-mail: vronskij@freemail.hu

Volume 48(1-4):77, 2004
Acta Biologica Szegediensis
http://www.sci.u-szeged.hu/ABS

DISSERTATION SUMMARY

Expression and a novel function of filamin-240 in lamellocyte development in *Drosophila*

Florentina Rus

Institute of Genetics, Biological Research Center, Hungarian Academy of Sciences, Szeged, Hungary

Drosophila has a very effective innate immune system with striking similarities to innate immunity in vertebrates. Cellular immune defense in *Drosophila* is mediated by three different classes of hemocytes: the plasmatocytes, the lamellocytes and the crystal cells. Lamellocytes represent a unique population of hemocytes, both in terms of morphology and function. The lamellocytes are large, flat, adherent cells, involved in encapsulation and neutralization of intruders or of abnormally developed tissues, too large to be engulfed by plasmatocytes. These cells are nonphagocytic and their cytoplasmic constituents are relatively sparse. Very few lamellocytes are observed in wild-type *Oregon-R* larvae. Parasitization by the Hymenopteran wasp, *Leptopilinia boulardi*, initiates the rapid differentiation of lamellocytes, which subsequently adhere to and surround the egg capsule. This capsule subsequently melanizes, locally generating cytotoxic compounds and creating a barrier. Bacterial challenge does not induce lamellocyte differentiation, but this can be induced artificially by objects placed in the larval haemocel that are too large to be phagocytated (Evans et al. 2003). They develop from small (8-10 μm), round stem cells and become large (40-50 μm) flattened cells capable of binding and encapsulating large foreign particles. The development of lamellocytes from stem cells to effector cells involves two major steps: first, the differentiation of small stem cells to the immediate precursors of the fully differentiated large cells. This step requires cell division and is terminated by the expression of the L1 antigen. Second, the terminal differentiation of the immediate precursors to the large flattened cells. This process does not require cell division but is characterized by the expression of L4 and L6 antigens and the most characteristic morphological changes. In this work we studied the role of a lamellocyte antigen in lamellocyte development, which turned out to be a unique, actin-binding component of the cytoskeleton in lamellocytes.

By screening *Drosophila* cDNA expression libraries with an antibody reacting preferentially with lamellocytes, positive clones were obtained and 5 DNA fragments were isolated. The analysis of the generated sequences showed that these correspond to 8 exons of *cheerio* gene, which encodes filamin, a protein that organizes filamentous actin in networks and stress fibers and also anchors various transmembrane proteins to the active cytoskeleton. All of our isolated cDNA sequences contain a so-called filamin-folding domain, a consensus motif profile, generated from the 25 existing filamin domain sequences. Filamin exists in two isoforms in *Drosophila*, as a result of alternative splicing. The longest form, filamin-240, contains an N-terminal actin-binding domain and so far it has been known to be specific for the ring canals in the ovaries. Our studies revealed that this isoform is expressed in lamellocytes too, and is possibly involved in the organisation in the actin-network during the terminal stage of lamellocyte development. To get further insight into the role of filamin-240 in lamellocyte development, we studied the possible effect of the lack of this protein in the *cher1/cher1* loss of- function type mutant stock. The results show that the lack of the isoform results in abnormal number and proportion of developing lamellocytes, suggesting that filamin-240 is involved in the regulation of lamellocyte differentiation, perhaps as an organizer of the rearrangement of the cytoskeleton.

References

Andó I, Laurinyecz B, Nagy I, Márkus R, Rus F, Váczi B, Zsámboki J, Fehér L, Gateff E, Hultmark D, Kurucz É (2003) Our archaic heritage: the innate immunity. The cellular immunity of *Drosophila*. Magy Immunol 2:39-45.

Evans CJ, Hartenstein V, Banerjee U (2003) Thicker than blood. Conserved mechanisms in *Drosophila* and vertebrate hematopoiesis. Dev Cell 5:673-690.

Supervisor: István Andó
E-mail: inarus2001@yahoo.com

Volume 48(1-4):79, 2004
Acta Biologica Szegediensis
http://www.sci.u-szeged.hu/ABS

DISSERTATION SUMMARY

Experimental analysis of input summation in neocortical neurons

János Szabadics

Department of Comparative Physiology, University of Szeged, Szeged, Hungary

Neurons receive and integrate signals from thousands of synapses arriving to the surface of their membrane. Understanding the arithmetic used by dendrites in combining afferent signals is a fundamental problem in neuroscience. The rules of input summation are crucial in determining neuronal output properties: linear summation would preserve the importance of individual inputs. Non-linear integration, i.e. when the algebraic sum of single postsynaptic responses differs from the neuronal response to simultaneous activation, would significantly increase the computational power of both single nerve cells and neural networks. Theoretical studies also predict that the modes of integration of coincident inputs depend on their subcellular location and timing. However, due to the lack of direct experimental analysis, the rules of neural input interactions are not clear.

To test these models experimentally, we simultaneously recorded from three or four neocortical neurons *in vitro* and investigated the effect of the subcellular position of two convergent inputs on response summation in the common postsynaptic cell. When scattered over the somatodendritic surface, combination of two coincident excitatory or inhibitory synaptic potentials summed linearly in layer 2/3 pyramidal cells as well as in GABAergic interneurons. Slightly sublinear summation with connection specific kinetics was observed when convergent inputs targeted closely placed sites on the postsynaptic cell. The degree of linearity of summation also depended on the type of connection and the relative timing of inputs (Tamás et al. 2002). Simultaneous activation of many co-aligned inputs might lead to more significant nonlinear interactions especially in compartments of relatively small diameter. The axon initial segment of pyramidal cells has a limited volume and it receives inputs only from a moderate number of axo-axonic interneurons yet the summation of unitary axo-axonic inputs was only slightly sublinear (9.4%; Tamás and Szabadics 2004).

These results suggest that the majority of afferent permutations undergo linear integration, maintaining the importance of individual inputs. However, compartment and connection specific nonlinear interactions between synapses located close to each other could increase the computational power of individual neurons in a cell type and connection specific manner.

We then tested how subthreshold rules of summation would be translated to suprathreshold firing behaviour of postsynaptic neurons. We recorded two simultaneous EPSPs arriving on the same interneuron and detected their effects on postsynaptic firing. The number of postsynaptic spikes in response to simultaneously arriving EPSPs was similar to the summed number of spikes triggered by individual EPSPs. However, simultaneous presynaptic activation caused significant nonlinearities by shifting the temporal distribution of postsynaptic spikes towards the presynaptic spike and by narrowing the time window for postsynaptic activity. Furthermore, asynchronous (<10 ms) presynaptic activation was nonlinearly translated to single postsynaptic action potentials. When triggering postsynaptic spikes, preceding inputs eliminated the spike triggering effectiveness of follower EPSPs. In turn, EPSPs arriving after subthreshold preceding inputs triggered spikes with shortened latency.

Our results provide evidence that the rules of summation can be switched by the operational state of postsynaptic neurons. Close to linear subthreshold input summation rules can turn to highly nonlinear interactions enhancing temporal precision of network processes and altering spike-triggering effectiveness of individual inputs.

References

Tamás G, Szabadics J, Somogyi P (2002) Cell type and subcellular position dependent summation of unitary postsynaptic potentials in neocortical neurons. J Neurosci 22:740-747.

Tamás G, Szabadics J (2004) Summation of unitary IPSPs elicited by identified axo-axonic interneurons cerebral cortex (in press).

Supervisor: Gábor Tamás
E-mail: szabadix@bio.u-szeged.hu

Volume 48(1-4):81, 2004
Acta Biologica Szegediensis
http://www.sci.u-szeged.hu/ABS

DISSERTATION SUMMARY

The role of proline in *Arabidopsis thaliana* osmotic stress response

Gyongyi Szekely

Institute of Plant Biology, Biological Research Center, Hungarian Academy of Sciences, Szeged, Hungary

Plants have evolved different ways of adapting to osmotic stress. Proline accumulation in higher plants is a characteristic physiological response to osmotic stress. Proline is considered to play an important role in defense mechanisms of stressed cells which can ameliorate shifts in redox potential by replenishment of NADP+ supply as well. Proline degradation can provide carbon, nitrogen and energy source after stress (Hare et al. 1999). In higher plants prolin is synthesized from glutamate or ornithine. Proline biosynthesis in the glutamate pathway is controlled by the first enzyme, the bifunctional 1-pyrroline-5-carboxylate (P5CS), which phosphorylates glutamic acid and reduces it to glutamyl-5-semialdehyde (G5SA). Proline is synthesized from G5SA via pyrroline-5-carboxylate (P5C), by the Δ1-pyrroline-5-carboxylate reductase (P5CR) enzyme (Delauney and Verma 1993). The rate-limiting step in this pathway is the γ–glutamyl kinase activity of the P5CS enzyme, which is controlled by feedback inhibition in plants as well as in bacteria (Zhang et al. 1995). Degradation of proline takes place via oxidation to P5C by proline dehydrogenase (ProDH) and subsequently to L-Glu by P5C dehydrogenase (P5CDH; Kiyoshue et al. 1996). Proline accumulation in salt stressed *Arabidopsis* plants follows the activation of P5CS1 and P5CS2 genes and repression of the ProDH gene, suggesting that transcriptional regulation is the main control of proline biosynthesis (Verbruggen et al. 1996; Strichov et al. 1997).

To study the role of P5CS1 gene function, we used *Arabidopsis* knock out mutants, *p5cs1*, with T-DNA insertion in the promoter or coding region of AtP5CS1 gene. The *p5cs1* mutants showed hypersensitivity to exogenous application of 200 mM NaCl. Decreased proline content was observed in *p5cs1* mutants during external NaCl supply, as compared with wild type plants. These results prove the role of P5CS1 in adapting plants to osmotic stress. NaCl treatment greatly increased *AtP5CS1* RNA levels in wild type plants. The transcript level of *AtP5CS1* was significantly reduced in mutants; this result was confirmed by Northern hybridization.

It was reported that the elevation of proline as an osmoprotectant in the mechanism of salt stress adaptation led to the enhancement of the enzymes scavenging the reactive oxygen species (ROS).

To further analyze the defense mechanisms of *p5cs1* mutants we measured the activity of ROS scavenging enzymes. Reactive oxygen species are produced in both unstressed and stressed cells. Even under optimal conditions, ROS, including superoxide, hydrogen peroxide, hydroxyl radicals and singlet oxygen, are metabolic by-products of plant cells. These ROS affect lipid peroxidation, protein denaturation and DNA structure. To remove ROS, plant cells possess an antioxidant system consisting of low-molecular-weight antioxidants, such as ascorbate, α–tocopherol, glutathione and carotenoids, as well as antioxidant enzymes. These include superoxide dismutase for scavenging the superoxide radicals and other key enzymes, ascorbate peroxidase and glutathione reductase, detoxifying hydrogen peroxide in the ascorbate-glutathione cycle. Under normal conditions, the production and destruction of ROS is well regulated in plant cells. Under environmental stress, the balance between the production of reactive oxygen species and the quenching activity of the antioxidant system is upset.

After the measurement of the activity of glutathione S-transferase, glutathione reductase, guaiacol peroxidase, ascorbate peroxidase, catalase and superoxide dismutase, we observed that the level of the mentioned enzymes, excepting superoxide, are elevated by salinity, due to the imbalance in the production and destruction of reactive oxygen species. Compared the wild type plants with the *p5cs1* mutants, we realized that the level of the measured enzymes was decreased, except guaiacol peroxidase, which enzyme level was increased in mutants. These results suggest that the defense mechanisms of *p5cs1* mutants are less effective, which is in accordance with the hypersensitivity of *p5cs1* mutants to salt.

References

Abraham E, Rigo G, Szekely G, Nagy R, Koncz C, Szabados L (2003) Light-dependent induction of proline biosynthesis by abscisic acid and salt stress is inhibited by brassinosteroid in *Arabidopsis*. Plant Mol Biol 51:363-372.

Supervisor: László Szabados
E-mail: szekelygy@yahoo.com

Volume 48(1-4):83, 2004
Acta Biologica Szegediensis
http://www.sci.u-szeged.hu/ABS

DISSERTATION SUMMARY

Glutamate and methionine transport in *Escherichia coli*

Attila Szvetnik

Bay Zoltan Foundation for Applied Research, Institute for Biotechnology, Szeged, Hungary

Integral membrane proteins represent a very important class of proteins, as they are involved in a wide variety of cellular functions. In *Escherichia coli*, more than 10% of all chromosomal genes code for membrane transport proteins. My work is focused on two *E. coli* amino acid transporter systems.

L-glutamate is an important molecule for *E. coli* and other members of *Enterobacteriaceae*. It is the focal point in the nitrogen assimilation, and known to be a major osmoprotectant. It is readily utilizable as a carbon and energy source via α-ketoglutarate.

In *E. coli*, there are three separate L-glutamate transporter systems. The normal transporter levels together are not sufficient to allow utilization of L-glutamate as a sole carbon source. Our experiments are focused on the GltS system, which is a Na^+-dependent, binding protein independent transporter. It is known to be the major L-glutamate transporter of *E. coli*. Only fragmented information is available on the regulation, structure and transport mechanism of this protein, so we started to explore these aspects.

To study the regulation of GltS, we created a translational promoter-β-galactosidase gene fusion. For expression analysis, we integrated this construct to the chromosome and the expression was monitored under oxygen limited growth conditions. We found about a three-fold increase in the expression level.

With translational riporter fusions we analized the two dimensional structure (topology) of GltS. Ten transmembrane segments were identified. The N- and C-terminal ends are localized in the periplasmic space. Based on these results we created insertions and deletions in certain loop-regions of the protein. Currently we examine the effect of these mutations on the structure and activity of the protein.

In *E. coli*, methionine is taken up by a high affinity (*metD*) and a low affinity (*metP*) system. The *metD* system is the only transporter of D-methionine, which is an effective methionine source for the bacterial cell. Based on earlier data and the whole genome sequence of *E. coli*, we have identified a gene cluster as a likely candidate for the *metD* locus. We deleted this region from the chromosome and the deletion was transduced to a methionine auxotroph strain. Unlike the parent this *metD* minus strain was unable to grow on M9 minimal plates containing D-methionine. Complementation studies showed that expression of all the genes in the cluster is needed for growth.

A fragment which contains the predicted promoter of the first gene was cloned into a β-galactosidase-based promoter-probe vector. The activity assay results showed that the segment behaves as a promoter, and it is regulated by the MetJ repressor.

Supervisor: Miklós Kálmán
E-mail: ati@baybio.bay.u-szeged.hu

Volume 48(1-4):85, 2004
Acta Biologica Szegediensis
http://www.sci.u-szeged.hu/ABS

DISSERTATION SUMMARY

Development of a protein expression system

Gabriella Urbán

Bay Zoltán Foundation for Applied Research, Institute for Biotechnology, Szeged, Hungary

The aim of the work is to develop a protein expression system which can be used to overexpress proteins. The system would be based on a methylotrophic *Pichia* strain which is capable to utilise methanol as a sole carbon and energy source. The strain was isolated from nature by the co-workers of the Institute, so the system – if developed – could be used without any legal restriction.

Known alcohol oxidases (AO) were compared at the nucleic acid and amino acid levels, evolutionary conserved motifs were identified, degenerate oligonucleotides were synthesised accordingly and used in PCR reactions to amplify segments of the AO coding regions. The templates in these reactions were genomic DNAs isolated from the *Pichia* sp. and from two other methylotrophic *Candida boidinii* strains for comparison. The amplified products were cloned and sequenced. The partial sequences revealed the presence of two genes (*aoxA* and *aoxB*) in the *Pichia* sp. and one in each *Candida boidinii* strain. Gene specific PCR primers were synthesised on the bases of the sequence information gained, and the complete AO ORFs were subsequently isolated in several steps.

The expression of *aoxA* and *aoxB* was analysed by RT-PCR. RNAs for templates in these reactions were isolated from yeast grown on dextrose or methanol. In the presence of dextrose a constitutive, low-level expression of *aoxA* but not *aoxB* was detected. Both genes were induced in the presence of methanol, although to different extent.

The DNA segments that contain the promoter of the genes were isolated in several successive steps. The isolated genomic segment is 1920 bp long in the case of *aoxB* and 1661 bp long in the case of the *aoxA*. The 3' non-translated regions which probably contain the transcriptional terminators were also isolated as a 469 bp (*aoxA*) and a 430 bp (*aoxB*) long PCR fragments, respectively.

For the localisation of the functional elements of the promoter and for the identification of the minimal functional promoter, a number of transcriptional fusions were constructed. For a reporter in these fusions we used the fluorescent protein DsRed2.

For a functional expression system, some kind of a selection is essential. Plasmids, therefore, were constructed that indicate the successful transformation through the manifestation of a resistance gene (zeocin). Zeocin, as an antibiotics, though works at a laboratory level, might not be used for commercial productions. For future usage we also isolated the entire *his4* gene from the *Pichia* sp. which could be used for selection, provided a strain carrying a mutant version of this gene was isolated, too.

The effective transformation requires the stable maintenance of the transformed DNA, either through integration into the genome, or by replication. For integrative stabilisation the *his4* sequence can be used. The replicative stabilisation requires genomic regions the presence of which confers replication to the transformed DNA by the cellular functions. Such autonomously replicating sequences were isolated from the *Pichia* sp. and their ARS function were confirmed.

Supervisor: László Dorgai
E-mail: urga@bay.u-szeged.hu

Volume 48(1-4):87, 2004
Acta Biologica Szegediensis
http://www.sci.u-szeged.hu/ABS

DISSERTATION SUMMARY

28D, a new component of the phytochrome B signal transduction, in *Arabidopsis thaliana*

Ildikó Valkai

Institute of Plant Biology, Biological Research Center, Hungarian Academy of Sciences, Szeged, Hungary

Phytochromes are regulatory photoreceptors that control plant growth and development in response to signals from the light environment. In *Arabidopsis*, the phytochromes comprise a five membered family, designated phyA to phyE. While the role of phytochromes is well described at the physiological level, the signal transduction pathways mediated by these photoreceptors are largely unknown. To identify possible elements of phytocrome B-mediated pathways, we conducted yeast two-hybrid screen. From this screen, a phytochrome B interacting factor was isolated and named 28D. This protein contains a pterin-4a-carbinolamin-dehydratase domain. We found homologus proteins in *Pseudomonas aeruginosa*, *Drosophila melanogaster* and in mammals. The mammalian pterin-4a-carbinolamine dehydratase is identical to the dimerization cofactor for hepatocyte nuclear factor 1 (DCoH), which suggested the possibility that this dehydratase may also regulate phenylalanin hydroxylase activity at the nucleic acid level by regulating the dimerisation of this factor.

In yeast two-hybrid experiments 28D forms dimers, binds to wild-type C- and N-terminal domain of PHYB, and the full length PHYB and PHYE.

We generated transgenic *Arabidopsis* plants expressing 28D fused to the yellow fluorescent protein (YFP) to describe intracellular localization of this protein. Surprisingly, it localizes almost exclusively to the chloroplast and shows a characteristic pattern.

Expression of sense or antisense 28D sequences in transgenic *Arabidopsis* perturbs photoresponsiveness in a manner indicating that 28D functions in phyB signaling pathways *in vivo*. Moreover, in these plants the circadian clock function is altered as well. This connection is strengthened by data obtained from yeast two-hybrid assays performed with 28D and certain molecules related to the circadian clock.

Supervisor: Ferenc Nagy
E-mail: valkai@nucleus.szbk.u-szeged.hu

Volume 48(1-4):89, 2004
Acta Biologica Szegediensis
http://www.sci.u-szeged.hu/ABS

DISSERTATION SUMMARY

In vitro analysis of the intracellular distribution of different calcium-binding proteins and their corresponding mRNAs

Szilvia Várszegi

Department of Zoology and Cell Biology, University of Szeged, Szeged, Hungary

Calmodulin (CaM) is a multifunctional, highly conserved Ca^{2+}-binding protein particularly abundant in neural tissue. It is involved in signalling pathways that regulate many crucial cellular processes. In the central nervous system, a vast majority of CaM is synthesized by neurons, whereas the glial CaM expression is much weaker. In higher vertebrates three CaM genes are collectively transcribed into at least eight different mRNAs, although each mRNA codes for the same protein. Messenger RNAs transcribed from all three CaM genes are significantly more abundant in dendrite-rich regions than in axon-rich regions of rat brain (Palfi et al. 2002). In order to investigate the intracellular distribution of CaM mRNAs in detail we carried out CaM gene-specific in situ hybridization cytochemistry (ISH) with digoxigenin-labeled riboprobes on rat primary hippocampal cultures. The perykaryon was heavily stained in neurons and strong dendritic mRNA targeting was detected for all three CaM genes. The color labeling exhibited a punctate distribution, suggesting that CaM mRNAs are transported in RNA granules. To identify the cells with nondetectable CaM expression, glia-specific S100 immunocytochemistry was carried out after the ISH protocol. The vast majority of the CaM negative cells proved to be S100 positive, whereas the neurons expressing the CaM genes did not express the S100 marker (Kortvely et al. 2003).

The number of known dendritically targeted mRNA species in mammalian neurons is growing and evidence indicates that these mRNAs are translated there. Many localized mRNAs contain specific targeting element in their 3'-untranslated region (3'-UTR). The mRNA of the Ca^{2+}/CaM-dependent protein kinase II α (CaMKIIα), which is one of the most important target protein of CaM, is also localized dendritically, and its 3'-UTR can mediate this localization (Rook et al. 2000). A cis-acting control element, the cytoplasmic polyadenilation element (CPE) can facilitate mRNA transport to dendrites (Huang et al. 2003). Since the 3'-UTR of the CaMI and CaMKIIα mRNAs contain CPEs, we assume that these mRNAs are cotransported to dendrites. To test our hypothesis, fluorescent in situ hybridization cytochemistry was carried out with biotin- and digoxigenin-labeled riboprobes for CaMI and CaMKIIα mRNA, respectively, on B104 neuroblastoma and cultured primary hippocampal cells. Our preliminary experiments indicate that these two mRNAs are colocalized in dendrites, raising the possibility of their local synaptic activity-dependent cotranslation.

References

Huang YS, Carson JH, Barbarese E, Richter JD (2003) Facilitation of dendritic mRNA transport by CPEB. Genes Dev 17:638-653.

Kortvely E, Varszegi Sz, Palfi A, Gulya K (2003) Intracellular targeting of calmodulin mRNAs in primary rat hippocampal cells. J Histochem Cytochem 51:541-544.

Palfi A, Kortvely E, Fekete E, Kovacs B, Varszegi Sz, Gulya K (2002) Differential calmodulin gene expression in the rodent brain. Life Sci 70:2829-2855.

Rook MS, Lu M, Kosik KS (2000) CaMKIIα 3' untranslated region-directed mRNA translocation in living neurons: visualization by GFP linkage. J Neurosci 20:6385-6393.

Supervisor: Károly Gulya
E-mail: nyulszi@freemail.hu

Volume 48(1-4):91, 2004
Acta Biologica Szegediensis
http://www.sci.u-szeged.hu/ABS

DISSERTATION SUMMARY

Characterisation of the promoter of *Medicago sativa* cyclin dependent kinase - Cdc2MsF

Miroslava Zhiponova

Institute of Plant Biology, Biological Research Center, Hungarian Academy of Sciences, Szeged, Hungary

The eukaryotic cell cycle is regulated at multiple points and most of these involve the activation of a special class of serine-threonine protein kinases, which functionally require binding for activity to a regulatory protein known as a cyclin and are therefore named cyclin-dependent kinases (CDKs). Alfalfa (*Medicago sativa* L.) is one of the most important forage crops and it is used as a model plant in molecular biology. It was demonstrated that at least six Cdc2 homologous genes, members of the CDK family, are expressed in tetraploid alfalfa (Magyar et al., 1997). The mRNA level of one of them – cdc2MsF – showed a peak during G2/M phases. Our aim is to characterize the cdc2MsF promoter (*fpr*), which would develop further the study of the cell cycle.

Cloning of *fpr*, plant transformation and histochemical assays

We cloned a genomic DNA fragment from tetraploid alfalfa, approximately 400bp upstream from the transcription start of cdc2MsF gene.

Since the G2/M specific expression of cdc2MsF mRNA and protein was described in synchronized cell cultures (Magyar et al. 1997), our main question was if *fpr* directed reporter genes have the same pattern in a living plant organism as the native cdc2MsF protein has.

In order to follow the promoter activity, we made pCambia3301-derived constructs where the *fpr* regulates reporter genes coding for β-glucuronidase (GUS) or luciferase. The constructs were introduced in alfalfa plants by *Agrobacterium*-mediated transformation. Throughout present work the spatial and developmental expression of *fpr* driven reporter genes was investigated by analysing callus tissue, somatic embryos and 2-3 week old plantlets. In addition, for first time, histochemical detection of the native cdc2MsF protein was performed and correlated to the expression of the recombinant GUS and luciferase proteins.

Different parts from GUS stained alfalfa plants were observed under light microscope. Ultrathin sections were made from GUS stained root tips and analyzed. Immunolocalization of cdc2MsF protein was done on sections from GUS stained emerging lateral roots. Single-labelling immunohistochemistry was performed on alfalfa root tip with cdc2MsF and luciferase antibodies. For visualizing the immunoreactions secondary antibodies conjugated with horseradish peroxidase and DAB (diaminobenzidine) substrate were used. Also, we examined the activity of the luciferase enzyme after addition of luciferin substrate.

The GUS staining experiments showed that in alfalfa the reporter product accumulates preferentially in meristematic regions in which the cell division is frequent. This observation was confirmed by the cdc2MsF and luciferase immunopositivity of alfalfa root tip in the apical root meristem. In addition, there is a correlation between the GUS staining and the cdc2MsF protein expression in emerging lateral roots. Light excitation was detected during the stages of active cell division.

Synchronization of cell cultures from transformed alfalfa plants

For detailed analysis of the cell phase expression of *fpr* regulated reporter genes, we cultivated *in vitro* cell cultures from transformed alfalfa plants. Samples were taken in order to check the cell cycle progression of synchronized cells. The luciferase and cdc2MsF (as a control) transcript levels were investigated by RT-PCR and by Northern blot assay.

Reference

Magyar Z, Mészaros T, Miskolczi P, Deák M, Fehér A, Brown S, Kondorosi E, Athanasiadis A, Pongor S, Bilgin M, Bakó L, Koncz C, Dudits D (1997) Cell cycle phase specificity of putative cyclin dependent kinase variants in synchronized alfalfa cells. Plant Cell 9:223-235.

Supervisor: László Szilák
E-mail: laszlo.szilak@freemail.hu

Volume 48(1-4):93, 2004
Acta Biologica Szegediensis
http://www.sci.u-szeged.hu/ABS

DISSERTATION SUMMARY

Characterisation of the ABA sensitivity influencing *Arabidopsis* PPR gene

Laura Zsigmond

Institute of Plant Biology, Biological Research Center, Hungarian Academy of Sciences, Szeged, Hungary

T-DNA insertion mutagenesis is a recently developed technique, allowing the identification and easy isolation of genes from higher plants, in this case from *Arabidopsis thaliana*. We initiated a mutagenesis program by generating a collection of T-DNA insertion mutants (Szabados et al. 2000). Using this technique, we are trying to genetically dissect signal transduction pathways mediating cellular and organ differentiation, developmental regulation and stress responses. In order to identify tagged genes, T-DNA insertions sites are characterized by random sequencing the flanking genomic plant DNA (Szabados et al. 2002). During this mutagenesis program, we identified a transgenic line with different behaviour possessing for osmotic and hormonally stress response, where the T-DNA insertion is in the exon of *At3g16890*. The tagged gene encodes a pentatricopeptide repeat-containing protein.

The pentatricopeptide repeat (PPR) is a degenerate 35-amino acid repeating motif, which was first described by Small and Peeters (2000). The PPR proteins have been identified in animal, fungi, and plant, but not in the procaryote and in *Archea*. This family is particularly large in plants, where the majority of family members are predicted to be targeted to mitochondria or chloroplasts. Most observations (Williams and Barkan 2003) suggested that PPR domains can function as nucleic-acid-binding domains (tipically as RNA-binding domains), but some protein-binding motifs are also known. The biological function of PPR proteins could be connected with organellar RNA metabolism, but the directed substrates are not known yet.

In the course of morphological examination a semidwarf mutant was identified from the studied transgenic line, and the segregation analysis suggested that it contains only one T-DNA insertion. We confirmed the linkage between the T-DNA insertion and phenotype by molecular analysis (Southern blotting, PCR). The semidwarf mutant is homozygous for the T-DNA-tagged locus. The homozygous plants showed an increased environmental stress sensivity such as salt and cold. ABA and glucose treatments greatly prevented the mutant germination and its growing. In order to test several stress-related gene expression in this transgenig line, we used quantitative and RT PCR technique. It was verified that there is no *At3g16890* mRNA production in the homozygous mutant plants. We observed that the *AtP5CS1* and *AtRD22* RNA levels were augmented in mutant plants compared to wild type *Arabidopsis* under normal conditions as well as after ABA and NaCl treatments. We concluded, that the *At3g16890* gene can play a role in an ABA-dependent stress signaling pathway.

To further analyze the biological function and localization of this protein, we cloned the full-lenght cDNA in a HA-epitope tagging binary vector, and transformated into the homozygous and wild type plants. We confirmed the transformation by Northern hybridization and Western analysing. The phenotype of the complemented mutants were similary to the wild type under stress (ABA, NaCl, glucose) and normal conditions. The overexpressing transgenic lines showed insensitivity to toxic concentrations of NaCl, glucose, and ABA treatments at germination level. To locate the protein by Western analysis, we isolated intact chloroplast and mitochondria from overexpressing plants, and compared the recombinant protein level in the two organelles and whole plant. The protein showed mitochondrial localization. Experiments are in progress to further characterize this protein and its RNA interacting partners.

References

Szabados L, Kovács I, Ábrahám E, Oberschall A, Nagy R, Zsigmond L, Krasovskaja I, Kerekes I, Ben-Haim A, Koncz Cs (2000) Arabidopsis genome project in Hungary: generating T-DNA tagged Arabidopsis genes. Plant Physiol Biochem 38:S98.

Szabados L, Kovács I, Oberschall A, Ábrahám E, Kerekes I, Zsigmond L, Nagy R, Alvarado M, Krasovskaja I, Gál M, Berente A, Rédei GP, Ben-Haim A, Koncz Cs (2002) Distibution of 1000 sequenced T-DNA tags in the Arabidopsis genome. Plant J 32:233-242.

Small I, Peeters N (2000) The PPR motif – a TPR-related motif prevalent in plant organellar proteins. Trends Biochem Sci 25:46-47.

Williams PM, Barkan A (2003) A chloroplast-localized PPR protein required for plastid ribosome accumulation. Plant J 36:675-686.

Supervisor: László Szabados
E-mail: zsigmond@nucleus.szbk.u-szeged.hu

Instructions to Authors

Submission of manuscripts

Submission of a manuscript to Acta Biologica Szegediensis automatically involves the assurance that it has not been published and will not be published elsewhere in the same form. Manuscripts should be written in English. Since poorly-written material will not be considered for publication, authors are encouraged to have their manuscripts corrected for language and usage by a trusted expert.

There are no explicit length limitations: a normal research article will occupy 4-6 printed pages; reviews might be considerably longer. Authors should submit three sets of the complete manuscript and illustrations, together with a computer disk containing an electronic version of their manuscript. The elctronic file is considered the final material. Both Macintosh and PC versions will be accepted. The disk should be labeled with the date, the first author's name, the file name of the manuscript and the software, disk format and hardware used. Acta Biologica Szegediensis will not return copies of submitted manuscripts and figures. Requests to return original figures will be honored as a courtesy, but cannot be guaranteed. If instructions are not followed, authors will be asked to retype their manuscripts.

Manuscript format

Only good-quality laser printouts will be accepted. All pages should be printed with full double spacing, 2.5 cm margins, and a nonjustified right margin. A standard 12 point typeface (e.g. Times, Helvetica or Courier) should be used throughout the manuscript, with symbol font for Greek letters. Boldface, italics or underlined text should not be used anywhere in the manuscript. Footnotes are not permitted. Each page should be numbered at the bottom as follows:

Page 1. Title page: Complete title, first name, middle initial, last name of each author; where the work was done (authors' initials in parentheses if necessary); mailing address, phone, fax, and e-mail of the corresponding author; a running title of no more than 48 characters and spaces.

Page 2. Abstract: no more than 200 words, followed by 4-6 key words.

Beginning on page 3: Introduction, Materials and Methods, Results, Discussion, Acknowledgments, References, Figure Legends, Tables. Each section should be begun on a new page.

The manufacturer's name and location should be given in parentheses for reagents and instruments. Sources for all antibodies and nucleotide sequences should be indicated. Customary abbreviations in common use need not be defined in the text (e.g. DNA or ATP). Other abbreviations should be defined the first time that they are used. Quantitative results must be presented as graphs or tables and supported by appropriate experimental design and statistical tests. Only SI units may be used. For studies that involve animals or human subjects, the institutional, national or international guidelines that were followed should be indicated.

References

Only work that has been published or is in the press may be referred to. Personal communications should be acknowledged in the text and accompanied by written permission. In the text, references should be cited by name and year, e.g. Bloom (1983) or (Schwarz-Sommer et al. 1990) or (Maxam and Gilbert 1977). In the References, references should be listed alphabetically by first authors (including all co-authors) and chronologically for a given author (beginning with the most recent date of publication). Where the same author has more than one publication in a year, lower case letters should be used (e.g. 1999a, 1999b, etc.). Periods should not be used after authors' initials or abbreviated journal titles (e.g. Acta Biologica Szegediensis should be cited as Acta Biol Szeged). Inclusive page numbers should be used. Examples:

Bloom FE (1983) The endorphins: a growing family of pharmacologically pertinent peptides. Annu Rev Pharmacol Toxicol 23:151-170.

Coons AH (1978) Fluorescent antibody methods. In Danielli JF, ed., General Cytochemical Methods. Academic Press, New York, 399-422.

Maxam AM, Gilbert WA (1977) A new method for sequencing DNA. Proc Natl Acad Sci USA 74:560-564.

Monod J, Changeux J-P, Jacob F (1963) Allosteric proteins and cellular control systems. J Mol Biol 6:306-329.

Schwarz-Sommer Z, Huijser P, Nacken W, Saedler H, Sommer H (1990) Genetic control of flower development by homeotic genes in Antirrhinum majus. Science 250:931-936.

Illustrations

Three complete sets, including a high-quality "original" for publication, must be submitted with the manuscript. The back of each figure or composite plate should be labeled in soft lead pencil, indicating the orientation, the figure number, and the first author's name. The back of the best set should be marked "use for reproduction" or "original". Authors are encouraged to submit digital images of photographs, line drawings or graphs for printing. Most major image editing and drawing/illustrator computer software files (both Macintosh and PC) in TIFF or EPS formats are acceptable. It is particularly important that adequate resolution (at least 300 dpi, preferably 600 dpi) is used in making the original image.

Figure legends

Figures should be numbered consecutively with Arabic numerals. Material in the text should not be duplicated and methods should not be described. The size of scale bars should be indicated when appropriate. The first figure in the text should be referred to as Fig. 1, and so on.

Tables

Tables should be numbered consecutively with Arabic numerals. A brief title should be included above the table. Each table should be printed double spaced, without vertical or horizontal lines, and on a separate sheet. Material in text should not be duplicated and methods should not be described. The first table in the text should be referred to as Table 1, and so on.